Vrije Universiteit Brussel

Development of an arm system for a gesturing system for the social robot Probo

Steven Depue

Promoter: prof. dr. ir. Bram Vanderborght

Co-promoter: prof. dr. ir. Dirk Lefeber

Supervisor: ir. Greet Van de Perre

Thesis submitted in partial fulfilment of the requirements for the Master :
Master of Science in Electro-mechanical Engineering Mechatronics-Construction

Academic year 2012-2013

Bruface

Brussels
Faculty of
Engineering

VRIJE UNIVERSITEIT BRUSSEL · SCIENTIA VINCERE TENEBRAS ·

Abstract

This document is written by Steven Depue during the academic year 2012-2013 to obtain a degree in Master of Science in Electro-mechanical Engineering Mechatronics-Construction. The title of this document is *Development of an arm system for a gesturing system for the social robot Probo*.

Keywords: gesturing arm social robot Probo

This document describes the development of a robotic arm system for the social robot Probo that will be used to increase the recognition rates of a select number of emotions that Probo can portray. First, the properties of the human arm are examined. The current state of the art of robotic arms is then established to review differences with the human arm and to determine frequently used mechanisms and their reasoning. Based on this, the properties of the arm system for Probo are established: not only the systems that allow the arm to portray gestures, but also the safety features. These chosen properties are then integrated into a first prototype. The prototypes of the arms are mounted to a temporary upper body, which is used to portray six basic gestures. Using an electronic survey, the recognition rates of this upper body are tested and the results are used to assess the performance of the current prototype and the future improvements that may be needed.

Dit document beschrijft de ontwikkeling van een robotisch arm-systeem voor de sociale robot Probo, dat gebruikt zal worden om de herkenningsgraad van een aantal emoties die Probo uitbeeldt te verbeteren. Eerst wordt de menselijke arm onderzocht. Daarna wordt de huidige staat van robotische armen bekeken om de verschillen met de menselijke arm op te lijsten en om vaak gebruikte mechanismen, met de achterliggende redenen, te onderzoeken. Resulterend uit dit worden de eigenschappen van het arm-systeem voor Probo opgesteld: niet alleen de mechanismen om gebaren uit te beelden, maar ook de veiligheidssystemen worden bekeken. Deze eigenschappen worden ingebouwd in een eerste prototype van de armen, die dan bevestigd worden aan een tijdelijke bovenlichaam dat gebruikt wordt om zes basisemoties uit te beelden. Door middel van een elektronische vragenlijst worden de herkenningsgraden van de emoties getest en de resultaten worden gebruikt om over de prestaties van het huidige prototype te oordelen en toekomstige verbeteringen voor te stellen.

Ce document décrit le développement d'un prototype de bras robotique pour le robot social Probo, qui sera être utilisé pour augmenter les taux de reconnaissance d'un nombre d'émotions que Probo peut montrer. D'abord le bras humain est étudié. Ensuite, l'état courant des bras robotiques est examiné afin d'énumérer les différences avec le bras humain et d'établir les mécanismes fréquents, ainsi que les raisons sous-jacentes. Résultant de ça, les propriétés du bras robotique pour Probo sont établies: pas seulement les mécanismes pour montrer les gestes sont examinés, mais aussi les systèmes de sécurité. Un prototype des bras est construit avec ces propriétés et ils sont fixé sur un torse provisoire, qui est utilisé pour dépeindre six émotions. Au moyen d'une enquête électronique, les taux de reconnaissance sont mesurés et les résultats sont utilisés pour juger les performances du prototype et pour proposer des améliorations.

Acknowledgements

I would like to thank a number of people for their assistance and support.

First of all, I would like to thank my promoter prof. dr. ir. Bram Vanderborght for his advice on how to approach the tasks at hand, for his regular checkups and for the technical input during the project.

I would like to thank my co-promoter prof. dr. ir. Dirk Lefeber for his advice and support throughout the work.

I would like to thank ir. Greet Van de Perre for sharing information and her support, and for being available for technical advice.

Next, I want to thank Quentin Desantoine from Kinesitherapie at the Vrije Universiteit Brussel for explaining the workings of the human arm and for his advice on how to best perform the gestures for the tests.

I would like to thank the people at the faculty MECH at the VUB, who helped me to produce and purchase some components; and the people at the FablabXL at the Erasmus Hogeschool for helping me to work with the laser cutter.

Lastly, I would like to thank anyone who was able to spare a few minutes of their time to fill in my survey.

Table of contents

5

TABLE OF CONTENTS

List of figures

List of tables

Introduction

Social robots are a very specific subsection of robots, constituting a different branch of robotics than for example industrial robots. The characteristics of a social robot can be described as following [1]:

'By giving a physical embodied, and (semi)autonomous robot artificial emotions and human characteristics like a personality, facial expressions, and gestures, the robot becomes able to interact and communicate with humans. When this human robot interaction (HRI) occurs by following social behaviors and rules, the interacting robot is called a social robot. The keywords to define a social robot are: physical embodiment, autonomy, communication/interaction and social behavior/rules. It is likely that at some point some physical interaction or communication between a human and a robot that shares the same workspace will be necessary. Some autonomy is required for a social robot.'

It is noted that social robots are different from sociable robots, which are characterized by their ability to learn, which requires a very advanced type of artificial intelligence [2].

Social robots come in many shapes and forms and with varying abilities. MIT (Massachusetts Institute of Technology) has produced a large number of social robots over the years, such as Kismet, an anthropomorphic robot with 21 degrees of freedom, all of them in the actuated head [2]; or Nexi, which has an actuated head and upper body (torso and arms) [3]. Of course, these are by far not the only social robots. One thing that a lot of social robots do have in common is that because of their complexity and number of degrees of freedom, they are very expensive; often running into tens of thousands of Euros. Because of this, it is difficult to integrate social robots into the environments that they were designed to work in (such as hospitals, schools, normal people's households, etc.), meaning they stay confined to research platforms, demonstrative purposes or learning platforms for robotics students. There are however a few examples of cheap social robots such as Furby [4], where a price tag of less than €100 is achieved by significantly limiting the number of degrees of freedom that the robot possesses and by way of mass production, as it is marketed as a toy intended for households.

Probo [1] [5] is a social robot, currently under development by the Robotics & Multibody Mechanics Research Group at the Vrije Universiteit Brussel (*fig. 1*). It is being developed for Robot Assisted Therapy, which is a new type of therapy in which social robots are used to comfort and communicate with patients [6]. Probo's design and applications are targeted specifically towards children [7]. The communication is also targeted towards this audience, using emotion expression to accompany or stand in for verbal communication.

To allow Probo to express emotions, there are currently 20 degrees of freedom in the head and neck [8], which are the only components that are actuated. In this research, the design, construction and gesture recognition rates of an actuation system for the upper body of Probo will be described. In Part 1, the human arm and the state of the art of robotic arm systems for gesturing are examined. The design properties for a prototype of an arm for Probo are established based on this and the realization of the prototype is described in Part 2. Lastly, in Part 3 a survey is made to test the recognition rates using the prototype and the results and possible improvements are discussed.

Motivation

As robots assume a larger role in society [1], the interaction between humans and robots (aptly called human robot interaction) needs to evolve. Where in the past, the communication was mostly targeted towards the robots in 'their' language (i.e. issuing commands by mouse and keyboard which are then translated to software code); if robots are to be used in everyday situations by people who are not specialized in this field of research, the communication needs to be targeted towards the person in a human language [9]. An important aspect of this communication is verbal, however, research indicated that up to 60% of all human communication is non-verbal [10]. This percentage however was only valid in specific circumstances and has been called into question since [11]. Nevertheless, it stands to reason that if social robots need to interact and cooperate with humans, both the recognition and interpretation and the execution of non-verbal communication need to be implemented.

Fig. 1 Complete exterior of Probo [1]
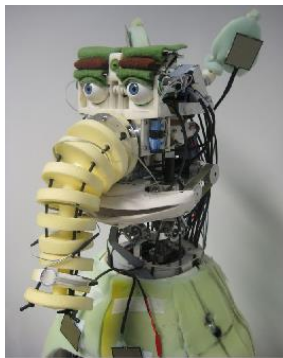
Fig. 2 Prototype of the actuation of the head of Probo [8]

This non-verbal communication is currently implemented in the design of Probo as the actuation of the head (including a trunk) and neck, allowing Probo to express emotional facial movements such as frowning, smiling or looking sad [8] (*fig. 2*).

The objective is to expand the actuation of Probo to the upper body, since movements of the arms and torso should not only make it easier to recognize what Probo feels or wants when observed from a distance when the face is hard to see; but there is also a heavy influence the actual recognition rates of emotions [12]. A test of the recognition rates of 7 emotions (*Anger*, *Happiness*, *Surprise*, *Disgust*, *Sadness*, *Fear* and *Perplexity*) was performed using KOBIAN, a social robot developed at the Waseda University in Tokyo, Japan. This experiment concluded that when performing an emotion with only the face, the emotion was correctly recognized 44.6% of the time. However, when accompanied with gestures performed by KOBIAN's body, the average recognition rate increased to 70%. It was also noted that not only the static posture of the gesture is important, but also the trajectory that the limbs follow to achieve this posture: there was an increase in recognition rates when using videos of the gestures instead of still pictures.

The selection of the gestures that Probo needs to be able to perform, is described in the preliminary work *Kinematics and Dynamics of the arm system of the social Robot Probo* [13]. Here, it was described how the gestures were recorded using motion capturing, then modified to fit Probo's skeleton (which has different proportions than a human skeleton) and finally the position trajectories were generated for simulating the gestures with 1 rotational joint in the hips and two 4 degrees of freedom arms (3 degrees of freedom in the shoulder and 1 in the elbow). The arms were simulated with 4 degrees of freedom to correspond to the data coming from the motion capture process, however, it will first be investigated how many degrees of freedom are deemed necessary to perform the gestures with a real mechanical version of the arm system.

Part I: Arm systems in social robots

Probo is by far not the first social robot that will portray gestures with an arm system. In Part 1, first the human arm itself is analyzed and the ways the arm can be modeled are described. An overview is given of the different mechanisms that social robots have used in the past to implement a shoulder joint, elbow, wrist and actuated hand. A number of compliance mechanisms that have been implemented are described, in addition to mechanisms that minimize the torque that the actuators need to be able to provide, such as gravity compensation.

1.1 Modeling a human arm

The human arm, which consists of the shoulder complex, the elbow, the wrist and the hand, is a very complicated system that needs to be simplified in order to be modeled and translated into a number of joints and links; with the objective of being implemented into a robotic arm, capable of performing gestures similar to a human arm.

1.1.1 The human shoulder and elbow

First, the basic movements that a shoulder can perform are described [14]. There are 3 rotations around absolute axes and a rotation around one local axis, which is the axial direction of the upper arm and is a combination of the 3 absolute axes (*fig. 3*). The neutral position from which the maximal rotational angles are calculated, is when the arm is stretched out, vertically next to the upper body.

The movements of the arm around the shoulder are divided in 4 types: abduction (moving the arm away from the body), adduction (moving the arm towards the body), anteflexion (moving the arm forwards) and retroflexion (moving the arm backwards).

The first set of rotations of the shoulder are the retroflexion (up to 50°) and anteflexion (up to 180°) in the sagittal plane (rotation around the transversal axis in *fig. 3*). This is pictured in *fig. 4*.
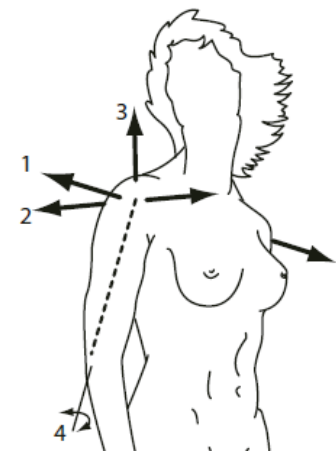
Fig. 3 **Rotational axes of the human shoulder: axis no.1 is the transversal axis, axis no.2 is the sagittal axis, axis no.3 is the vertical axis and axis no. 4 is the longitudinal axis [14]**
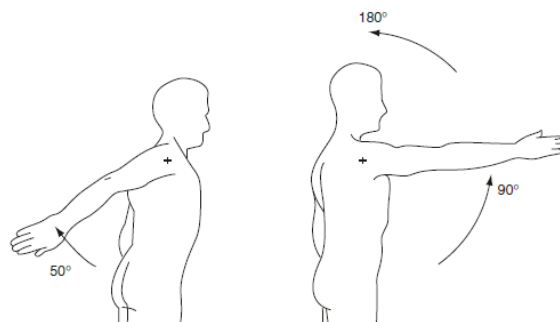
Fig. 4 **Retroflexion and anteflexion in the sagittal plane of the shoulder complex [14]**

The second set of rotations are the adduction around the sagittal axis in *fig. 3*, which is divided in retroflexion (only a few degrees) and anteflexion (up to 30°), and the abduction around the same axis, which is possible up to 180° (pictured in *fig. 5*). In this last case, the entire shoulder complex and even the spine are involved in performing the movement.

13
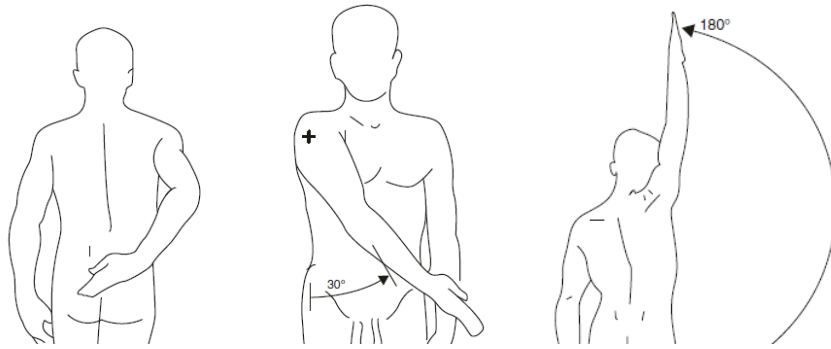
Fig. 5 Retroflexion & adduction, anteflexion & adduction and abduction in the vertical plane [14]

The third rotation is around the longitudinal axis in *fig. 3* (an exorotation outwards up to 80° and an endorotation inwards up to 95°), pictured in *fig. 6*.

Fig. 6 Rotation around the longitudinal axis of the shoulder complex [14]

The fourth set of rotations are the anteflexion and adduction around the vertical axis in *fig. 3* (up to 140°) and retroflexion and abduction (up to 30°) around this axis (*fig. 7*).

Fig. 7 Anteflextion and adduction and retroflexion and abduction in the horizontal plane of the shoulder complex [14]

It is clear that during these rotations, the center of rotation is not always the same, since the shoulder girdle itself moves. Additionally, the spine also bends to allow for some movements of the arm. In conclusion, the movement of the shoulder complex is due to the intricate collaboration of different bones, ligaments and muscles, considered impossible to classify into a number of degrees of freedom, but is more commonly described in a degree of motion or a workspace that can be reached.

Anatomically, the elbow constitutes 1 joint, however there are a number of possible rotations [14]. The pronation (up to 85°) and supination (up to 90°) of the elbow (pictured in *fig. 8*) are the axial rotation of the forearm, which is a rotation that is in robotics often attributed to the wrist, in order to reduce the mass that actuator needs to rotate.
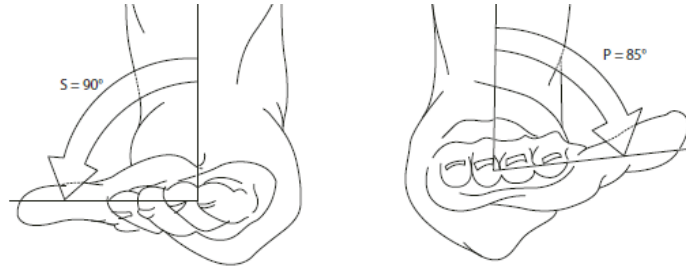
Fig. 8 Supination and pronation of the elbow [14]

The other rotations are the flexion and extension of the elbow, however due to the flexibility of the ligaments, the forearm can slightly rotate (a few degrees) around the longitudinal axis of the upper arm after the elbow joint (*fig. 9*).
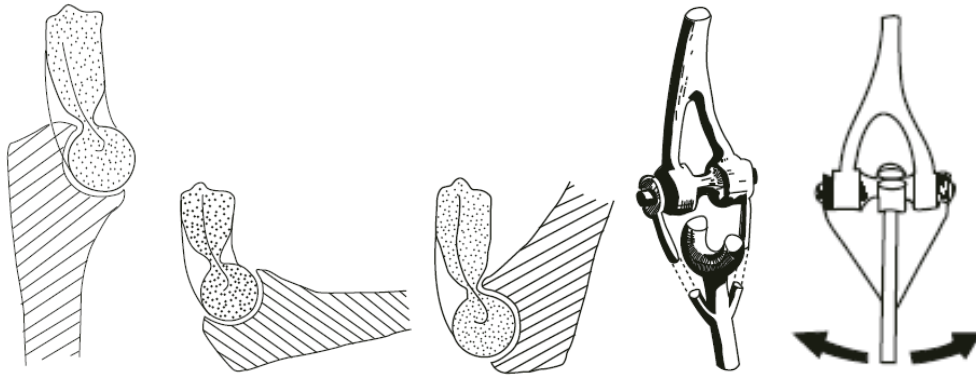
Fig. 9 Flexion and extension of the elbow, mechanical model and flexibility of the ligaments [14]

1.1.2 Kinematic models of the human shoulder and elbow

One possible kinematic model for simulating the human shoulder complex and the elbow is analyzed [15]. The anatomical structure is not simulated, rather the trajectory of the approximate center of rotation of the wrist (point *W* on the left side of *fig. 10*) is plotted.
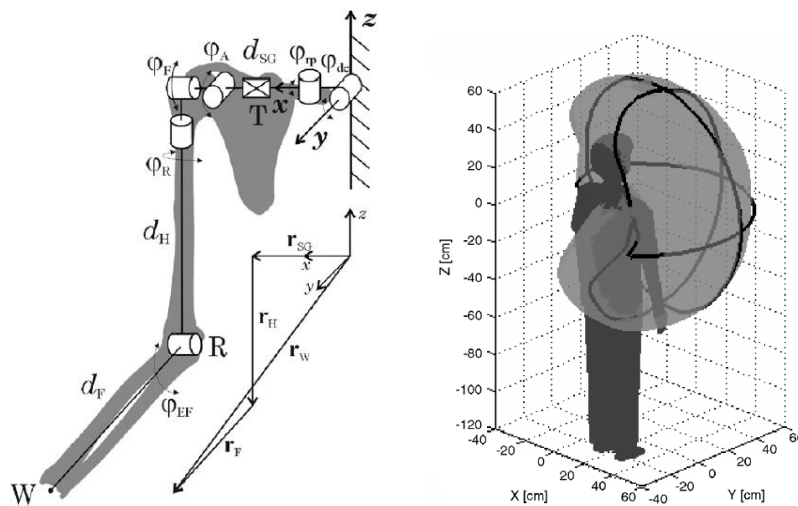
Fig. 10 Kinematic model and reachable workspace of a human arm [15]

In this model, the base of the shoulder consists of 3 joints: a rotation φ_{de} which accounts for the depression and elevation of the shoulder complex, φ_{rp} which accounts for the retraction and

protraction and a translational joint d_{sg}. The shoulder itself is modeled with 3 Euler angles: φ_A, φ_F and φ_R. The elbow is modeled as 1 joint, because the orientation of point W is not taken into account.

The arm-reachable workspace (the maximal volume that is covered by moving the arm) of the model was compared to that of a healthy human with identical dimensions of the right arm and it was concluded that there is a general agreement between the two (right side of *fig. 10*).

Due to the high mobility of the shoulder complex, there are other kinematic models which have been developed, varying in number of degrees of freedom (ranging from 6 in the aforementioned research to 12 or even higher [16]) or in the order of the rotations [17].

What is also important to consider, is the trajectory generation for different gestures when simplifying the kinematics of the human arm into a lower number of degrees of freedom. One of the easiest ways to generate human-like gestures is by motion capturing a human actor and then extracting the information on the rotations of the joints. In the preliminary work [13], it is described how the gestures that Probo will perform, were generated using motion capture. It is argued that attention needs to be given to the trajectory generation, because a difference in '*actual kinematics and joint structures […] between human and robot bodies […] could in some cases result in visibly different motion*' [18]. For this reason, the gestures that have been recorded by way of motion capture and are applied to the shoulder and elbow joints, should be subjected to a visual inspection after they are performed by Probo and modified if necessary.

1.1.3 The human wrist and hand

Regarding the wrist, there are 2 sets of rotations: flexion (up to 85°) or extension (up to 85°) and adduction (up to 45°) or abduction (up to 15°) (*fig. 11*) [14].
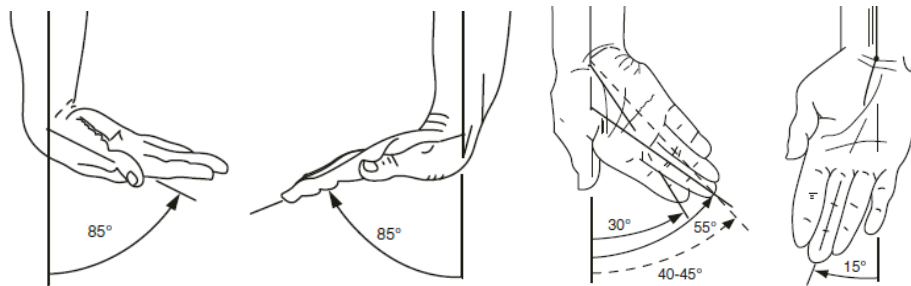
Fig. 11 Flexion, extension, adduction and abduction of the wrist [14]

The human hand is described as having 4 degrees of freedom in each finger (3 for extension and flexion and 1 for adduction and abduction), while the thumb has 5 degrees of freedom [19]. The interaction between these degrees of freedom to achieve different grips and gestures is very complex and will not be expanded on.

In conclusion, in this Chapter 1.1 the human arm is examined. The movements of the arm are an intricate combination of the degrees of freedom in the spine, shoulder girdle, shoulder, elbow, wrist and hand. When modeling the human arm, it is possible to approximate the workspace of the arm with a reduced number of degrees of freedom, however there is no clear consensus on how many degrees of freedom are actually needed. In the following Chapter 1.2, the number of degrees of freedom commonly encountered in robotic arms of social robots are examined.

1.2 State of the art of robotic arm systems

There are currently a large number of social robots with actuated arms available on the market or in development. However, a considerable number of these arm systems are geared towards manipulation of objects, instead of being developed solely to portray human gestures. Of course, there is an overlap between the components and abilities of the aforementioned two types of arm systems: for example both use a number of actuators to achieve (usually) 3 degrees of freedom in the shoulder, both can have integrated elements of compliance to allow for safe human robot interaction, etc. Robots with arm systems that can manipulate objects can almost always perform gestures, since the task of object manipulation is much more complex. However, an arm system targeted towards object manipulation may lack some degrees of freedom that an arm system for gesturing can possess: for example, the base of the shoulders may be actuated to allow the robot to shrug or move the complete shoulder complex in another fashion; this is not a necessary feature for an arm system geared solely towards handling objects.

Some key differences between arm systems for gesturing and for object manipulation are listed. For manipulation of objects, a larger amount of degrees of freedom in the arm itself is needed: the end effector (usually shaped as a hand) needs to be in a very specific position or orientation to grab and release an object. A more robust construction and powerful actuators are needed to carry an object in addition to the weight of the arms, instead of only carrying the weight of the arm itself; and moving the arms is often quite slow because a large accuracy is needed [20]. For example, the robot ASIMO needs about a minute to open a bottle and pour the contents into a glass [21]. All these factors contribute to a much higher development cost and ultimately, a much higher purchasing price. Another aspect is that the trajectory, the end position and orientation and the movement speed are often not human-like, for example lacking fluidity in the movement (which is claimed to play a large role in making the movements seem natural to human observers [22]).

1.2.1 Comparing arm systems of current social robots

In order to establish the design requirements for the arm system for Probo, a number of current social robots that have similar abilities are compared in *Table 1*. This table shows a list of social robots with their abilities from document [1], updated with a number of more recent social robots.

The data that is collected on the social robots is the following. First the name of the robot is given. The number of degrees of freedom in one arm is split up as accurately as possible over the different relevant components. Next, it is indicated if the arm system is suited for or has been used for gesturing and/or object manipulation. Lastly, it is indicated if the arm system incorporates any form of compliance, be it in the form of active compliance (through software control), SEA (series elastic actuation), variable stiffness, or using another method (see Chapter 1.2.5).

Table 1 Comparison of state of the art arm systems for social robots and the human arm

Name	Relevant DOFs	Gestures	Object manipulation	Compliance	Reference
Human arm	Shoulder: Range of motion Elbow: 2 Forearm: 1 Wrist: 2 Hand: 21	Yes	Yes	Yes: Tendons & ligaments	[14]

1.2 STATE OF THE ART OF ROBOTIC ARM SYSTEMS

Social robots with arm systems capable of object manipulation					
Name	Relevant DOFs	Gestures	Object manipulation	Compliance	Reference
Justin	Shoulder: 3 Elbow: 1 Wrist: 3 Hand: 12	Yes	Yes	Yes: Active	[23]
Leonardo	Shoulder: 3 Elbow: 1 Wrist: 2 Hand: 3	Yes	Yes	Yes: Voice coil	[24]
Nexi	Shoulder: 3 Elbow: 1 Wrist: 3 Hand: 2	Yes	Yes	Partial (unknown method)	[25]
iCub	Arm: 7 Hand: 9	Yes	Yes	No	[26]
WE-4RII	Shoulder: 3 (+2) Elbow: 1 Wrist: 3 Hand: 6	Yes	Yes	No	[27]
NAO	Shoulder: 3 Elbow: 1 Wrist: 1 Gripper: 1	Yes	Yes	No	[28]
Infanoid	Shoulder: 3 Elbow: 1 Forearm: 1 Wrist: 1	Yes	Yes	No	[29]
ARMAR II	Shoulder: 3 Elbow: 1 Wrist: 3 Hand: 8	Yes	Yes	No	[30]
PR1 / PR2	Shoulder: 3 Elbow: 1 Wrist: 3 Hand: 1	Yes	Yes	Yes: Parallel elastic	[31], [32]
Baxter	Shoulder: 3 Elbow: 1 Wrist: 3	Yes	Yes	Yes: SEA (and gravity compensation)	[33]
KOBIAN	Shoulder: 3 Elbow: 1 Wrist: 3 Hand: 4	Yes	Yes	No	[12]
Asimo (2011)	Shoulder: 3 Elbow: 1 Wrist: 3 Hand: 13	Yes	Yes	No	[34], [35]
ECCE	Right shoulder: 3 Elbow: 1 Wrist: 2 Hand: 1	Yes	Yes	Yes: SEA	[36]

Social robots with arm systems incapable of object manipulation					
Name	Relevant DOFs	Gestures	Object manipulation	Compliance	Reference
WE-4R	Base shoulder: 2 Shoulder: 3 Elbow: 1 Wrist:3	Yes	No	No	[27]
Repliee Q2	Base shoulder: 2 Shoulder: 3 Elbow: 1 Wrist: 3	Yes	No	Yes: Pneumatic (variable)	[18]
QRIO	Shoulder: 3 Elbow: 1 Forearm: 1	Yes	No	No	[37]
Robovie-IV	Shoulder: 3 Elbow: 1	Yes	No	No	[38]
Robota	Shoulder: 3 Elbow: 1 Forearm: 1 Gripper: 1	Yes	No	No	[39]
Kaspar II	Shoulder: 3 Elbow: 1 Forearm: 1	Yes	No	No	[40]

The main design characteristic of the arm systems designed for object manipulation for social robots is that there are 6 or 7 degrees of freedom in the arm and that attached to the wrist, is a multi-degree of freedom end effector, mostly taking the shape of a human hand.

1.2.2 The shoulder joint

The shoulder joint is usually implemented as a spherical joint, meaning that there are 3 degrees of freedom in this joint. Research is being performed on developing fully integrated spherical joints to accurately simulate the ball-and-socket connection between the human scapula and the humerus [41]. However because of the cost, difficulty of actuation and compliance and a limited range of motion, only a very limited number of social robots have implemented these designs. An example is the ECCEROBOT (which stands for *Embodied Cognition in a Compliantly Engineered Robot*), a robot currently under development and funded by the EU [36]. More conventionally, designers have always opted for 3 separate actuators to achieve 3 degrees of freedom. The degrees of freedom in the shoulder can be XZX as in the typical configuration of a spherical wrist (this is the case in most arm systems, for example in iCub [26] (pictured in *fig. 13*). Another possible configuration consists of (from the upper body towards the elbow) 2 rotation joints and one axial rotation joint (for example in PR-1 and PR-2 [31]) (*fig. 12*).
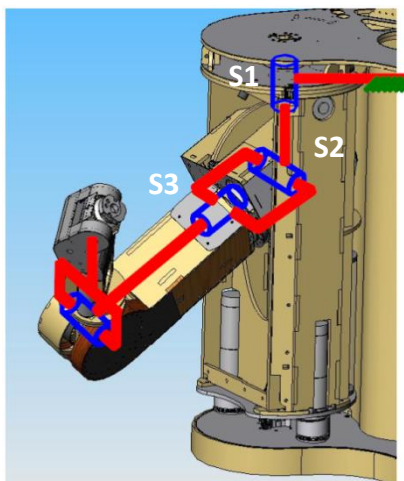
Fig. 12 Configuration of the shoulder joint in PR-1 [31]

The names that will be given to the actuators in the shoulder joint are as following, from the upper body towards the elbow: Shoulder1 (S1), Shoulder2 (S2) and Shoulder3 (S3). The choice to design the shoulder with S1 as an axial joint (as in *fig. 13*) instead of a 'rotational' joint as in *fig. 12*, offers the ability to make the design more compact, because S1 can be integrated into the upper

Fig. 13 Configuration of the shoulder joint in iCub [26]

body, often taking the place where the clavicle would be positioned in the human body. In the other case (*fig. 12*), S1 takes the place of S2 in the XZX configuration of *fig. 13*, meaning that the joints have to be positioned to the outside of the upper body. The downside of the XZX configuration is that S1 needs to compensate for a gravitational load when the arm is rotated to the front or back, whereas in the other case, S1 never has to account for gravitational load on the arm, meaning that a smaller, less powerful actuator can be used. However, with the availability of very small actuators with integrated gearboxes that are able to deliver high torques, many robot builders decide that compactness is the preferred target.

In some social robots, the base of the shoulder is actuated, meaning that the spherical joint in the shoulder is translated or rotated. An example is WE-4R (*Waseda Eye No. 4 Refined*, which is an extension of WE-4, which is an actuated robotic head), a robot which consists only of an upper body that is approximately human-sized, built at the Waseda University in Tokyo, Japan [42]. In this robot, there are in total 9 degrees of freedom in the arm system, consisting of 2 actuators at the base of the shoulder to move it up and down and to the front and back, 3 actuators in the shoulder, 1 in the elbow and 3 in the wrist (pictured in *fig. 14*). The hand is a non-actuated hand-shaped block. Additionally, there are 24 degrees of freedom in the head to portray the facial gestures.
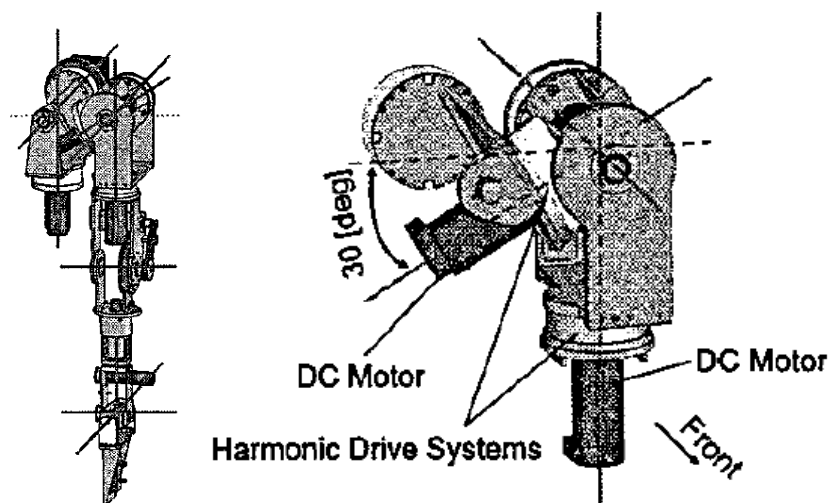
Fig. 14 Actuation of the base of the shoulder in WE-4R [42]

There is no substantiated reason given for the inclusion of the 2 degrees of freedom in the base of the shoulder, other than '*We considered that these motions played a very important role in the emotional expressions*'. The recognition rates of 6 basic emotions (*Happiness*, *Surprise*, *Anger*, *Disgust*, *Sadness* and *Fear*) were examined: a comparison was made of the recognition rates of only the head of WE-4R, the complete upper body, and the face of a human actor. The group of test subjects was composed of 22 people (20 males, 2 females, average age 23). The results are plotted in *fig. 15*.
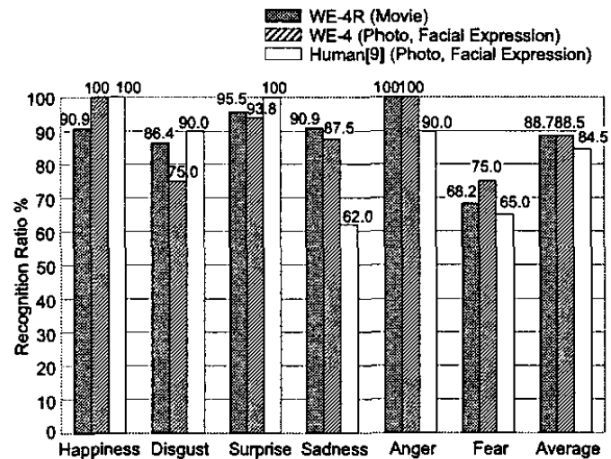
Fig. 15 Recognition rates of gestures performed by WE-4R, only the head of WE-4R and a human face [42]

It was concluded that the arm system contributes to the recognition rates but that the gestures themselves could be improved. However, there was no test performed in which the 2 degrees of freedom in the base of the shoulder were deactivated, so no conclusion on the usefulness or necessity of these degrees of freedom was drawn.

1.2.3 Elbow and wrist joints

In every single social robot with an actuated elbow in the arm, be it designed either for object manipulation or for social interaction, it consists of one joint. This is adequate in simulating a human elbow (see Chapter 1.1.2). Anatomically, the rotation of the forearm is also attributed to the elbow. In robotics however, this actuation is attributed to the wrist. This is done because with this placement of the actuator, it does not have to rotate the weight of the forearm (which can be the weight of the structure but also cables or electronics), meaning that a smaller actuator can be used, while the load on the actuator in the elbow is barely influenced.

In comparison to the arm systems geared towards object manipulation where 3 degrees of freedom are preferred in the wrist to allow for redundancy and collision avoidance, the arm systems of social robots designed mostly or purely for gesturing don't always employ all 3 degrees of freedom. A first example of a social robot with one degree of freedom in the wrist is the NAO robot, which is a small humanoid robot (with a height of only 58cm) made by the French company Aldebaran-Robotics [28]. It has 3 degrees
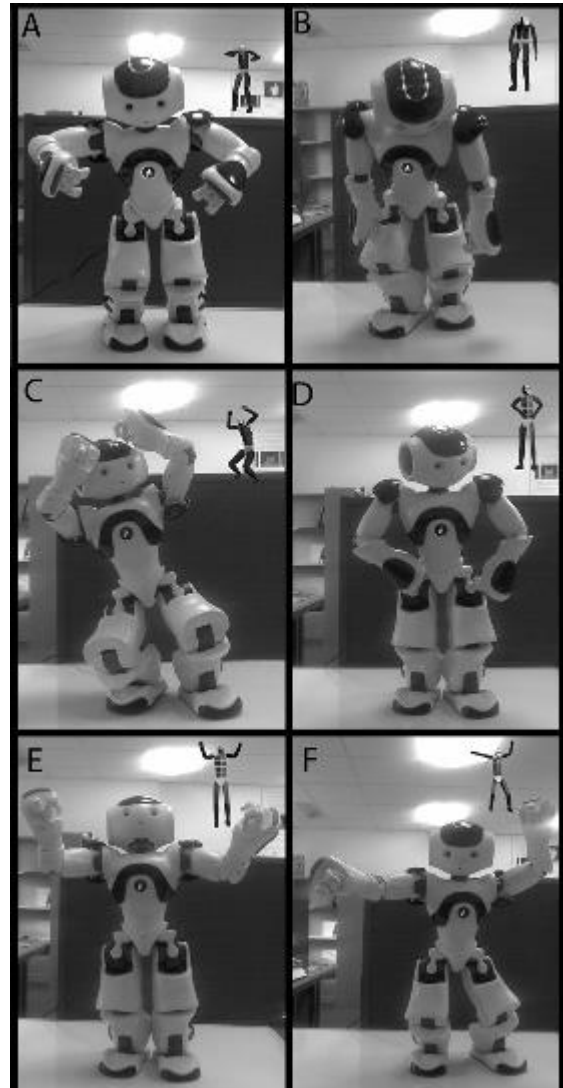
Fig. 16 Gestures for Anger, Sadness, Fear, Pride, Happiness and Excitement of the robot NAO [43]

of freedom in the shoulder (XZX), 1 joint in the elbow and one rotational degree of freedom in the forearm. However, the axial rotation of the forearm is used mostly for rotating the hands into the correct orientation, either for grabbing items or for using the back of the hand to push itself up after falling over. The recognition rates for six static poses (*Anger*, *Sadness*, *Fear*, *Pride*, *Happiness* and *Excitement*) are described [43]. These poses were recorded by means of motion capturing an actor and actuating the robot to approximate the stance. Images of the poses were shown to an audience of 26 adults, with an average age of 29. The head itself is not actuated and the legs and torso do not contribute greatly to the pose, meaning that the emotions are portrayed mostly by the arms and tilting of the head (*fig. 16*).

The six gestures were shown each three times to the participants of the study, once with the head looking straight ahead, once with the head tilted downwards and once with the head looking up. The results of the experiment are listed in *Table 2*.

Table 2 Recognition rates of the robot NAO [43]

Percentage of participants that identified correctly the emotion at least once during the three rounds (Chance level would be 42%) [43]					
Anger	Sadness	Fear	Pride	Happiness	Excitement
88%	85%	92%	88%	73%	73%

The results indicated that the recognition rates were significantly higher than chance level, meaning that adequate recognition rates can be achieved using arm systems with less than 7 degrees of freedom. The experiment continued to conclude that the tilting of the head has a large impact on the recognition rates (this research will be further examined in Chapter 3.2).

Another very similar robot is QRIO [37]. It has a height of 58 cm, weighs 7 kg and has 5 degrees of freedom in the arms: XZX in the shoulders, 1 degree of freedom in the elbow and a rotation of the forearm (*fig. 17*). The robot KASPAR II, of which the arm is pictured in *fig. 18* and which was built at the university of Hertfordshire, uses the same degrees of freedom in the arms [40].
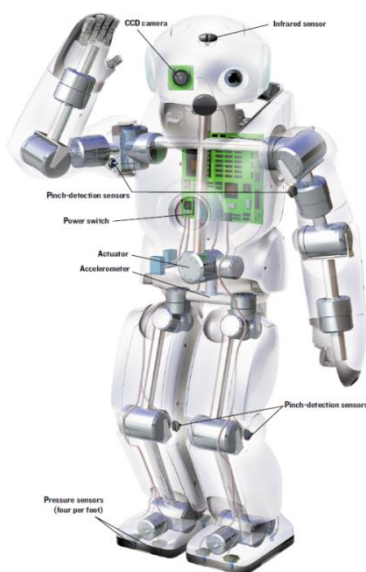
Fig. 17 Configuration of QRIO [37]
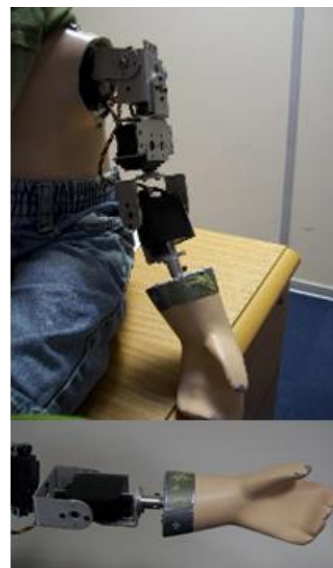
Fig. 18 Configuration of KASPAR II [40]

Some social robots use even fewer degrees of freedom in the arm system. Robovie [44] is a social robot which has been built at the Advanced Telecommunication Research Institute International in Japan (*fig. 19*).

Fig. 19 The robot Robovie [44]   **Fig. 20 A later iteration: Robovie-IV [38]**
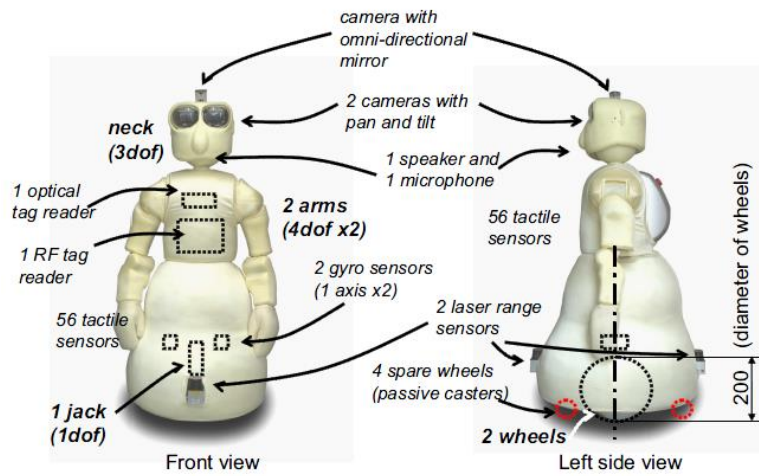
The arm system is composed of 4 degrees of freedom: 3 in the shoulder and 1 in the elbow. There is no actuation of the forearm, as the first generation of Robovie had spheres instead of hands. However the gestures that this robot is capable of performing, are geared towards practical tasks such as pointing to a certain object or direction or moving an object [45]. A later generation, Robovie-IV, has hands instead of spheres (as pictured in *fig. 20*), however there are no published recognition rates of relevant gestures [38].

1.2.4 The hand

The complexity of the end effector of the arm depends on the intended purpose of the robot and can make the arm very expensive. Some robots are equipped with a simple 1 degree of freedom gripper, such as the NAO robot [28]. Here, the objective for the hands is to handle small objects with simple shapes. When used for gesturing, the gripper (shaped as 2 fingers and a thumb) can be used to portray an open hand or a fist, but the fingers cannot move independently (*fig. 21*).
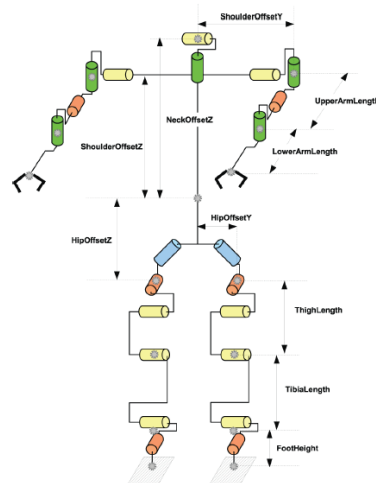
**Fig. 21 Configuration of the NAO robot with 1-DOF grippers as end effector
(Note: the axial rotation of the lower arm is absent on the diagram) [28]**

On the other side of the spectrum, the WE-4RII robot is equipped with the RCH-1 hand, which has 5 fingers, resulting in a total of 16 degrees of freedom and 6 degrees of motion [46] (*fig. 22*). It has 16 contact sensors and two 3D force sensors, which are necessary to grab an item and interact with it without letting it slip or crushing it with excessive gripping force.

Fig. 22 RCH-1 5-fingered hand module [46]

The usefulness of a complex actuated hand for gesturing can be examined [27]. In this study, the recognition rates of a number of gestures performed by the robots WE-4R and WE-4RII are compared. The only difference between both robots is that the RII (*Refined version 2*) is equipped with the RCH-1 hands, whereas WE-4R is equipped with non-actuated hand-shaped blocks (*fig. 23*).
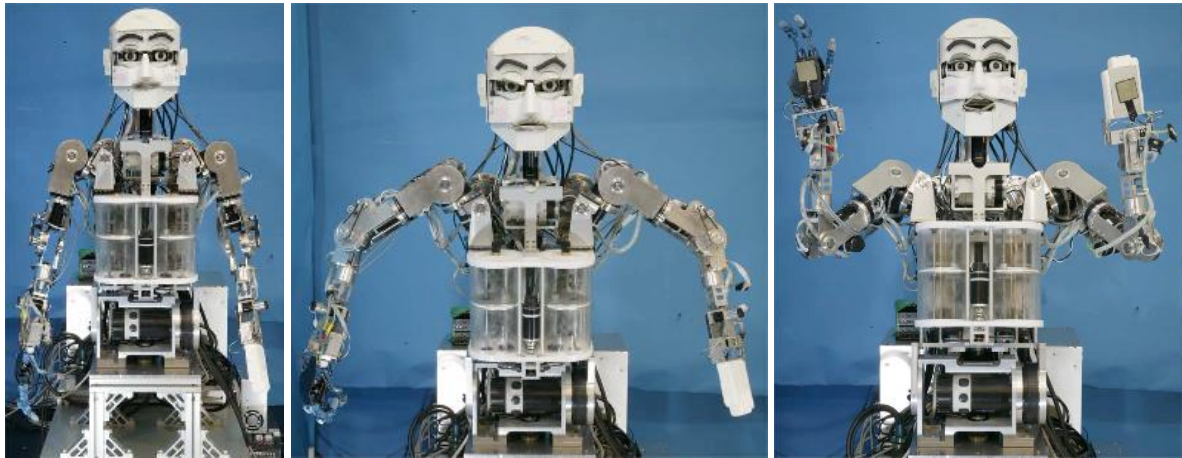
Fig. 23 WE-4R equipped with a 3-fingered RTR-3 hand as right hand and a non-actuated block as left hand performing the following emotions: *Neutral*, *Anger* and *Surprise* (Note: the recognition rate tests were performed with the RCH-1 hand with 5 fingers) [27]

The recognition rates of 6 emotions (*Happiness*, *Surprise*, *Anger*, *Disgust*, *Sadness*, and *Fear*) were tested with an audience of 18 male subjects with an average age of 21 years old. The members of the audience were shown videos of the complete robot (torso, arms and head) performing the emotive gestures. The results are depicted in *fig. 24*.
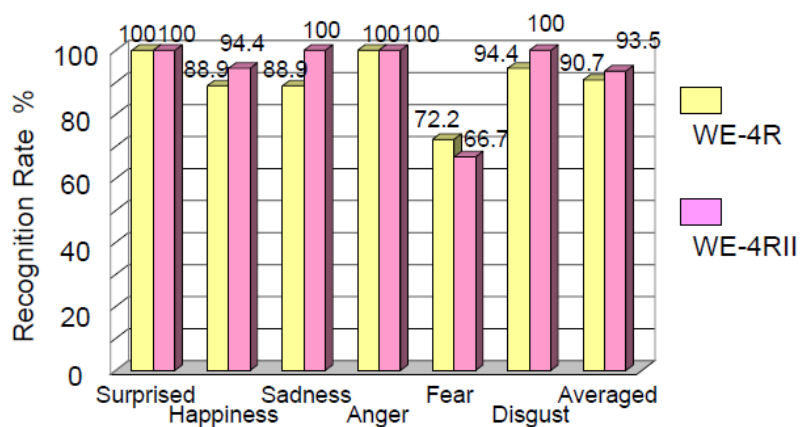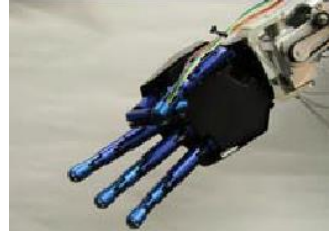
Fig. 24 Results of recognition rates tests of WE-4R and WE-4RII [27]

It was concluded from the study that on average, the recognition rates of the emotions were augmented slightly by equipping the robot with elaborate actuated hands. In particular, the largest visual differences were in the gestures *Sadness* (where the hands almost fully closed) and *Anger* (where the hands form fully closed fists).

The RCH-1 robotic hands themselves are capable of performing more complicated gestures [46]. The recognition rates of different gestures of the RCH-1 hands have been tested with an audience of 14 male students with an average age of 21 years old. The results indicating how many participants perceived which gestures can be found in *Table 3*.

Table 3 Gestures performed by the RCH-1 hand and perception by audience [46]

Hand gesture	Perceived gesture by audience	Hand gesture	Perceived gesture by audience
	OK: 14		Lovers: 7 Engagement: 7
	Number 1: 7 Pointing: 7		Rock (from Rock-paper-scissors): 13 Aggressiveness: 1
	Peace sign: 9 Number 2: 2 Victory: 2 To smoke: 1		Number 4: 10 To cut: 3 Karate: 1
	Ok: 9 Money: 3 Number 3: 2		

The conclusion is drawn that the members of the audience recognize that the hand is performing a gesture, however without any context or visual information from the rest of the body, it is hard to identify what gesture is actually being performed.

1.2.5 Compliant actuators and gravity compensation

When a robot has to perform its tasks in the vicinity or even during physical contact with a human, safety precautions need to be taken [47]. When a social robot moves its arms to perform a gesture, the actuators are delivering considerable amounts of torque, meaning that if the arms were to hit a person while moving, it is possible that the person will get injured. For this reason, compliant actuators can be implemented in the design of social robots. Compliant actuators differ from stiff actuators in that they offer a certain degree of flexibility. This means that a person is able to move the component(s) moved by the compliant actuator away from the planned trajectory by exerting a force on it, without the robot (in this case, the controller) treating it as a disturbance that needs to be uplifted as soon as possible.

There are different types of compliance that can be implemented [48]. First, the distinction is made between passive and active compliance. In passive compliance, there are non-stiff components such as springs or dampers integrated into the design, which simulate to a certain degree the elasticity that is inherent to tendons and ligaments in the human body [49]. In active compliance control, the compliance is done within the controller: the effect of elastic components such as compression or torsion springs are simulated in the controller [50]. For example, the robot Justin is equipped with this sort of compliance (*fig. 25*) [51] [20].
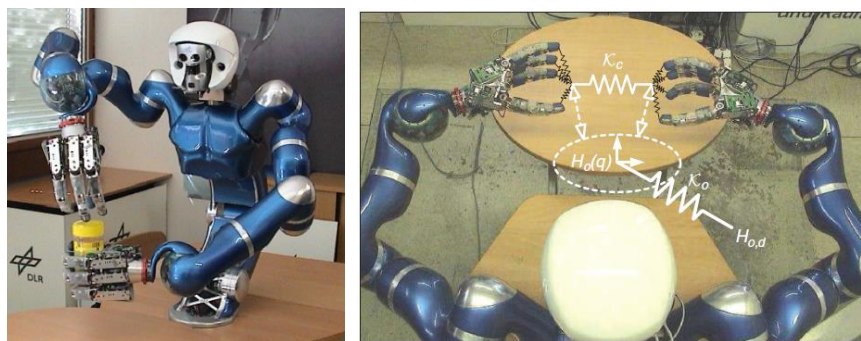
Fig. 25 Active compliant impedance behavior for the arms of Justin when manipulating an object [51]

The advantage of using active compliance is that the actuators in the design do not need to be physically elastic, meaning that the use of for example spring setups is not needed and that a compacter design can be achieved. However, there are also a number of important drawbacks. There is no storage of the energy that is coming from the gravitational pull or an external force, and the robot itself is not compliant when the controller is turned off. There is also only a limited absorption of shocks coming from external sources, because of the limited bandwidth of the controller and the time delay [48]. In comparison, passive compliant actuators offer compliance even when the controller is turned off (called *soft touch* [1]) and very short impulses (shocks) can be absorbed, but since elastic components are needed, the actuators setups are larger, heavier, in some cases louder and generally, make the design more complex and expensive. Another downside is that controlling the actuators becomes more difficult and can lead to lower operating speeds and worse accuracy in following the planned trajectory [1]. A dangerous situation can also emerge if the controller happens to fail or shut down, as the stored energy in the compliant parts can suddenly be released in an uncontrolled way.

There are two main categories of conventional passive compliant actuators: fixed compliance actuators and variable compliance actuators [48]. Fixed compliance actuators will always have the same degree of compliance, while variable compliance actuators can be either very stiff, very loose or somewhere in between, depending on the application. The downside of a variable compliance actuator is that another mechanism is always needed to alter the compliance (for example increasing the pretension on a spring with another actuator), which increases the size, complexity and cost.

There are many different ways of realizing passive compliance. One solution is to use springs in the design to transfer the power and to store the energy. An example of a social robot that uses this sort of compliance is TOFU, a small robot built at the MIT Media Lab [52]. A second possibility is to use pneumatic pistons. Social robots equipped with these kinds of actuators are Repliee Q2 and HI-1 [53]. Another possibility is to use voice coil actuators [54]. These are electromagnetic actuators where compliance is achieved though manipulation of the magnetic field generated by the coil. An example of a social robot using this type of actuators is Leonardo [3].

Passive compliant actuators can be classified into 4 categories of compliance design methods [48]. A first method is equilibrium-controlled stiffness. Here, an elastic component (such as a spring or a Bowden cable) is put in series with an actuator to transfer the power to the next link. These types of actuators are also called SEA, or Series Elastic Actuators [55]. It is possible to combine the use of cables and springs into one design, as illustrated in *fig. 26* [56].
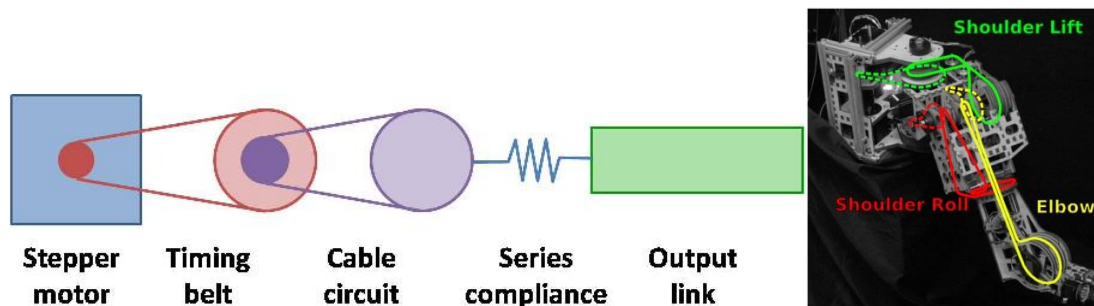
Fig. 26 Series elastic actuation of two rotations of the shoulder and one rotation in the elbow [56]

In this design, the timing belt is used to reduce the speed and increase the torque from the actuation of the stepper motor, while cables are used to transmit the power to the SEA elements in the joints themselves. An advantage of this design is that the motors can be integrated in the upper body of the robot, however the reduction and cable mechanisms occupy a large volume in the arm.

Another example of a robot using SEA compliance is the ECCEROBOT [36]. Here, a set of cables and springs are actuated through a number of pulleys (a schematic representation is added in *fig. 27*), to simulate human muscles and tendons [57].
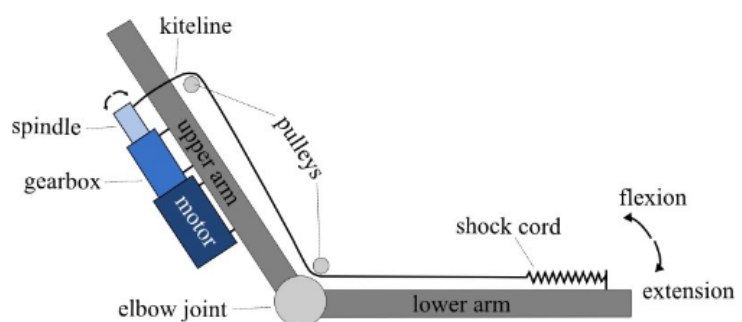
Fig. 27 Schematic illustration of the series elastic actuation of the ECCEROBOT [57]

The second method to achieve compliance is called antagonistic-controlled stiffness. This requires 2 non-linear elastic elements to work antagonistically to each other [58]. A third method is structure-controlled stiffness, which is altering the flexibility of the compliant part of the setup and the fourth method is mechanically-controlled stiffness, where the length of the compliant part is altered, thus changing its elastic properties.

Elastic elements can also be used to store energy, more specifically in order to reduce the power that actuators need to provide to perform a movement or to compensate for static forces such as gravity. Gravity compensation can be performed purely by the presence of elastic elements or can be done in accordance with the robot's controller [59]. In the first case, the properties of the elastic elements and the properties of the robot's design are carefully selected.

One such method of passive gravity compensation is done by carefully selecting the spring constant and attachment points of the spring [60].
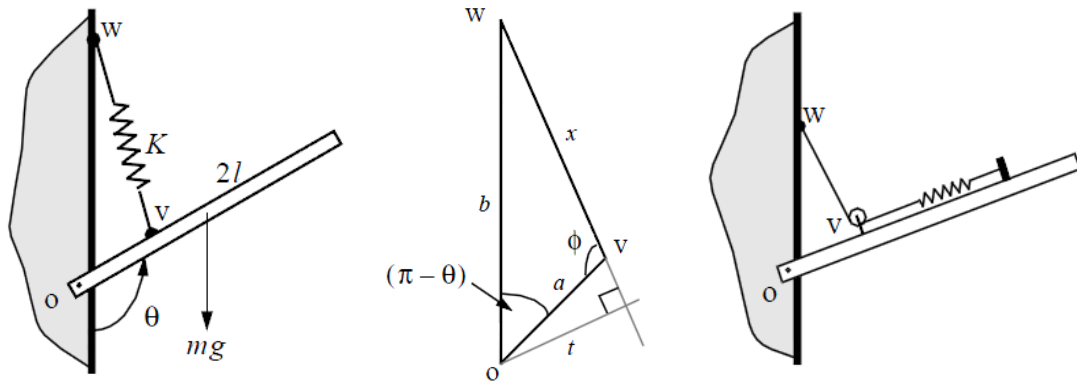
Fig. 28 (left) Passive gravity compensation of one link, (middle) geometric representation, (right) reducing unstretched spring length to zero [60]

In order to statically balance the 2D system given on the left and middle of *fig. 28* for all values of θ between 0° and 180°, the following equation has to be true:

$$K = \frac{mgl}{ab}$$

under the condition that the unstretched length of the spring is chosen 0. This can be done by moving the spring outside of the line WV (right side of *fig. 28*). The result of this configuration is that the actuator needed for the rotation θ is not loaded under the gravitational forces, but is only loaded with the inertia of the link when it is rotating, meaning that a smaller actuator can be used, depending on the contribution of the gravitational loads compared to the torques needed to overcome the inertias of the rest of the arm. This type of gravity compensation can easily be expanded to multiple links in the same plane (*fig. 29*).
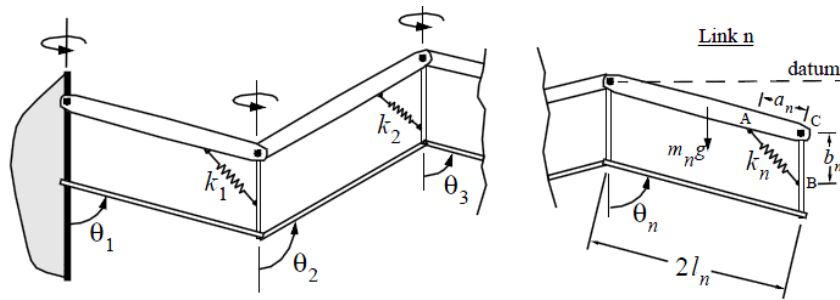
Fig. 29 Passive gravity compensation of multiple links [60]

By using this type of passive gravity compensation, the gravitational load on an arm with 4 degrees of freedom (three in the shoulder, one in the elbow) can be compensated for all positions with two springs [61] (*fig. 30*). However, a rigid link is needed to transfer the angle of the elbow joint back to the shoulder, meaning that this can interfere with the implementation of compliance in the upper arm.
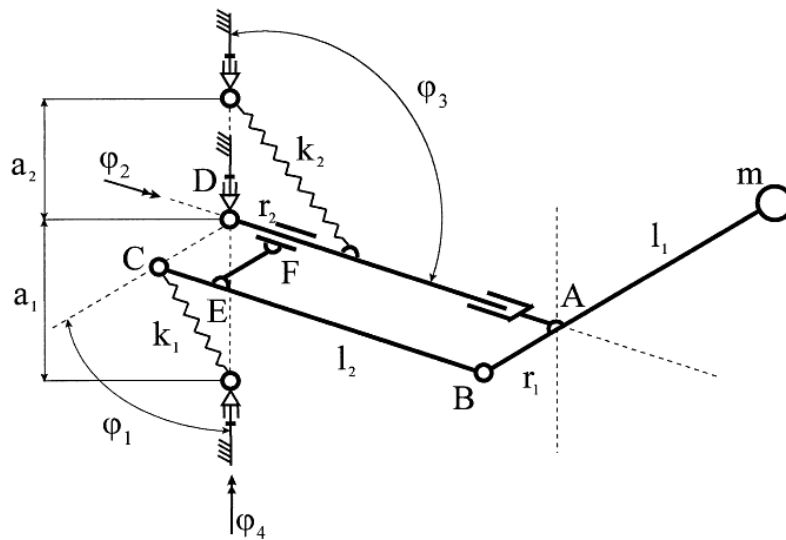
Fig. 30 Passive gravity compensation of a 4-degrees of freedom arm:
Shoulder rotation φ_2 is balanced by spring k_1, φ_3 is balanced by spring k_2, φ_4 does not need balancing, Elbow rotation φ_1 is balanced by spring k_1 [61]

An example of a robot equipped with this type of gravity compensation in one of the shoulder joints is PR-1 (*fig. 31*) [31]. However, it is worth noting that some of these types of compliance have been patented [62].

A social robot that is equipped with controller-based gravity control is Baxter [63], however this type of gravity compensation will not be elaborated on as it goes beyond the scope of this research.

Fig. 31 The arms of PR-1 incorporate passive gravity compensation [31]

1.3 Conclusions from the state of the art

In Chapter 1.2, the arm systems of a number of social robots are examined. Robotic arms can be developed for two different objectives: gesturing or object manipulation. There is a large overlap in properties between the two types, but there are also some key differences such as the fact that arm systems for manipulation can incorporate redundant degrees of freedom and can carry a higher load, while arm systems for gesturing can incorporate additional degrees of freedom to simulate a human arm. The most traditional number of degrees of freedom in an arm system which can perform both object manipulation and gesturing is seven: 3 degrees of freedom in the shoulder, 1 in the elbow and 3 in the wrist.

Regarding the shoulder, the ball and socket joint in the human arm is usually replaced by three separate degrees of freedom. The most used configuration of these degrees of freedom is XZX (pictured in *fig. 13*): this means that from the upper body to the elbow, there is first an axial rotation (S1), followed by a rotational joint (which constitutes the center of rotation of the replaced ball and socket joint, called S2), followed by the axial rotation of the upper arm (S3). Even though there are other configurations in which the actuators are less heavily loaded, this design is the most compact solution and is therefore the most popular. There is no real proof that adding extra degrees of freedom in the base of the shoulder increases recognition rates of various gestures.

One degree of freedom is considered to be sufficient to simulate the human elbow and all social robots in the current state of the art employ this. Regarding the wrist, one degree of freedom to axially rotate the lower arm is often incorporated in the design if the orientation of the end effector needs to change when performing the gestures. The end effector often takes the shape of a human hand and can range from a one degree of freedom 'gripper' to sixteen separate degrees of freedom. A study that compares the recognition rates of an actuated upper body, first with blocks as hands, then with fully actuated 5-fingered hands, notes a slight increase. However, without any context, it is indicated that gestures performed purely with a robotic hand are hard to recognize and label consistently.

If there is a chance of physical interaction between the robot and the human observer or if this is a specific objective of the robotic arms, a form of compliance can be integrated. Compliance can be active or passive: in active compliance, the controller simulates elastic elements, meaning that no physical springs are built into the design. In passive compliance, physical elastic elements are integrated and used to store energy, that is then released in a safe way. There are four categories of passive compliant actuators, of which the Series Elastic Actuators (in which the elastic element is put in series with the force or torque transducer) is the easiest and most popular variant. Related to this, elastic elements can be used to compensate the gravitational pull downwards of the arm. Use of a setup of springs with very carefully chosen parameters can statically balance the gravitational load for all positions of the arm and reduce the load torques on the servomotors.

At the beginning of Part 2, the relevant information from the study of the state of the art will be examined and used to determine the properties with which the first prototype of the arm system for Probo will be designed, regarding the number of degrees of freedom and their configuration, the compliance and the gravity compensation.

Part II: Designing an arm system for Probo

In Part 2 of this document, the complete design of an arm system for Probo will be examined. First, in Chapter 2.1, the general properties that the design of the arm will have are established, in particular the number of degrees of freedom and in which of those joints compliance will be implemented. In Chapter 2.2, the type of actuation and methods to transfer power from the actuator to the joint itself are examined. Next, a complete overview of the 3D design of the prototype of the arm is included with the argumentation for certain design choices. In Chapter 2.3, the 3D model of the arm is used in a dynamic simulation to establish the torques that the joints are loaded with and based on this, the specific actuators are chosen. In Chapter 2.4, the compliance in the chosen joints is explained and the chosen mechanisms are compared to each other. In Chapter 2.5 the method of gravity compensation is examined and in Chapter 2.6, the system for collision detection is described and implemented.

2.1 Design properties

Based on the state of the art of robotic arm systems (see Chapter 1.2), the number of degrees of freedom that this first prototype will have are chosen, followed by an argumentation of the choice of the compliant joints and the type of gravity compensation.

2.1.1 Selection of degrees of freedom

In Chapter 1.2, a number of arm systems for social robots are examined. The recognition rates of gestures of arm systems ranging from 5 degrees of freedom to 9 degrees of freedom are all at greater than chance levels. It is first decided that the degrees of freedom at the base of the shoulder will not be implemented, because of the high complexity, added cost and the uncertainty that adding these degrees of freedom improves recognition rates. There will be 3 degrees of freedom implemented in the shoulder (called S1, S2 and S3 in *fig. 13* in an XZX configuration as this improves compactness) and 1 degree of freedom in the elbow (called E). Regarding the wrist, a decision is made on the degrees of freedom in accordance with the gestures that are selected to be portrayed in the preliminary work [13]. The 6 basic emotions that are to be portrayed are illustrated in *Table 4*.

Table 4 Static poses of the gestures that Probo will portray, as simulated in 20-sim 4.1 with 4 DOF arms and 1 DOF hips [13]
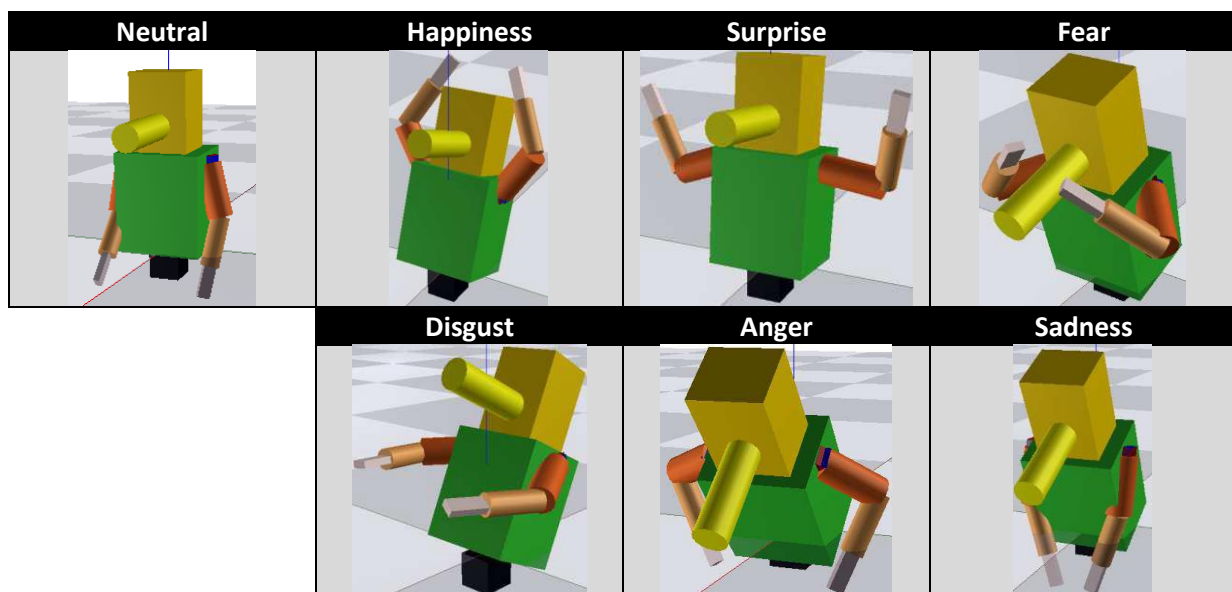
These gestures are portrayed with a fixed joint in the wrist, meaning that there are no degrees of freedom. The assessment is made at this point that the only gesture which is expected to benefit significantly (meaning closer to the way that the actor portrayed the gesture in the motion capturing) from movement in the wrist is *Disgust*: here, it would be beneficial to rotate the wrist in such a way that the palms of the hands are facing the viewer. However, since it is very probable that Probo will be placed higher than the children it is interacting with to reduce the risk that they would knock Probo over, the palms of the hands will be more or less facing the viewers since they are positioned lower. It is therefore decided that there will be no degrees of freedom in the wrist implemented in the first prototype.

Regarding the hands, it is concluded that the best use of a robotic hand for gesturing only, would be a 1 degree of freedom hand where the transition can be made from an open hand with outstretched fingers and thumb to a fully closed fist. In order to realize this motion, either a number of actuators or one actuator and a number of Bowden cables and springs can be used. However, either way adds complex components (which drives up the cost) and weight (meaning that a stronger construction and more powerful actuators are needed in the rest of the arm) to the arm system. For this reason, it is decided not to equip the arm system for Probo with actuated hands in this first design.
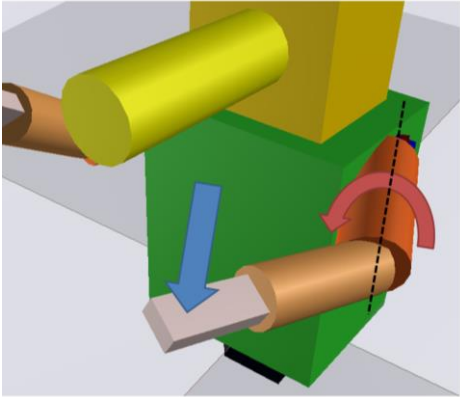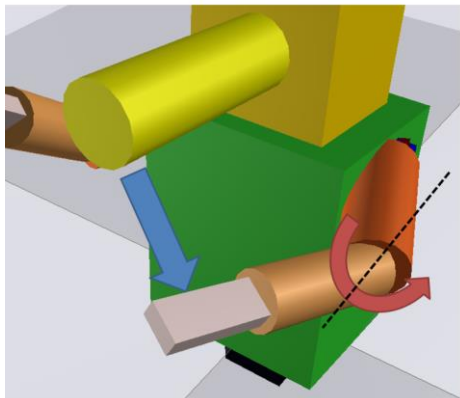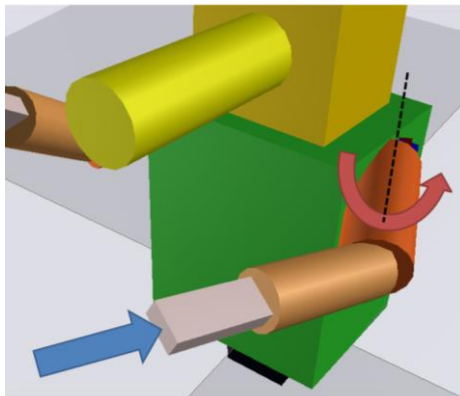
Regarding a rotation of the upper body, it is decided to implement 1 degree of freedom in the hips (as in the gestures in *Table 4*), in order to rotate the upper body to the front and back for the recognition rates tests. This way, the touchscreen that is positioned in the belly of Probo will not be damaged by torsion, while still allowing a close approximation of the way the gestures are portrayed by a person. The mechanism to rotate the upper body is examined in Chapter 3.1.

2.1.2 Choice of compliant degrees of freedom and gravity compensation

The choice to use electrical actuators is done in accordance with the current actuation in the head and neck of Probo: they are quieter and safer to use in a hospital or domestic environment than other types of actuators such as combustion engines of hydraulic actuators [1]. The type of compliance that will be used is passive compliance, with the advantage over active compliance of the soft touch property. SEA (Series elastic actuation) will be implemented to realize this compliance, as it is expected to be the cheapest solution and the easiest to implement.

The decision is made to not implement compliance in all actuated joints. The placement of the compliant elements is chosen in accordance with the direction of the external forces, as illustrated in *Table 5*. Here, it is assumed that the external force will be exerted on the hand, as this is the component that is moving at the highest velocity and may thus cause the largest injuries when it comes into contact with a person or object. The important factor in the design is that the elbow will always be bent, therefore the axial directions of the upper arm and lower arm will never be coincident.

Table 5 The 3 possible external force vectors and resulting moments

Direction of external force (Blue arrow)	External force direction and axial direction of upper arm are skew, external force direction is perpendicular on plane formed by axes of lower and upper arm
Resulting moment (Red arrow)	Rotation of the upper arm around axial direction (joint S3)
Direction of external force (Blue arrow)	**External force direction and axial direction of upper arm are intersecting, external force direction is situated in plane formed by axes of lower and upper arm**
Resulting moment (Red arrow)	Rotation around the elbow joint (joint E)
Direction of external force (Blue arrow)	**External force direction and axial direction of lower arm are coincident**
Resulting moment (Red arrow)	Combined rotation of the shoulder joints (joints S1 & S2)

All directions of the external forces on the hand will be a combination of the 3 situations given in *Table 5*. This means that in order to implement compliance for all possible external forces on the hand, compliant elements need to be integrated in all 4 joints. However, since none of the gestures that Probo will perform includes a motion in which the arm is thrust forward (resulting in an external force coincident with the axial direction of the lower arm), the compliance will be implemented only in the joints in the elbow and the rotation of the upper arm. The joints S1 and S2 will therefore not be designed to incorporate compliance.

Passive gravity compensation will be implemented in the shoulder to reduce the torques that the actuators need to deliver to keep the arms in a certain pose. However, this gravity compensation will be implemented as a single spring setup per arm in parallel with S2, in order to simplify the design and decrease the cost. This setup will not compensate the gravitational forces working on the arms for all rotations of the elbow: one gesture will be selected, for which the gravitational forces will be fully compensated. It makes sense to choose the *Neutral* pose, as this is the posture that Probo will assume most of the time.

In conclusion, in this Chapter 2.1 it is established that the prototype will implement four degrees of freedom in one arm: 3 degrees of freedom in the shoulder (XZX) and 1 degree of freedom in the elbow. Additionally, for the recognition rates tests, one degree of freedom will be implemented in the hips of the upper body in order to rotate to the front and to the back. Passive compliance will be implemented under the form of SEAs in the elbow joint and in the axial rotation of the upper arm. By implementing compliance in those two joints, all directions of external forces on the hand, except along the axis of the lower arm, will be taken into account and will be partly absorbed by the compliance. Additionally, a basic type of passive gravity compensation will be implemented in the second rotation of the shoulder (S2), to ensure that none of the actuators are loaded at the neutral pose.

2.2 Transmission of power and 3D model

In this chapter, the methods of power transmission from the actuators to the joints are discussed, followed by an overview of a 3D model of the arm that is built in Autodesk Inventor Professional 2013. The design of the arm is done in multiple iterations, since the torque that the actuators need to provide is dependent on the mass of the arm, in which the actuators themselves have a large share.

2.2.1 Power transmission and actuation

Before starting to design an arm, the method of transferring the torque from the actuators to the links is decided. The choice is made to transfer the torque both through a direct connection between the actuator and the structure for rotation S3 (which is the axial rotation), and through chain drives for the other rotations (S1, S2 and the elbow joint E). The actuators for the joints S2, S3 and the elbow will be placed in the arm itself, which means that their mass will need to be carried by the actuators closer to the upper body. This is done to simplify the construction and to avoid having to use cables or another mechanism in addition to the chain drives. The 'gears' around which a chain drive rotates are called sprockets and the sprocket on which an actuator provides a torque will be called the powered or actuated sprocket, while the sprocket that is rotated by the chain is called the driven sprocket.

Using a chain drive offers multiple advantages:

1. The actuator (with the powered sprocket) can be placed at a considerable distance from the driven sprocket, meaning that the actuators can be placed closer to the upper body to reduce the torque that the actuators S1 and S2 need to deliver, while still resulting in a compact construction. This, together with the fact that the load is distributed over multiple teeth, gives it a significant advantage over using gears.
2. A chain drive has a relatively high efficiency. The results of an investigative study on losses in a bike chain are examined [64]. A comparison is made to a bike chain instead of a chain drive in an industrial application because in the arm system, much like in a bike chain, the chain will be subjected to variations in torque and rotational speed, a possible deficiency or lack of lubrication and possible misalignment of the sprockets. First, the relevant properties of the highest loaded chain in the arm, which is in joint S1, will be established. An explanation of the chosen properties is given in Chapters 2.2.2 and 2.3.

$$\text{Maximal power in chain S1: } 0.675Nm * \frac{180°}{sec} = 0.675Nm * 30rpm = 2.12W$$

$$\text{Teeth ratio of sprockets} = \frac{22}{17}$$

The experimental results of the study take into account the friction between the links, the sprocket misalignment and the friction between the links and sprocket teeth. The first conclusion from the study is that going from smaller sprockets to larger ones (in the study teeth ratio 52:11 to 52:21) increases the efficiency (from 92.5% to 95.2%). A second conclusion is that as the rotational speed increases, the efficiency decreases (in this case an increase of speed from 30rpm to 90rpm lowers the efficiency from 96.7% to 85.45%). The third conclusion is that as the power increases, the efficiency goes up (an increase from 50W to 200W increases the efficiency from 81% to 95.8%). The last conclusion is that small sprocket misalignments and type of lubrication have a negligible impact on efficiency, however no conclusion is drawn on a total absence of lubrication. Extrapolating the results of this study to the chain drives used in the design of the arm is difficult because of the large difference in power transmission, absence of a device that keeps a certain tension on the loose side of the chain, absence of lubrication and difference of used materials (plastic chain links with MDF teeth instead of steel on steel), however it is expected that the efficiency of the used chain drives will be somewhere around the same order as in the study, i.e. around or higher than 90%. This will be examined at the end of Chapter 2.3.

3. A high load can be put on a chain, without the slip that would occur when using a regular belt. Compared to using a timing belt, there is less deformation and a longer lifetime. Another advantage is that the length of the chain can easily be altered by removing one or multiple links when the distance between the sprockets is chosen. There is no need for cutting a belt, which usually come in standardized lengths, which may lead to problems when the location of the modification is pulled onto the pulley during rotation.
4. Chains are easy and cheap to buy, plastic chains are very light, and there are numerous designs that produce very low noise [65] [66].

The chain that will be used is purchased from Servocity [67], which has a (supplier-given) breaking force of 245N and a measured weight of around 3g per 10cm of chain. The dimensions (in inches) are displayed in *fig. 32*.

The actuators themselves will be Savöx digital coreless servomotors [68]. These are available in the range of torques that were indicated in the preliminary work [13], they are widely available for purchase and are not overly expensive. One thing to take into consideration is that they are not able to rotate more than 160°, meaning that if a rotation of more than 160° is

Fig. 32 Dimensions of the chain links in imperial units [67]

needed, a decrease in delivered torque will occur due to a to be determined gearing ratio.

2.2.2 3D design of the different modules

The design of the arm is divided into multiple separate modules. The primary objective is to design different modules that can be replaced when any aspect of their function needs to be altered, without having any significant influence on the operation of the other modules. However, a significant increase in weight of one component can have an influence on the choice of the actuators in the other modules.

The secondary objective is to design the modules in such a way that they can easily be assembled, disassembled and connected to each other. This objective will be achieved by designing the connections between the different modules as bolt and nut connections, with the intention that the whole arm can be assembled and disassembled with only one screwdriver. A third objective is that it is preferable that all servomotors, cables and other internals are completely sealed away in the design or at least as much as possible.

An overview of the different modules, from the hand towards the upper body, will be given. The design itself is constructed from thin slices of MDF wood (with thicknesses 2, 2.5 or 3mm), which are cut from large MDF plates using the laser cutter at the Erasmushogeschool Brussel. They are glued together where necessary and coated with a layer of varnish, mostly to contain the unpleasant smell of burned wood that the slices emit after being cut with a laser. The remark is made that the 3D model is that of a left arm, while the finished physical prototype is that of a right arm. The reason for this is that the first physical prototype was a left arm, based on the 3D model. This prototype was analyzed for possible failures and improvements, which were then implemented in the 3D model. The choice was made to keep the first prototype as the left arm for the recognition rates tests (see Chapter 3.1), while the design with the improvements was built as a right arm, so that 2 physical arms were available for the recognition rates tests, a left arm and a right arm. A visual overview of the different modules is given in *Appendix A* and images of the physical prototype of the right arm and a guide to assembling the modules is added in *Appendix E.*

The first module is the lower arm (called **module H**). Since the choice was made to not include any degrees of freedom in this module (see Chapter 2.1.1), the hand is rigidly connected to the lower arm. The base of the lower arm is an axis with a driven sprocket, this axis will become the elbow joint. The rest of the module has an eccentricity to this axis, allowing the lower arm to rotate further before colliding with the upper arm. The accelerometer for the collision detection (see Chapter 2.7) is mounted on the small surface close to the axis (*fig. 33*).The length of the lower arm needs to be

chosen in proportion with the rest of the body, depending on the objective: these can be human proportions or exaggerated cartoonish, for example short, fat and tapered arms are often used to portray a *'cute'* character [69] [70]. In this prototype, it chosen in human proportion to the stuffed version of the head of Probo that will be used for the recognition rates tests (see Chapter 3.1). The actuated head of Probo may differ in size from the stuffed version, meaning that the length of the module (and the dimensions of the hand) will need to be modified.
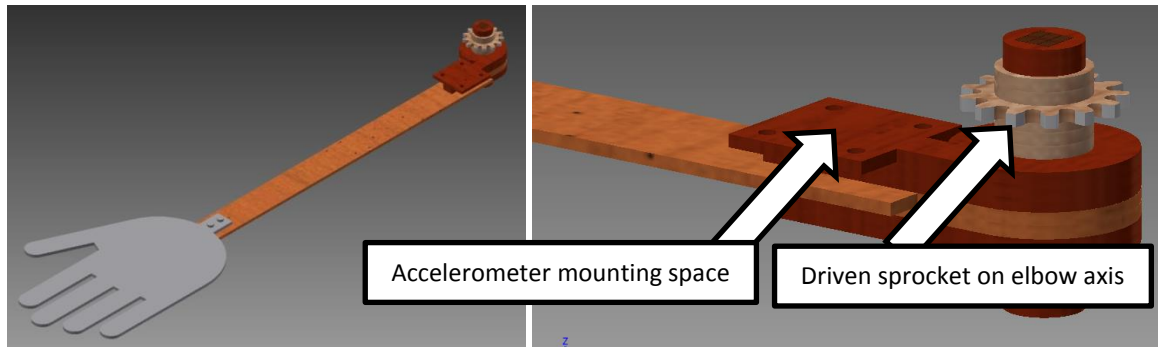
Fig. 33 Module H with the elbow axis and accelerometer mounting space

The following modules constitute the lower part of the upper arm (**modules A and B**). Module A (on the left of *fig. 34*) houses the servomotor that is used to rotate the driven sprocket on the elbow axis through a chain transmission (not pictured in the 3D model), while module B is used to close the arm up and protect the motor and transmission (right side of *fig. 34*). The outside cover of the modules was completely filled in the first prototype, however to reduce the weight, some MDF slices were removed, with minimal impact on the stiffness of the structure. The elbow axis rotates in two SKF 61802 bearings to reduce friction when turning. The elements that hold the bearings are not glued to the rest of module A, because they need to be disconnected from the rest of the design to mount the elbow axis. The chain transmission that connects the actuated sprocket on the servomotor and the driven sprocket on the axis, provides the force to keep the elements into place in module A. Two slices of MDF (light brown in the 3D model) are designed with a hole with a smaller diameter than the outside diameter of the bearings; these ensure that the bearings don't fall out of the design.
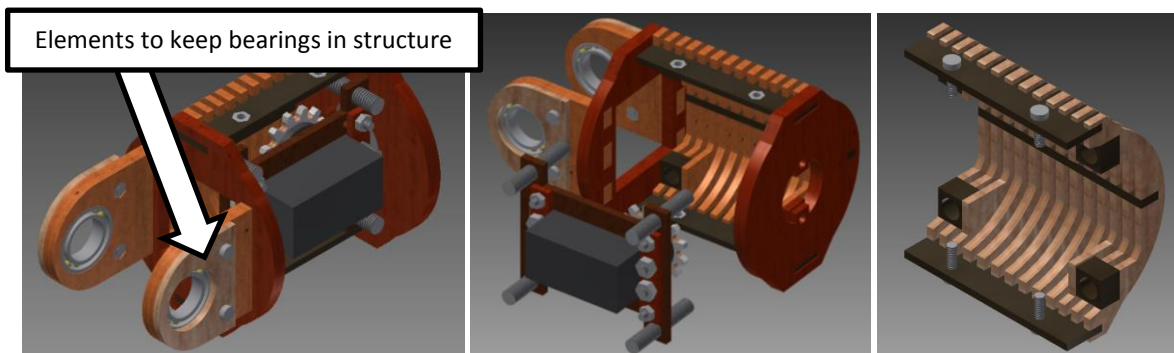
Fig. 34 Module A, the removable servo holder and module B

The servomotor is held into place in a holder, in which four M6 screws are bolted (middle of *fig. 34*). These bolts are slid into 8 straight holes that are aligned both in module A and B, holding the servo holder firmly into place when module A and B are connected. The purpose of these 4 screws is that by turning them, the location of the actuated sprocket along the elbow axis is modified and will ultimately be used to align (within a range of about 15mm) the actuated sprocket with the driven

sprocket, should the location of the driven sprocket be modified for whatever reason. The sprocket that is mounted on the servomotor is chosen small enough to fit inside the design, which results in a sprocket with outside diameter 29.6mm. At the end of the module, two M4 nuts are glued, these will form the connection with the upper part of the upper arm (module D). In between these nuts, there is a hole to allow the cables of the servomotor and the accelerometer to stay inside the design.

Module B, as previously stated, will be used to protect the internals of module A. It has the same outside shape as module A, and will be connected to module A with four M3 screws.

The actuated sprocket (called E_actuated) and the driven sprocket (called E_driven) are chosen to have the same dimensions, so a 1:1 transmission ratio will be used. This is the case because the servomotor can rotate up to 160° degrees, which is enough for the elbow joints, and because the weight of the lower arm is low enough so that there is no need to increase the torque (see Chapter 2.3). The largest possible sprockets that fit in the design will be used (because larger sprockets have a higher efficiency, see Chapter 2.2.1), which means that sprockets with 13 teeth will be used. The key properties of modules H, A and B are given in *Table 6*.

Table 6 Key characteristics of modules H, A and B

Key characteristics of modules H, A and B (error on the mass is ±2g)	
Weight of module H (with polyethylene tube cover, with accelerometer)	90g
Weight of module A (without servomotor, with bearings, with chain)	122g
Weight of module B	27g
Length of the hand	173mm
Length of the lower arm (without hand)	300mm
Length elbow axis	50mm
Outside diameter of modules A and B	70mm
Length of module A (connection with module D to elbow axis)	105.5mm
Distance between axes of actuated and driven elbow sprockets	82mm
Sprocket outside diameter of E_actuated and E_driven	29.6mm
Sprockets module	2.04mm
# teeth on sprockets	13
Type of bearings used	SKF 61802

Module C forms the connection between modules A and the servomotor that will form the third rotation of the shoulder, S3. This module will rotate inside a bearing that is part of module D, so that the axial force in the joint is not carried by this element, but by the bearing. This bearing is placed around the orange MDF slices in the 3D model on the left on *fig. 35*, which are surrounded on both sides by elements with a bigger outside diameter, so that the module is stuck around the bearing and cannot fall out of the design. The white element on top is a standard duty servo saver which constitutes the compliance in joint S3 (see Chapter 2.4.2). The servomotor will be connected to this element. This servo saver is nailed onto an MDF slice which has a very particular shape: this shape is needed so that it can be slid onto the module, between the two M4 screws used to connect the module to the backside of module A (on the right on *fig. 35*). This is needed because the servomotor for S3 (in module E) needs to be slid into the design from the side, due to space constraints. There is enough space left so that the cables coming from the lower modules can pass internally through the connection.

Bearing is mounted around these orange elements
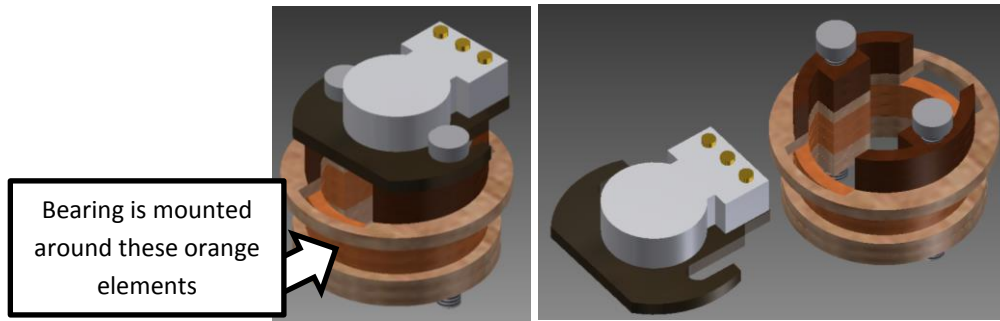
Fig. 35 Module C, with the removable servo saver and attachment

Module D, together with **module E**, makes up the upper part of the upper arm: it provides the connection between the bearing in which module C rotates and the shoulder axis which forms joint S2. The bearing is not glued into place, it is axially kept into place by module C, which in itself is axially kept into place by the servomotor in module E. The shoulder joint, which is made out of aluminum, has a hexagonal shape on 1 side, which slides into the top of module D. The circular slices through which the shoulder joint fits (which are colored red in the 3D model on the left side of *fig. 36*) are used to wind the cable that is used for the gravity compensation of the arm (see Chapter 2.5).

Winding the cable for gravity compensation
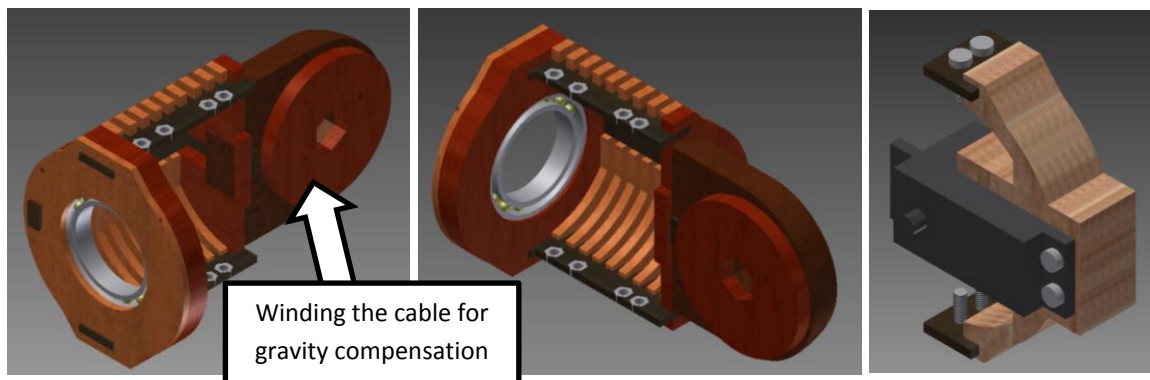
Fig. 36 Module D, back view of module D and module E

Module E (on the right on *fig. 36*) is used to hold the servomotor for joint S3 into place. It is connected to module D with four M3 screws that are bolted into the four M3 nuts that are the furthest away from the bearing. The other four M3 nuts that are glued in module D can be used to connect an extra, smaller module to enclose and protect module C inside module D. This module is not included in this prototype. The key characteristics of modules C, D and E are summed in *Table 7*.
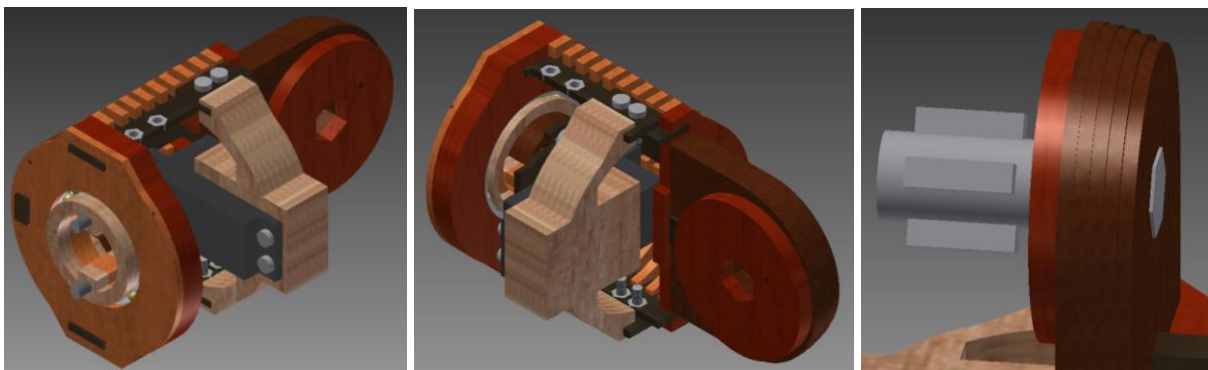
Fig. 37 Modules C and E mounted on D, back view, and the shoulder axis in module D

Table 7 Key characteristics of modules C, D and E

Key characteristics of modules C, D and E (error on the mass is ±2g)	
Weight of module C	16g
Weight of module D (with bearing)	106g
Weight of module E (without servomotor)	21g
Length of module D (connection with module A to shoulder axis)	96.5mm
Outside diameter of modules D	35mm
Inside diameter of module C (through which wires pass)	25mm
Hole through which wires exit can module C	15x10mm
Type of bearing used	SKF 61806

On the shoulder axis, there are 4 keys visible (on the right side of *fig. 37*), on which the driven sprocket to rotate the axis is mounted. This is part of **module F**, in which the servomotor for the actuation of joint S2 is mounted, but this whole module also needs to be able to rotate in a static housing to form joint S1. Module F is for this reason also referred to the shoulder insert since it rotates inside the shoulder housing. The shoulder axis and module D are mounted in module F in three bearings, which are held in place by bolting different elements together (pictured on the left side of *fig. 38*). The servomotor is bolted into place, so that the actuated sprocket (called S2_actuated) on the servomotor and the driven sprocket (called S2_driven) on the shoulder axis are aligned for the chain transmission (on the right side of *fig. 38*, the chain transmission is not pictured in the 3D model). Again, the servomotor will provide enough torque to the joint, so that a 1:1 chain transmission can be used (see Chapter 2.3). The sprockets are chosen with the largest dimensions that fit in the design, meaning that sprockets with 17 teeth will be used.
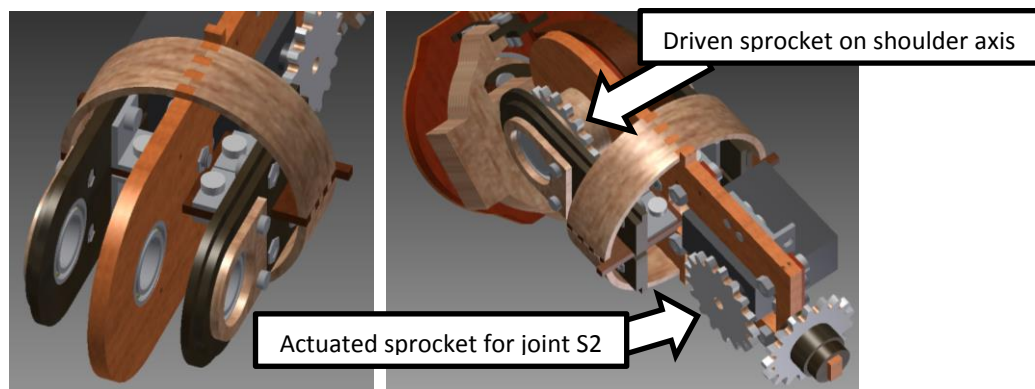
Fig. 38 Mounting location for the shoulder axis in module F, actuated and driven sprockets for joint S2

A corner joint is mounted above the servomotor, this piece will be used to attach the cable for the gravity compensation (pictured on the left side of *fig. 39*, the mechanism is examined in Chapter 2.5). Four round elements (light brown on the 3D models on the right of *fig. 39*) are created by glueing MDF slices together. These elements are not glued to the rest of the design, but are put into the grooves on the orange and dark brown elements, which keep them axially into place, and then tape is put around these elements to keep then radially together. The reason for this is that these elements need to be removable to access the bolts and nuts underneath them.

Grooves to keep round elements into place

Round elements around which needle bearing is mounted

Corner joint for connecting gravity compensation

Pin to keep needle bearing on module F
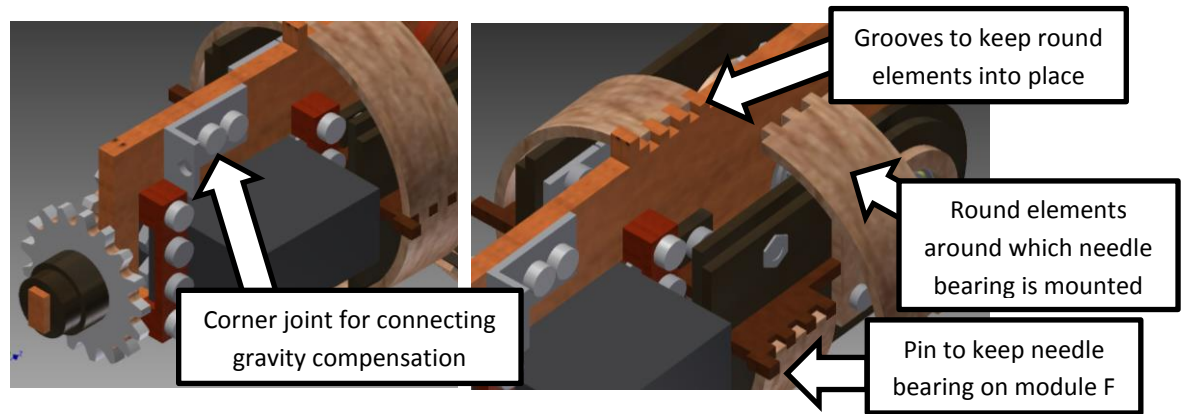
Fig. 39 Gravity compensation mounting location and mounting the round elements on module F

There are two elements on module F to allow it to rotate in the static housing to form joint S1. First, around the aforementioned four round elements, a needle bearing is placed. Use of a needle bearing is preferred over the use of a ball bearing, since the outer diameter of a ball bearing, with this dimension of inner diameter (which is 72mm), would be very big. To limit the friction when using the needle bearing, the outer diameter of the inner module F and the inner diameter of the outer module G need to be very precise, otherwise the needles can get pushed inwards or outwards in their frame, increasing the friction or even outright blocking the needles from rotating. There are 4 small 'pins' (90° apart) on module F that prevents the module from being pulled out of the needle bearing, should there be a force exerted that pulls the arm away from the upper body (pictured on the right side on *fig. 39*).

The second element is that the end of module F, which is a small cylinder, will be placed inside a bearing which is mounted in the static housing, forming the second part of the hinge joint (the needle bearing being the first) for joint S1. Next to this cylinder is the sprocket that will be driven with a chain transmission to rotate module F in the housing (pictured in *fig. 40*).

Needle bearing

Driven sprocket for joint S1

Small cylinder to insert in bearing in module G
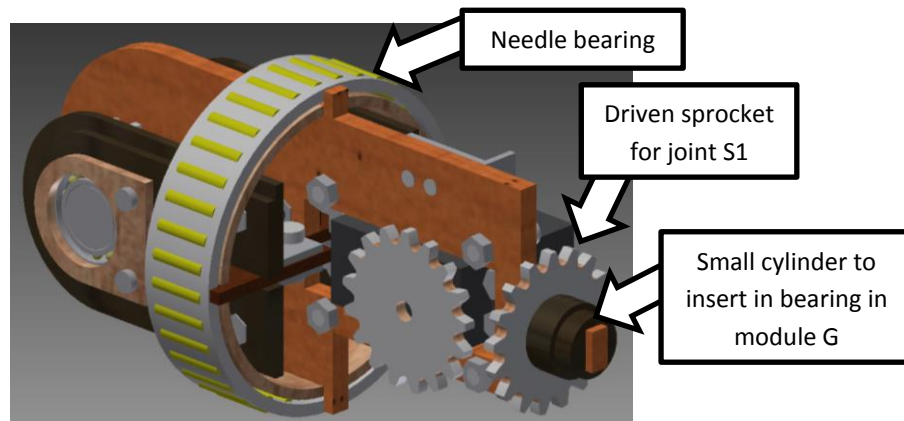
Fig. 40 Needle bearing and driven sprocket for joint S1

The housing is called **module G** and consists of 2 parts: an upper and a lower part (*fig. 41*). The upper part is connected to the lower part with six M3 bolts. The outside edges of both parts have a slightly smaller inner diameter than the outer diameter of the needle bearing, ensuring that the needle bearing cannot be pulled out of the housing. Together with the 4 'pin' on module F, it is ensured that the arm will not be pulled out of module G. At the other end of the lower part, the bearing in which the end of module F is placed, is mounted and prevented from being pulled out.

2.2 TRANSMISSION OF POWER AND 3D MODEL
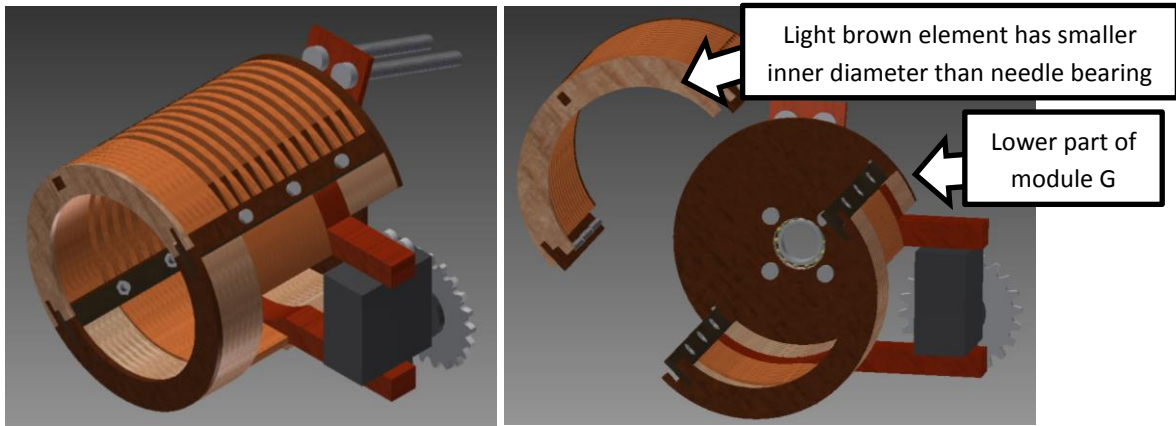
Fig. 41 Module G, which can be opened to mount module F

The servomotor is placed outwards to the backside of the upper body, on the lower part of module G. On this servomotor, a sprocket with 22 teeth will be placed, which will drive the driven sprocket with 17 teeth. This ratio is chosen because joint S1 will need to rotate 180° for the gesture *Happiness* (see Chapter 2.1.1) and the servomotor that will be used can only rotate 160°. With a transmission ratio of $\frac{22}{17}$, the joint will be able to rotate slightly more than the necessary 180°, while still maintaining around 80% of its torque. This is one of the reasons that a servomotor with a higher possible torque than established in the dynamic simulations (see Chapter 2.3) will be chosen.

There are three M4 holes foreseen in the plate at the inside of the shoulder. Here, a protective cover for the servomotor and chain transmission for rotation S1 can be mounted. This is not the case in this prototype. The reasons both for the placement of the servomotor and for the fact that the upper two M6 connection screws are at an angle of 20° to the two horizontal screws, are the shape and space availability of the current frame in the upper body of Probo.
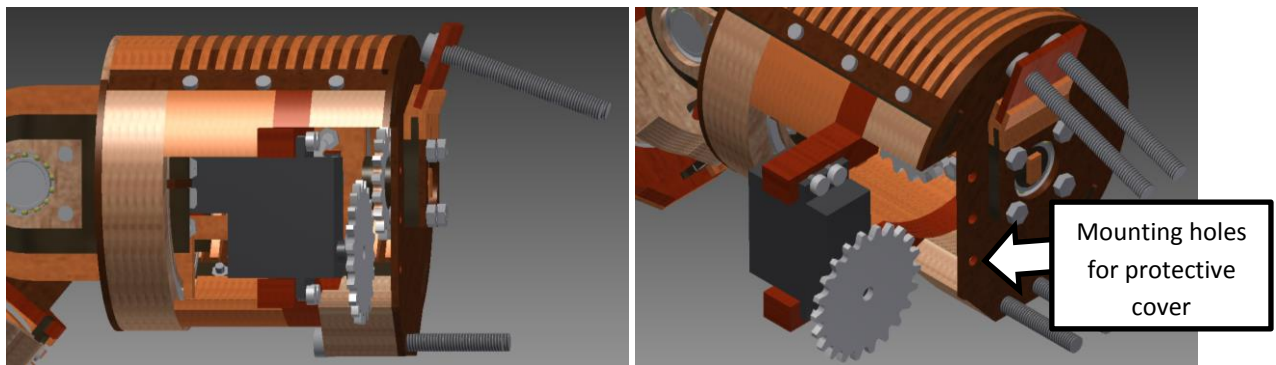
Fig. 42 Aligning the sprockets for joint S1 and location of the mounting holes for the protective cover

The current frame in the upper body of Probo consists of aluminum T-profiles (*fig. 43* and *fig. 44*). Towards the neck, they are bent inwards with an angle of 20°. The T-profiles are 25mm wide and 2mm thick. The servomotor is put at the back of module G, because there is no space underneath the shoulder or on the other side of the T-profile due to the presence of various microcontrollers used to control the head. This first prototype will be adapted to fit the current frame, rather than the other way around (pictured in *fig. 45*). The decision is made to put the servomotor for joint S1 on Probo's backside instead of on the front, both shielding the mechanism from users and hiding a noticeable visual bulge on the shoulder. The key characteristic of modules F and G are given in *Table 8*.

Fig. 43 Location of the frame in Probo's upper body [1]
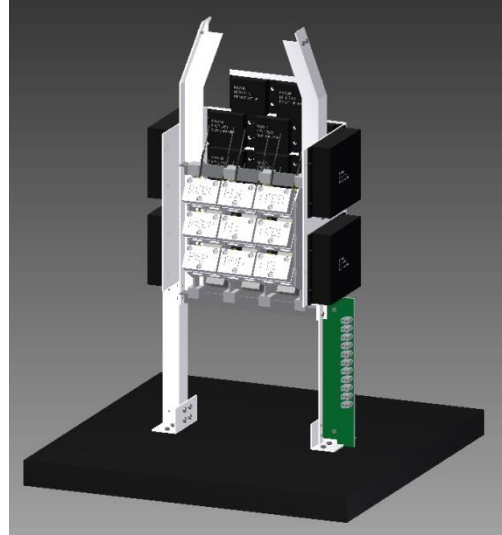
Fig. 44 Detailed view of the frame with the microcontrollers
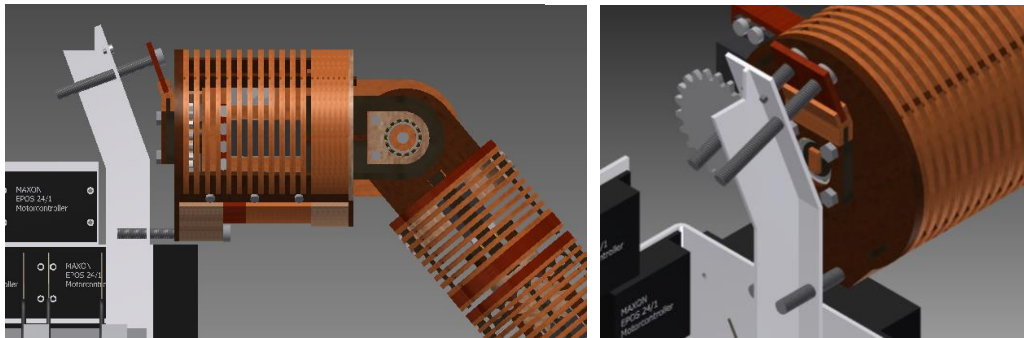
Fig. 45 Mounting location of the arm on the frame (front view), four holes are needed in the frame to mount the arm

Table 8 Key characteristics of modules F and G

Key characteristics of modules F and G (error on the mass is ±2g)	
Weight of module F (without servomotor, without (needle) bearings)	196g
Weight of module G (with servomotor/chain, without bearing)	329g
Length of module G (from frame to shoulder axis)	128.5mm
Outside diameter of module G	100mm
Length of shoulder axis	50mm
Distance between axes of actuated and driven S2 sprockets	88mm
Distance between axes of actuated and driven S1 sprockets	70mm
Hole through which wires can exit module G	37x54mm
Sprocket outside diameter for S1_driven, S2_actuated, S2_driven	37.8mm
Sprocket module for S1_driven, S2_actuated, S2_driven	2.04mm
# teeth on sprockets S1_driven, S2_actuated, S2_driven	17
Sprocket outside diameter for S1_actuated	48.0mm
Sprocket module for S1_actuated	2.04mm
# teeth on sprockets S1_actuated	22
Type of ball bearings used	SKF 61802
Type of needle bearing used	SKF K72x80x20

2.2 TRANSMISSION OF POWER AND 3D MODEL

In conclusion, in this Chapter 2.2 the methods of transferring the power from the actuators to the joints are established and based on this, the 3D design of the structure is made. The decision is made to use a chain transmission in joint S1, S2 and E, where the actuated axis of the servomotor is parallel to the axis of the driven joint. Using a chain drive offers many advantages: they are strong, flexible and light, it is easy to alter the length, the actuator can be placed far away from the joint and they offer a high efficiency. The other joint S3, where the actuated axis of the servomotor is aligned with the axis of the joint, will be realized with a direct connection (in which a compliant element is integrated, see Chapter 2.4.2). This is done because in Chapter 2.3, it is established that there is no need for an increase in torque through the transmission when rotating joint S3 with the chosen servomotor. It is established that servomotors will be used in the design, however it needs to be taken into account that they can only rotate up to 160°, so a transmission ratio in the chain drives can be needed to achieve rotations of 180° or more.

The design of the arm is done modular: different modules are built, which are changeable without having a significant impact on the rest of the design. For example, the modules for joint S3, which are modules C, D and E, only need to have a correctly sized hexagonal hole at one end for connection to the shoulder axis, and correctly spaced holes for two M4 bolts at the other end to connect to the lower modules. The rest of the design of this part is variable.

From the hand to the upper body, the first module is module H. This is the lower arm which does not include any degrees of freedom (as established in Chapter 2.1.1). At the end of this module is the elbow axis, which will rotate in two bearings. The length of this module is variable and needs to be adapted to be in proportion to the rest of the arm and the upper body. The following modules are modules A and B, which constitute the lower part of the upper arm. Module A houses the bearings in which the elbow axis is placed and houses the servomotor and chain drive to actuate joint E. The position of the servomotor is adjustable so that the sprockets can be aligned. Module B is used to close up this part and cover the servomotor and chain drive. Module A is connected through module C to the upper part of the upper arm, which consists of modules D and E. Module C rotates axially in a bearing in module D to constitute joint S3, while guiding the wires and cables coming from the lower modules and keeping them inside of the arm. Module E contains the servomotor for joint S3 and is slid sideways into module D.

Module D is connected to the shoulder axis, which rotates in module F. This is the inside of the shoulder and contains the servomotor and chain drive to rotate the shoulder axis, forming joint S2. This whole module F rotates in module G, constituting joint S1. Module G is closed so that module F is protected, and four M6 screws are used to connect the whole arm to the frame inside the upper body. The design of the first prototype of the arm is done in such a way that all modules can be disassembled individually, with the objective that only one screwdriver is needed to assemble the whole arm. The assembly guide is added in *Appendix E: Assembling the robotic arm for the social robot Probo in 23 steps*.

2.3 Dynamic simulations and choice of actuators

After the arm has been designed in Autodesk Inventor Professional 2013, it is imported into MSC Adams 2012 Student Edition to perform the dynamics simulations to establish the torques needed to actuate the arm. The model is imported in 19 separate pieces (as some components made out of the same material are taken together) with the properties given in *Table 9*. The masses are either given by the manufacturer or measured on a scale with an error of ±2g.

Table 9 Properties of the parts as entered in MSC Adams 2012

	Adams Part	Includes	Material	Mass
1	**H**	Module H	Mostly MDF	86g
2	**A**	Module A without bearings or servomotor	Mostly MDF	107g
3	**ServoE**	Servomotor that is mounted in module A	Various	45g
4	**SKF61802_1**	Bearing that is mounted in module A	Steel	7.5g
5	**SKF61802_2**	Bearing that is mounted in module A	Steel	7.5g
6	**B**	Module B	Mostly MDF	27g
7	**C**	Module C	Mostly MDF	16g
8	**DE**	Modules D & E, without servomotor or bearing	Mostly MDF	102g
9	**SKF61806**	Bearing that is mounted in module D	Steel	27g
10	**ServoS3**	Servomotor that is mounted in module E	Various	45g
11	**ShoulderAxis**	Shoulder axis that connects modules D and F	Aluminum	25g
12	**SKF61802_3**	Bearing that is mounted in module F	Steel	7.5g
13	**SKF61802_4**	Bearing that is mounted in module F	Steel	7.5g
14	**SKF61802_5**	Bearing that is mounted in module F	Steel	7.5g
15	**F**	Module F	Mostly MDF	196g
16	**ServoS2**	Servomotor that is mounted in module F	Various	80g
17	**SKFneedle**	Needle bearing that is mounted in module F	Steel	98g
18	**G**	Module G with servomotor for joint S1	MDF, various	329g
19	**SKF61802_6**	Bearing that is mounted in module G	Steel	7.5g
		Total lower arm and upper arm mass		470g
		Total rotating shoulder insert mass		421g
		TOTAL MOVING MASS		**891g**
		Total shoulder housing mass (static)		336g
		TOTAL ARM MASS		**1227g**

These masses are entered in the properties of the bodies in Adams. After the prototype was build, the complete mass (including all bolts, cables, connections, etc., but excluding the microcontroller) of the modules was measured: the physical total moving mass is **927g**, while the total arm mass is **1278g** (both ±2g), meaning that the masses used in the simulations are a very close approximation.

Module G is connected to the ground, ensuring that it is the only non-moving component. The parts that cannot move relatively to each other are connected with Fixed Joints, while the 4 degrees of freedom are created with Revolute Joints. Gravity (the big red arrow on *fig. 46*) is pointing downwards and the initial position of the arm is at a 20° angle with the vertical, which will be the neutral position for the physical prototype.

The decision is made to not examine all the different gestures that are to be portrayed but rather the poses that cause the different actuators to be maximally loaded. This ensures that the servomotors will be able to perform any gesture that is modified to increase the recognition rates or new gestures that are to be added in the future. A safety margin for the torques will also need to be taken into account due to a number of unknown factors: the friction in the joints, the losses in the chain transmissions, the added loading from covering the arm with Probo's fur and other external forces that can be exerted on the arm.

Fig. 46 3D model of the arm imported in MSC Adams 2012

Joint S1 is considered to be maximally loaded when the arm is fully stretched out to the back or to the front. However, due to the construction, the upper arm cannot go closer than around 17° to the upper body. The angles for S2 and S3 are therefore unchanged and only the elbow rotates to bring the mass of the lower arm as far away from joint S1 as possible. Joint S2 is maximally loaded when the arm is in a T-pose. Joint S3 is maximally loaded when the lower arm is rotated 90° to the upper arm and is lying in the horizontal plane. Finally, joint E is maximally loaded when the lower arm is in the horizontal plane, with the palm of the hand lying in the vertical plane. The rotations of the joints are performed with the 'STEP' function in a span of 1 second in MSC Adams 2012, while the rotations for the gestures of the physical prototype will be done with cubic splines. The 'STEP' function in Adams approximates a step in angular acceleration (*fig. 48*). This function is used because the cubic spline option in Adams simply seems to be faulty. All types of friction are kept at the default values (see *fig. 47*). The results of the simulations are given in *Table 10*.

Fig. 47 Friction values in MSC Adams 2012
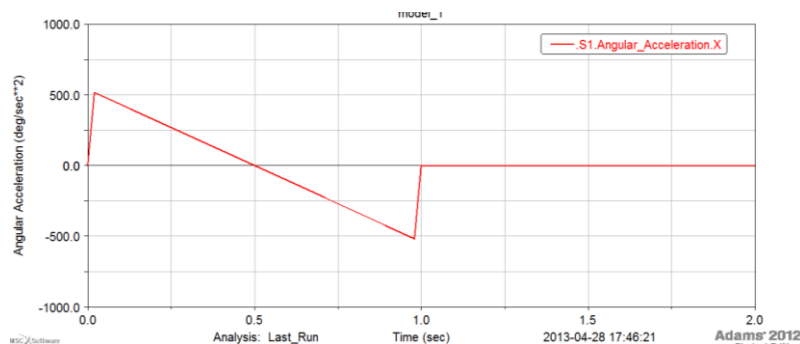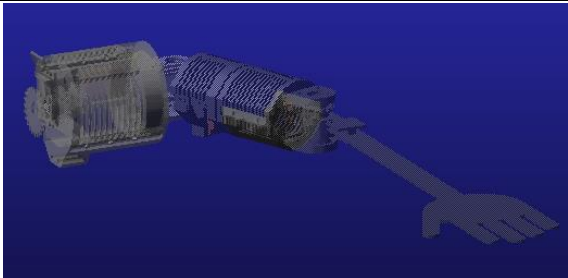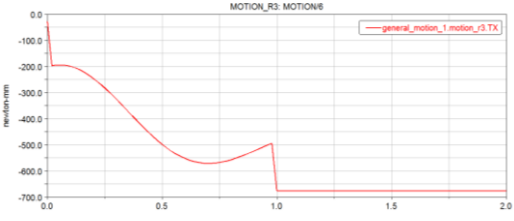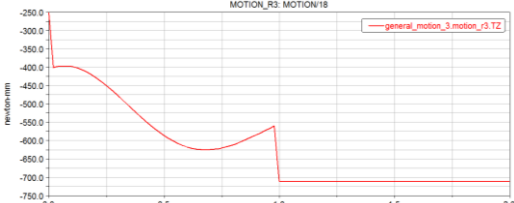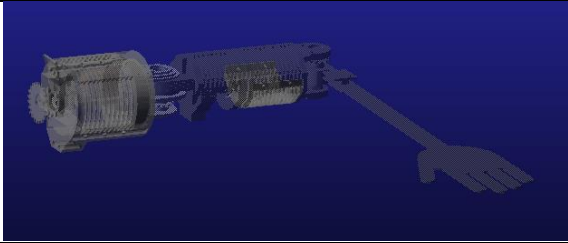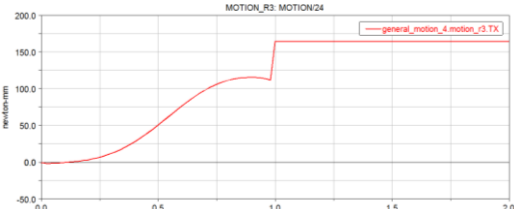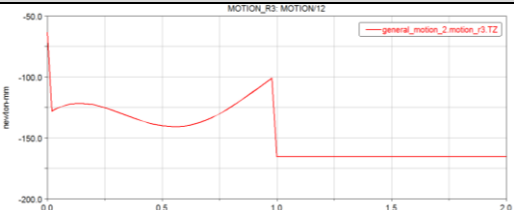
Fig. 48 STEP function in MSC Adams 2012 when rotating joint S1 90° in 1 second

46

Table 10 Torque curves and results from MSC Adams 2012

Joint	Rotations to maximally load the joint	Torques on the loaded joint
S1		
	Rotations: S1 rotates 90°, E rotates 20°	Maximal torque in joint S1: **0.675 Nm**
S2		
	Rotations: S2 rotates 70°	Maximal torque in joint S2: **0.710 Nm**
S3		
	Rotations: S1 rotates 90°, S2 rotates 70° E rotates 90°	Maximal torque in joint S3: **0.165 Nm**
E		
	Rotations: S2 rotates 70°	Maximal torque: **0.165 Nm**

The torque curves resulting from the simulations in MSC Adams 2012, displayed in *Table 10*, indicate that for joints E and S3, servomotors with a maximal load torque of 0.165Nm can be used, while for joints S2 and S1, servomotors with a maximal load torque of around 0.7Nm can be used. During a preliminary test, a Savöx servomotor with a maximal load torque of 9kgcm (0.88Nm, supplier-given) is used in joint S2. While it is possible to lift the arm with the actuator (confirming the hypothesis posed in Chapter 2.2.1 that the chain drives have minimal losses), the slightest amount of external loading (tested only empirically by blocking the hand of the arm), causes the motor to stall. Additionally, due to the inherent flexibility of the compliant elements (see Chapter 2.4) and the sometimes counteracting effect of the gravity compensation (see Chapter 2.5), the servomotors of joints E, S3 and S2 will be additionally loaded. Therefore, because the amount of loading (both from the added weight of a fur or protective coat around the arm or from external loading) on the arm is highly variable and unknown, in addition to the compliance and gravity compensation which were not included in the simulations, servomotors with an excess of torque will be used. The properties of the servomotors are listed in *Table 11*.

Table 11 Properties of the selected servomotors

Source: [68]	Joints E and S3	Joints S2 and S1
Manufacturer and type	Savöx SC-1251MG Coreless digital	Savöx SC-1283SG Coreless digital
Resolution	4096	4096
Gears	Metal	Steel
Weight	44.5g	80.0g
Output spline	25 teeth Futuba	25 teeth Futuba
Rotational speed at zero load @ 4.8V	0.1 sec/60°	0.16 sec/60°
Maximal torque @ 4.8V	7.0 kg-cm	25.0 kg-cm
Rotational speed at zero load @ 6V	0.09 sec/60°	0.13 sec/60°
Maximal torque @ 6V	9.0 kg-cm	30.0 kg-cm
Dimensions (mm)	40.8*20.2*25.4	40.8*20.2*36.4

As the design of the arm has evolved through multiple iterations, it has been adapted to fit the dimensions of the two types of servomotors. The servomotors will be supplied with a voltage of 6V to achieve the maximal torque and rotational speed. A major drawback of servomotors in general is that they are very noisy when heavily loaded. The chosen servomotors are no exception to this, therefore the videos made for the recognition of the gestures (see Chapter 3.1) will be muted.

In conclusion, in this Chapter 2.3 a dynamic simulation is performed with the 3D design of the arm in MSC Adams 2012 to establish the load torques on the actuators. These simulations will not be used to establish the torques for each individual gesture, instead they will be simulated for the poses in which the different joints are maximally loaded. This is done to ensure that the actuators can cope with higher load torques when new gestures are added. The results from the simulations are quite close to the experimental results. However, if an actuator is fitted that has a maximal torque just above the simulated load torque, the slightest amount of external loading causes it to stall. Since the amount of external loading due to a fur covering or a modified end effector are unknown at the time, and the compliant elements and gravity compensation mechanism may increase the load torque, the actuators are chosen with a fairly large safety factor: in joints E and S3, servomotors with a maximal torque of 9.0kgcm will be fitted and for joints S2 and S1, servomotors with a maximal torque of 30.0kgcm are selected.

2.4 Implementation of compliant elements

The selection of the joints in which passive compliance will be added, is discussed in Chapter 2.1.2. If the elbow of the arm is always bent, all external forces on the hand except for when the force is aligned with the axis of the lower arm, will cause a moment in either joint E, joint S3 or in both. For this reason, only in those two joints will a compliant element be implemented. The type of passive compliance that will be used is SEA (Series elastic actuation), as discussed in Chapter 2.1.2. Two different types of SEA will be used in the two joints, in order to compare the advantages and disadvantages.

2.4.1 Compliance in joint E

Compliance will be implemented in joint E through the use of two linear springs in the chain transmission. Using springs in the chain transmission has both advantages and disadvantages:

+ Springs can be bought in a wide array of static lengths, outside diameters and spring rates. For this reason, it should be possible to find the correct springs needed that fit in the current chain transmission. The compliance can be implemented in the design or deactivated (by simply replacing the springs with chain links) without significant modifications.

- If the joint is loaded with the weight of the lower arm, one side of the chain transmission will be stressed, while the other side will be loose. If the springs are not infinitely stiff, a part of the power in the chain transmission will always be used to elongate the spring in the stressed side, meaning that there is a difference in rotated angle at the actuator and the angle at the driven sprocket. The springs need to be stiff enough to minimize the difference in angle, while still being soft enough so that a small external load can elongate the stressed spring.

- If one spring is extended at the stressed side of the chain transmission, the other side will become very loose. To retain some stress in the loose side of the chain, an initial preload will need to be put on the springs. This preload will be realized by removing one or two chain links from the transmission, effectively making the chain too short and elongating the springs at no load.

- The springs need to have a length (both free and extended) that is short enough to not be pulled onto the sprockets during rotation.

The need for two springs in the chain is examined below:
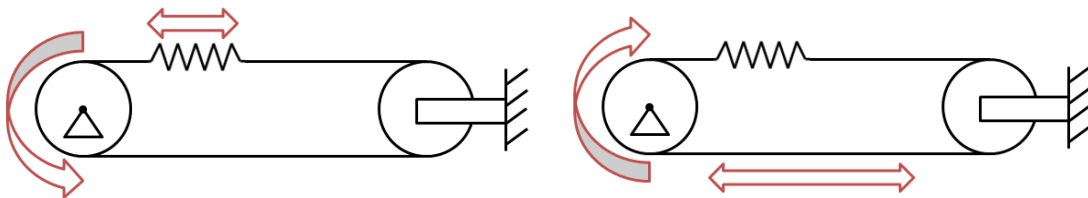
Fig. 49 Forces on the chain drive from an external loading in both rotation directions

On *fig. 49*, the left wheel is the driven sprocket on which an external moment (colored red) is applied, while the right wheel is the actuated sprocket which is kept static at a certain angle by the servomotor (signified by the clamping on the right). On the left side of *fig. 49*, the external torque is applied in such a way that the spring is elongated. This means that the joint is behaving in a compliant way. However, if the external moment is reversed (as on the right side of *fig. 49*), a stress is induced in the side of the chain without spring. In order to have compliance in both rotating directions, a spring is put in both sides of the chain. For simplicity, two identical springs will be used in the chain transmission, however it may be beneficial to use a stiffer spring in the side of the chain which is loaded during the gesturing in order to minimize the difference in angles due to elongation of the spring.

The maximal length of the springs needs to be calculated to make sure that the springs are not pulled onto the sprockets. The distance between the axes of the sprockets of joint E is 82mm, as measured in the 3D model on *fig. 50*. This distance is also the length of the chain between the two contact points with the sprockets, should those be perfectly round. The sprockets are designed with a pitch
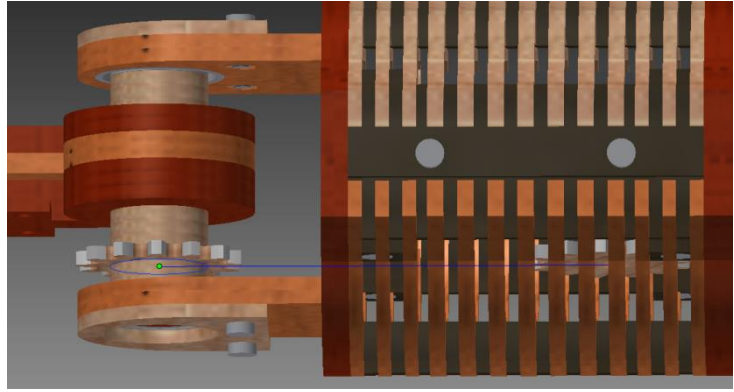
Fig. 50 Distance between actuated and driven axis for the elbow joint

diameter of 1.045" (26.54mm), to accommodate the dimensions of the chain links (*fig. 32*). The maximal rotation of the elbow starting from the initial position (lower arm aligned with the upper arm) is estimated at 160°. At this angle, further rotation of the lower arm will be blocked by the structure itself, therefore it is not possible to go beyond this angle with an external load. The length of the chain that is pulled onto the sprocket during a rotation is calculated as:

$$160° * \frac{\pi}{180°} * \frac{26.54mm}{2} = 37.06mm$$

which means that of the 82mm chain between the contact points, 37mm is pulled onto the sprockets, which leaves a possible maximal elongated spring length of 45mm. However, since the sprockets are not completely round and have teeth that may prematurely come into contact with the springs, and because there is on both sides a short distance where the spring needs to be attached to the chain, this length is estimated to be reduced to 37.5mm.

Since the external loading on the joint is unknown, the stiffness of the springs will instead be calculated to respect the maximal elongated spring length that is calculated above. The maximal torque on the elbow joint, as simulate in MSC Adams 2012 (see Chapter 2.3), is 0.165Nm. This means that the maximal tensile force on the springs in the chain will be:

$$\frac{0.165Nm}{\frac{26.54mm}{2}} = 12.43N$$

The formula for the force on a linear spring is:
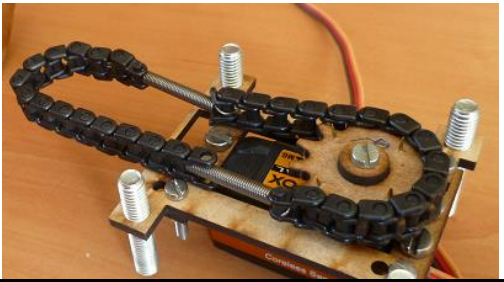
$$F = k * \Delta x$$

which means that if the initial length of the spring is around 25mm, the spring rate is equal to:

$$k_{spring} = \frac{12.43N}{(37.5mm - 25mm)} = 0.99N/mm$$

A set of springs that best approximates the calculated properties is ordered from RS Components Online [71], the properties of which are displayed in *Table 12*.

Table 12 Properties of the springs in the elbow joint [71]

Free length	26.4mm
Initial tension	15.7N
Material	Steel
Maximum extended length	41.1mm
Outside diameter	3.5mm
Spring rate	0.9N/mm
Wire diameter	0.55mm

The rotational stiffness of the setup is calculated in *Appendix B*. Experimentally, after the springs have been mounted in the chain, the lower arm feels rather loose, i.e. the joint is a bit too compliant and the difference in rotation angle between the actuated sprocket and the driven sprocket is too big. If the joint is loaded in one direction of rotation with the weight of the lower arm, the stiffness in the other direction of rotation is very low due to the spring in the looser side of the chain losing much of its prestress. Another drawback of the springs is that due to the small outside diameter, they are difficult to attach to the chain links. It would therefore be beneficial to use springs with the same free length, an outside diameter of 5mm and a higher spring rate. However, if the spring rate is chosen too high, the stress on the structure coming from preloading the springs in the chain may become too high. This may bend the elbow axis or damage the MDF structure and makes assembling the axis in the bearings very hard. With the current springs, the elongation of the springs when the joint is not loaded is around 5mm. This means that the force on the structure can be calculated as:

$$F = 2 * 0.9 \frac{N}{mm} * 5mm = 9N$$

Although the structure will in all probability not be damaged by fitting slightly stiffer springs (for a small finite elements simulation, see *Appendix C*), it becomes harder to elongate the springs enough to fit the elbow axis. For this reason, the current springs are left in the chain transmission.

2.4.2 Compliance in joint S3

Joint S3 is the axial rotation of module A (and modules attached to A) relatively to module D and E. To achieve compliance in this joint, a servo saver will be used. A servo saver is a small component that is mounted directly on the output shaft of a servomotor. Inside a servo saver is either a round wound linear spring (pictured on the left of *fig. 51*), a torsion spring or another flexible component.

Servo saver

Fig. 51 Inside of a round wound servo saver [72], it is attached to the servomotor used for steering on an RC car [73]

Traditionally, a servo saver is mounted on the servomotor that controls the steering of an RC car (pictured on the right side of *fig. 51*). Its use is to protect the servomotor when the steered wheels of the RC car violently hit an obstacle and the output shaft of the servomotor would be subjected to heavy shocks and forces. Because it has been designed to absorb shocks and small rotations, and needs to accurately transfer the desired rotation from the servomotor to the steered wheels, it is a rather stiff element that allows a limited amount of internal rotation (in this case the compression or extension of the round wound spring).

A servo saver with an internal round wound spring will be used to implement compliance in joint S3. It is a small module (outer diameter 17.7mm, with a thickness of 8.6mm), is made out of plastic and weighs only 2.5g. As neither the stiffness nor the maximal rotations are given by the supplier, the servo saver is mounted on a Savöx SC-1283SG servomotor (maximal load torque 30kgcm, to ensure that the servo saver starts giving way first) and will be loaded.

Fig. 52 Setup for testing the rotational stiffness of the servo saver (the bucket is filled with sand until the whole mass attached to the servo saver is 860g)

The servo saver is loaded with a mass of 860g, with the lever arm of the force being 14mm (*fig. 52*). This results in a rotation of the servo saver of around 4° (middle of *fig. 53*). The rotational stiffness of the servo saver is then calculated as:

$$k_{rot,servosaver} = \frac{0.860kg * 9.81\frac{m}{s^2} * 0.014m}{4° * \frac{\pi}{180°}} = 1.69\frac{Nm}{rad}$$

There is no visible difference when the servo saver is loaded with a moment in one direction compared to the other. The maximal torque on joint S3 is calculated in MSC Adams 2012 (see Chapter 2.3), where it was simulated to be 0.165Nm. With the calculated stiffness of the servo saver, this means that the difference in angle between the actuator and the link of joint S3 in the maximally loaded position is only 5.6°.

Lastly, the module is loaded by hand to reach the maximum possible rotation before damaging the module: this is estimated to be around 35° in both rotating directions (pictured on the bottom of *fig. 53*). At this point, the spring is either compressed as much as possible in one rotation direction or the plastic back sides of the spring connection points touch each other, which means that this maximal rotation is inherent to the construction of the element.
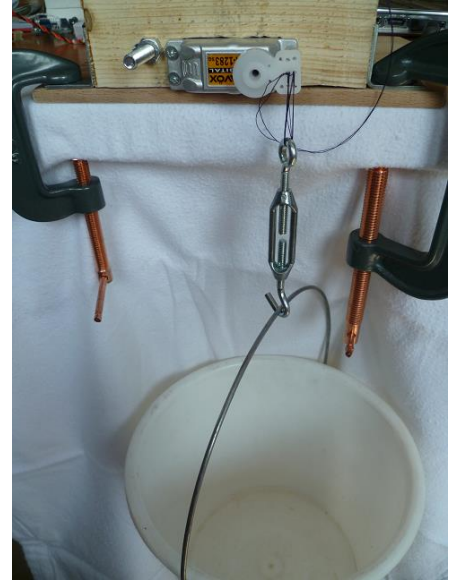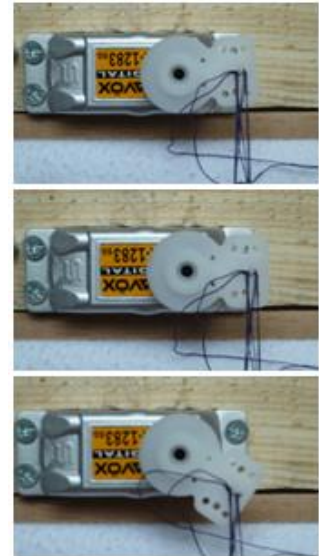
Fig. 53 Rotation of the servo saver at (top) no load (middle) moment of 0.118Nm (bottom) maximal rotation

2.4.3 Comparison of compliance systems

Both types of implemented passive compliance systems have advantages and disadvantages when compared to each other. A comparison is made in *Table 13*.

Table 13 Comparison of the two types of compliance

	Joint E	Joint S3
Type of compliance	Two springs in chain transmission	Servo saver (round wound spring) = simulates torsion spring
Rotational stiffness of the compliance	$0.158 \frac{Nm}{rad}$ (at no load)	$1.69 \frac{Nm}{rad}$
Maximal deflection under own weight	59.6° at 0.165 Nm (see *Table 10*)	5.6° at 0.165 Nm (see *Table 10*)
Weight of adding compliance	Mass of springs = 2 x 0.7g Mass of chain links that are replaced = 2 x 0.8g	2.5g
Maximal compliant rotation	Depends on spring rates and position of forearm but >35°	≈35°, inherent to construction
Does the compliance put a stress on the structure?	Yes	No
Ease of implementation	Moderately easy, connect springs in the chain and mount the elbow axis with the preload on the springs	Very easy, just slip on output shaft of the servomotor
Ease of expansion to variable stiffness	Difficult: increase of preload on both springs is not proportional and changes during certain positions	Difficult to dynamically increase preload on a torsion stiffness element

Comparing the two methods of compliance, it is clear that using a servo saver (which simulates a torsion spring) offers great benefits over using springs in the chain transmission. The fact that there are two springs of which one is either elongating or shortening and the other vice versa, combined with the necessary preload on the springs to keep the chain from getting too loose at one side during the rotations, makes the total stiffness of the joint hard to predict for both directions of rotation. If a higher stiffness is desired, stiffer springs are needed, which means that a higher preload needs to be put on the springs to keep the chain from becoming excessively loose at one side during compliant behavior. However, this preload is put on the structure that maintains the distance between the two sprockets of the chain drive and can deform or break if the necessary preload is too high. In comparison, use of a torsion spring is much easier, since there is no need to put a preload on the spring or on the structure. If a stiffer joint is desired, a torsion spring with a higher rotational stiffness can be easily implemented. However, with the use of only one torsion spring, there is a difference in the stiffness between the two rotational directions once the joint is loaded in one direction.

In conclusion, in this Chapter 2.4 the two types of compliance that are integrated in the structure are examined and compared. In joint E, two springs are attached in the chain drive in an attempt to integrate the compliance in the power transmission, while in joint S3, a variant on a torsion spring is used. It is concluded that use of a torsional spring (or round wound linear spring) is preferable over using two springs, due to the lack of a necessary preload on the structure and ease of implementation.

2.5 Passive gravity compensation

A type of passive gravity compensation will be implemented, as discussed in Chapter 2.1.2. A cable made out of Kevlar will be wound around the shoulder axis and will be connected to a spring, which will be connected to module F (the rotating inside of the shoulder), placing the spring in parallel with the actuator. The stiffness of the spring that is necessary to balance the arm at an angle of 20° with the vertical axis (this has been chosen as the neutral position of the arm) will be computed.

The mass of the part of the arm which rotates around the shoulder axis and will need to be balanced, is calculated in MSC Adams 2012. Along with the mass, the center of mass of this part will be calculated relatively to the coordinates of the shoulder axis. This is indicated on *fig. 54*.

The resulting moment around the shoulder axis that needs to be balanced is equal to:

$$0.460kg * 9.81 \frac{m}{s^2} * 0.0554m = 0.250Nm$$

The Kevlar cable on which the spring is mounted, is attached and wound around a cylinder on the shoulder axis. This cylinder has the maximal possible diameter to reduce the force on the spring which compensates the load torque. However, the diameter is kept smaller than the two elements next to it, so that the cable cannot slide off the cylinder and is kept in its place (pictured on *fig. 55*).

Mass to be balanced: 0.460kg

Distance in vertical plane: 55.4mm
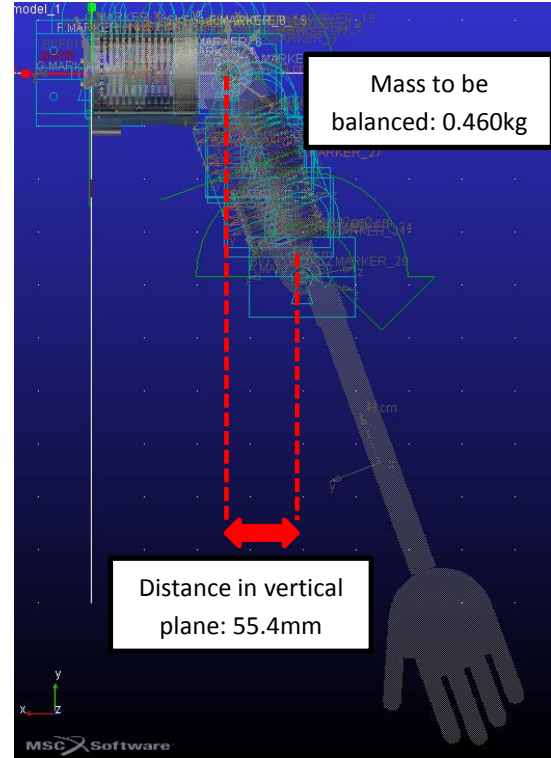
Fig. 54 Center of mass and mass to be balanced by gravity compensation

Designing the cylinder with the aforementioned requirements, results in a radius of 26mm. The force with which the spring is loaded to compensate the load torque is calculated as:

$$\frac{0.250Nm}{0.026m} = 9.62N$$

The stiffness of the spring will be chosen in such a way that there is always some tension on the cable instead of hanging very loose when the arm is in a position in which the gravity compensation has no effect.

Kevlar cable is wound around this cylinder

Connection point of cable and spring to module F

Fig. 55 Connection points for the gravity compensation mechanism

The maximal rotation of joint S2 is considered to be 70°, as the initial orientation is an angle of 20°

with the vertical and the arm is never lifted higher by joint S2 than the horizontal plane (for the gesture *Surprise*). The length of the cable that is wound on or off the cylinder is calculated as:

$$70° * \frac{\pi}{180°} * 26mm = 31.76mm$$

This length is the minimal elongation of the spring at full load, so that there is still some tension in the cable when the upper arm is aligned with the horizontal plane.

$$k_{spring} = \frac{9.62N}{31.76mm} = 0.30 \, N/mm$$

In the first prototype (pictured in *fig. 56*), due to the unavailability within time constraints of a spring with the necessary properties, a spring with a stiffness of 0.4 N/mm is mounted in the design, meaning that the cable is rather loose when the upper arm lies in the horizontal plane.

Fig. 56 Passive gravity compensation implemented in the physical prototype

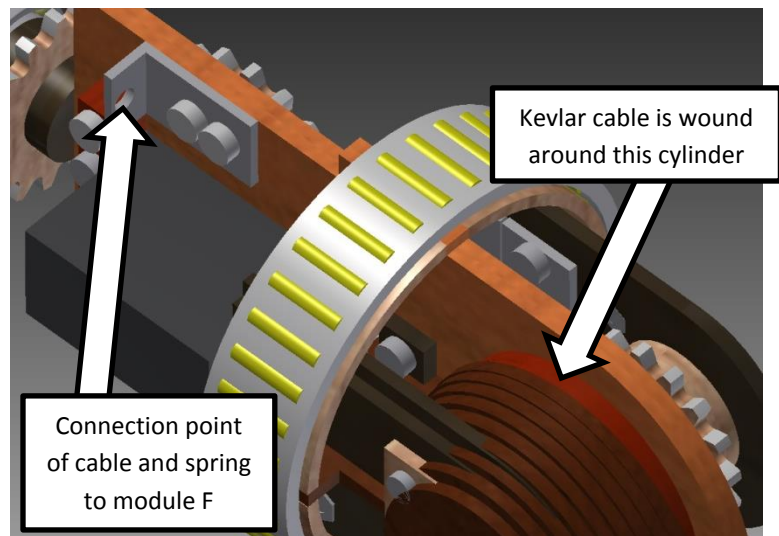In conclusion, in this Chapter 2.5 the method of passive gravity compensation is explained. The gravity compensation is done by winding a cable around the shoulder axis, instead of using a setup as in Chapter 1.2.5 that compensates the gravitational load in all static positions of the arm, because there is not enough space in the design. Additionally, because of the compliance in joint S3 in the upper arm, it would be very difficult to get the elbow angle the back to the upper body, which is needed to balance the arm in all poses. A spring is connected on one side to this cable and on the other side to the rotating inside module of the shoulder (module F). Compared to other passive gravity compensation techniques that balance the static load of the arm in all positions (see Chapter 1.2.5), this method is more compact but only balances the arm in 1 orientation. This orientation is chosen as the neutral pose, so that none of the servomotors are loaded when the arm is in the neutral pose (which is expected to be most of the time).

A drawback of this method is that when the arm moves down from an expressive pose in which the arm is lifted by joint S2, the load on the servomotor increases as the spring exerts a force when it is being elongated, but this is not a problem if the arm is lowered slowly enough. However, due to choosing the orientation of the servomotors to be XZX (as described in Chapter 2.1.1) and having the neutral position of the arm with the back of the hand to Probo's front, moving the arm upwards is mostly done by a rotation in joint S1, rather than with joint S2. Unfortunately, this introduces another drawback: if the arm is lifted upwards by joint S1 which rotates the inside of the shoulder, the whole gravity compensation mechanism is rotated with it, sometimes up to 180° if the arm is fully raised. This means that the spring which was originally pulling the arm upwards, is now pulling the arm down which elevates the load torque on joint S2. This is an additional reason that the servomotor in joint S2 is chosen with an excess of torque in Chapter 2.3.

2.6 Collision detection

In order to provide a safe way of interacting with the robotic arm, a method of collision detection will be implemented in addition to the compliant elements in joints S3 and E. This way, if the arm hits an object or person, not only is the impact of the hit reduced due to the flexibility in the joints, the arm will subsequently stop moving for a number of seconds and then go back to its neutral position.

Colliding with another object that diverts the arm from the planned trajectory can be seen as a disturbance on the system. The most simple way to detect this disturbance would be to measure the angles of all the joints during the rotations (with for example potentiometers) and if a measured angle differs from the angle that is given as input to the servomotor, an appropriate reaction of the system can be implemented. This can be done by implementing a PID controller to correct the disturbance: however, this is not the desired reaction for the arm, as it would mean that the servomotors would keep rotating until the arm has reached the expressive pose. A better solution would be to implement a threshold so that if the difference between the angle given as input and the measured angle becomes larger than this threshold, the arm is considered to be blocked and no further rotation of the actuators is allowed. The difficulty with implementing this method is due to the presence of the elastic elements in the joints: there will always be a difference in angle at the servomotor and at the following link. Moreover, this difference will differ for each joint due to the various methods of compliance, looseness of the chain drives, etc.; meaning that different thresholds need to be implemented. Additionally, as the arm goes to the expressive poses, the joints are loaded and the elastic elements are elongated, purely by the own weight and inertia of the arm. This means that the threshold cannot be static: as the joint is heavier loaded, the threshold needs to increase, otherwise this would lead to incorrect detection of collision. This can all be done in dynamic simulations (calculating the torques with inclusion of the elastic elements), but it is decided that another easier method of collision detection will be implemented in the first prototype.

The decision is made to attach an accelerometer to the last link, which is the lower arm. This accelerometer will measure the accelerations around three axes during a number of test runs in which the arm can perform the gesture without external loads. If the measured accelerations during the real operation differ too much from the calibrated values, a collision is detected and the arm is stopped. Ideally, the accelerations would be integrated twice to get the actual position of the lower arm in task space, however currently the arm is controlled in joint space by directly sending rotations to the servomotors. Since there are currently no measurements of the joint angles and no kinematic or dynamic equations implemented in the controller, having access to measurements of the position in task space is not useful at the moment.

The accelerometer that will be mounted on the first prototype is an inexpensive TinkerKit Arduino 3-axis linear accelerometer, based on the LIS344AL accelerometer, made by ST Microelectronics (pictured on the left on *fig. 57*). This accelerometer can measure accelerations of up to ±3.5g on three orthogonal axes. Ideally, this module would be mounted on the lower arm as close to the end of the hand as possible: here, the widest range of accelerations and decelerations can be measured. However, due to the fact that the compliance of the elbow joint is too soft (see Chapter 2.4.1), it is expected that there will be a variation of the acceleration of the lower arm each time the same gesture is performed. In order to limit the variation of the accelerations that the accelerometer measures, it is not mounted in the hand but at the base of the lower arm, close to the elbow.
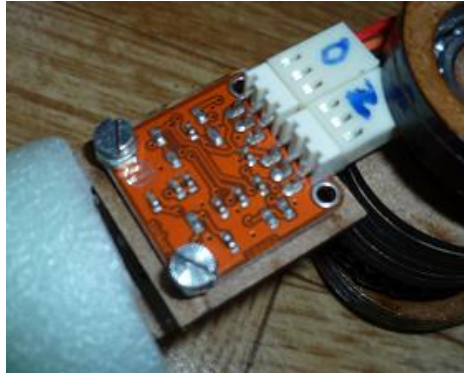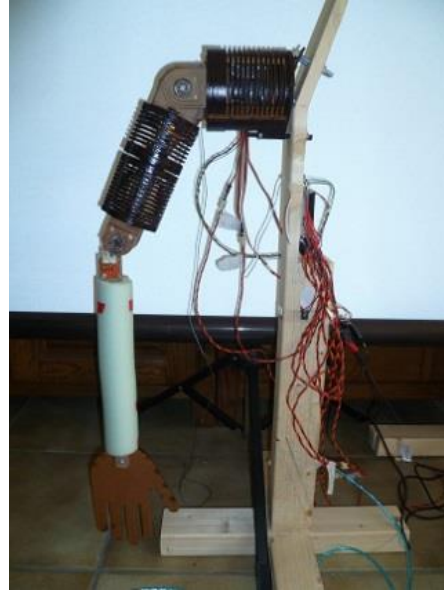
Fig. 57 (top) Mounting location for the accelerometer and (right) calibration setup

The accelerometer is calibrated using a slightly modified version of the gesture *Fear*. The rotations that are applied during this gesture to the servomotors are displayed in *Table 14*.

Table 14 Rotations for the gesture for which the accelerometer is calibrated

	Initial position	With cubic splines (initial and final velocity 0) in 1.5 seconds to	Expressive pose
Joint E	170°		60°
Joint S3	30°		60°
Joint S2	43°		60°
Joint S1	170°		100°

The accelerations are measured during five separate test runs, divided over multiple days and after assembling and de-assembling the arm from the frame. Afterwards, the data is averaged and the thresholds are established. The three orthogonal axes along which the accelerations are measured, are pictured in *fig. 58*. Examining the results, there is much more noise on the measurements of the Z-axis due to the apparent absence of any type of filtering, therefore the threshold will be chosen larger for this axis. The graphs with the measured data (the 'stream' of yellow, blue or green points) and the thresholds (the upper and lower limits) are given in *fig. 59* and *fig. 60*.
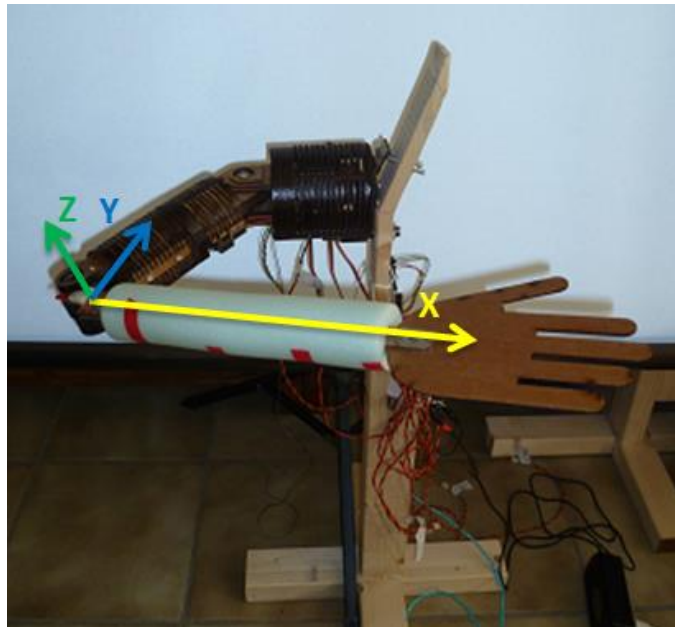

Fig. 58 The local axes along which the accelerometer measures the accelerations, during the expressive pose
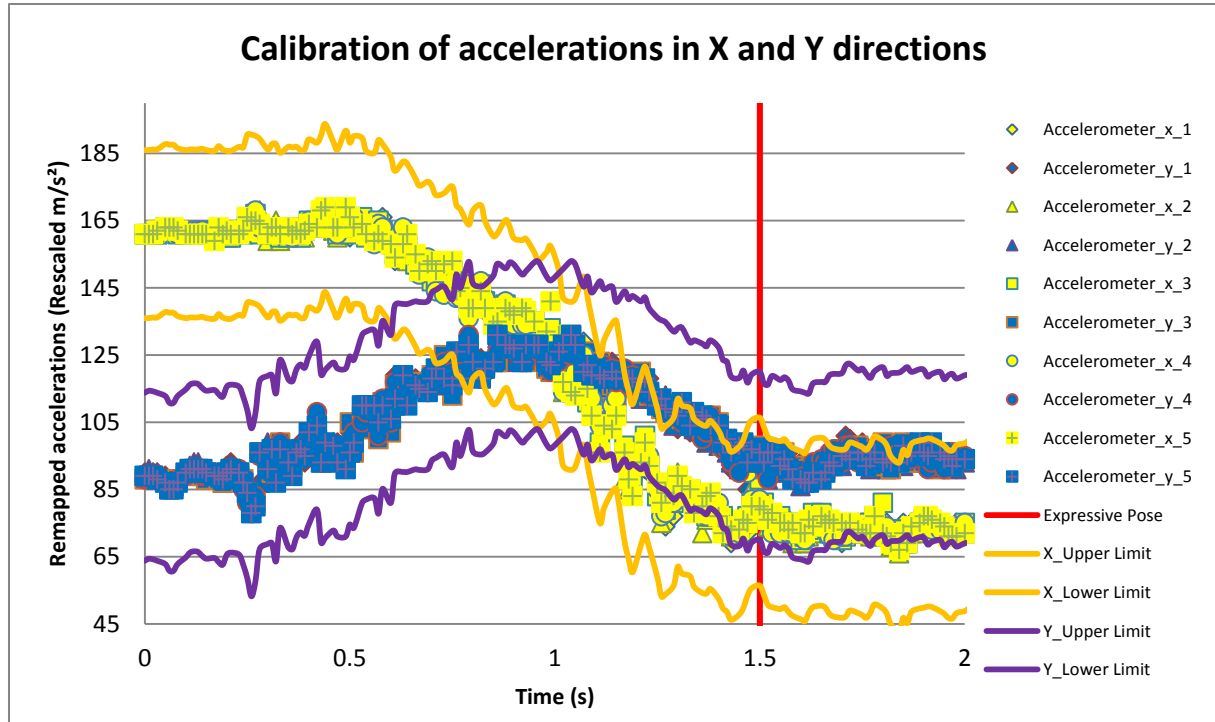
Fig. 59 Calibration of the accelerations in X and Y directions
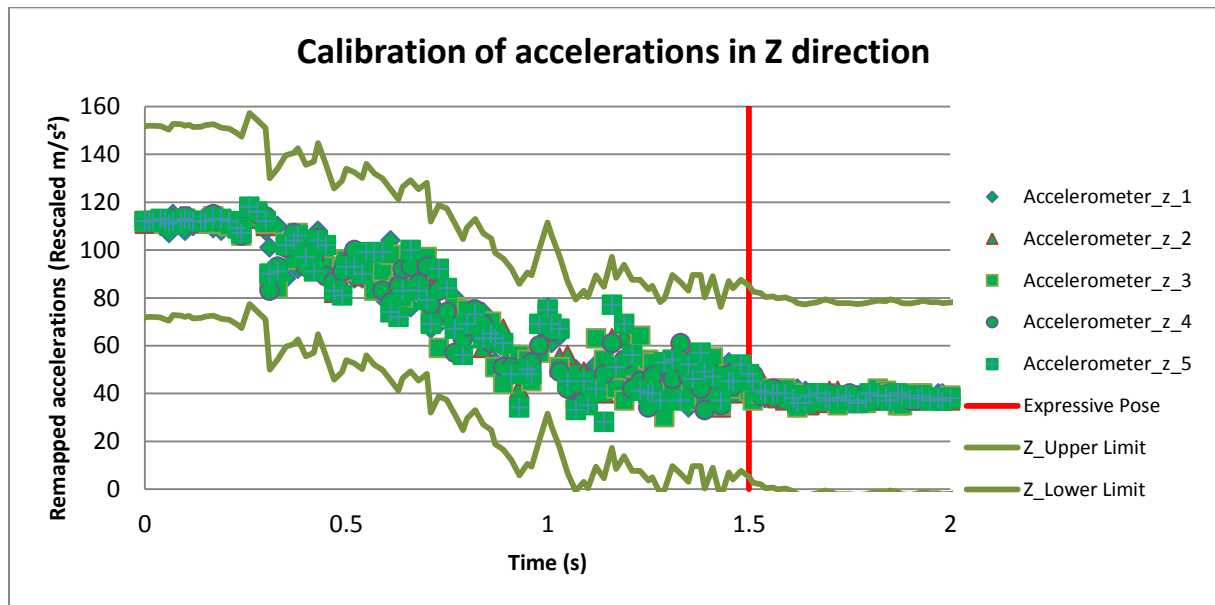
Fig. 60 Calibration of the accelerations in the Z direction

The red vertical line indicates when the expressive pose is reached (after 1.5 seconds), however it can be observed that there are slight variations in acceleration after the pose has been reached, indicating that the arm is still moving due to the softness of the elbow joint. The threshold of the X and Y-axes are calculated as the instantaneous mean value ± 25 and for the Z-axis the instantaneous mean value ± 40. These thresholds are chosen as constant values instead of calculating the traditional 6σ at each point in time to simplify the algorithm. In *fig. 61*, for the Z-direction the thresholds (mean value ± 40 and mean value ± 3σ) are compared: it is concluded that in the worst cases, both threshold methods give about the same results. These worst cases are considered to be

the most important: it is preferable that the threshold interval is chosen larger and that the arm stops a bit later than when the interval is chosen smaller and that there is a chance that a collision is incorrectly detected. For this reason, the constant thresholds will be used.

Fig. 61 Comparison of the thresholds for accelerations in the Z direction
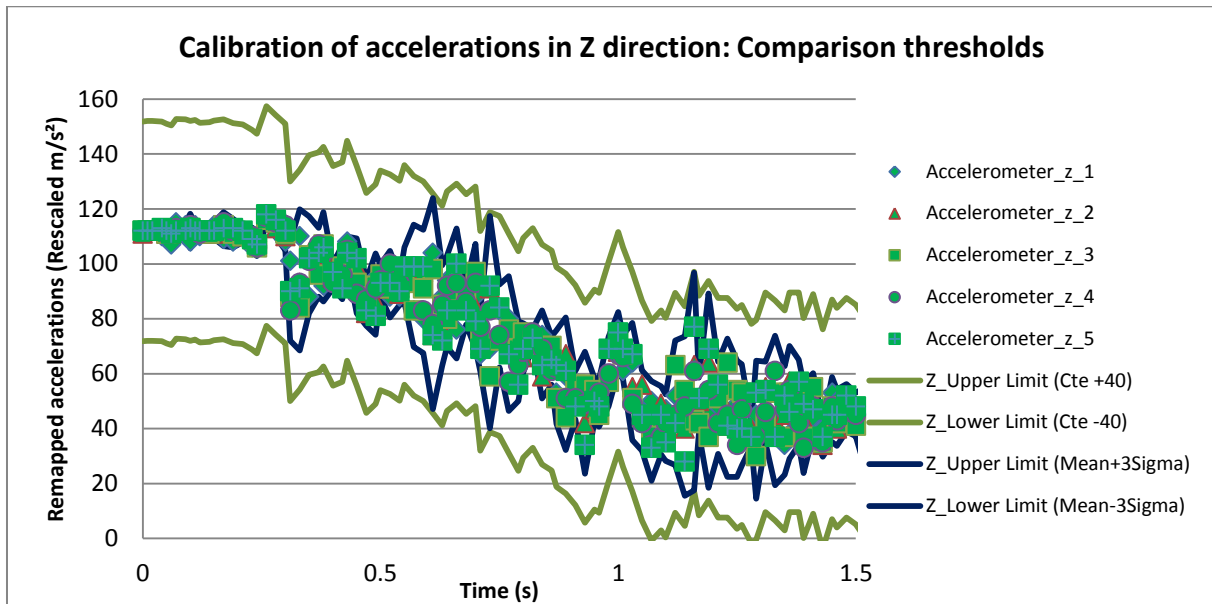
The algorithm works in the following way: the mean calibrated value for the X, Y and Z axes are given around every 10ms. When the arm is moving to the expressive pose, the measured values are compared to the aforementioned threshold values that are assigned to the point in time closest to the current measured time. If the measured value exceeds the threshold, the servomotors are kept at the same place for a number of seconds, then they linearly rotate back (1° per 10ms for joints S1, S2 and S3 and 2° per 10ms for joint E) to the neutral position.

In conclusion, in this Chapter 2.6 the method of collision detection is examined. The choice is made to attach an accelerometer to the lower arm, close to the elbow considering that the current method of compliance in the elbow joint is too soft (see Chapter 2.4.1). For a certain gesture, the accelerations in three orthogonal axes are measured five separate times. These values are averaged and inserted along with the according points in time into the program. During a run, the measured accelerations are compared to the mean values with a certain constant threshold interval. If the measured value exceeds the threshold, the arm stops for a few seconds, then goes back to the neutral position. The drawback of this method is that for each different gesture, difference in positioning of the accelerometer, etc., the accelerations need to be recorded or calculated in a dynamic simulation to establish the 'path' in accelerations that the arm needs to follow.

In a later prototype, once the stiffnesses of the compliant elements in the elbow joint and in joint S3 are optimized in such a way that they do not significantly deform under the own load of the arm but only when an external load is applied, the method of measuring the angles in the joints can be implemented. With this method, there is no need for preliminary calibration, as the comparison of measured and desired angle is done instantaneously in the controller. Another method of collision detection that can be used, is to implement pressure sensors in the fur of Probo.

2.7 Conclusions and future improvements of the design of an arm system

In Chapter 2.1, the design properties of the arm are established, based on the study of the current state of the art. The first prototype of the arm is designed with 4 degrees of freedom: three degrees of freedom in the shoulder (in XZX configuration) and one degree of freedom in the elbow. It will be examined in Part 3 during the recognition rates tests, if additional degrees of freedom are needed. Compliance will be implemented under the form of series elastic actuation in the elbow joint and in the axial rotation of the upper arm, which will allow for compliant behavior for the selected gestures. A form of passive gravity compensation is decided be implemented in the shoulder.

In Chapter 2.2, it is established that chain transmissions will be used to transfer power to three of the four joints. The choice to use chain drives is based on their low weight, high strength, ease of changing their length and high efficiency. A full 3D model of the arm is examined in this chapter. This design is done in different modules, which can be replaced should their functionality change. A possible improvement for the design is that the lower arm (module H) will need to be reinforced, should an additional degree of freedom or an actuated hand be fitted to the lower arm. Currently, the servomotor for joint S1 is placed outside of the design (on the backside of the arm, since this is the only place where there is space on the current frame in the upper body of Probo). It would be better to integrate this servomotor in the design, either by putting it on the inside of the frame so that it would be aligned with the axis of joint S1, or by moving it closer from the current position and possibly replacing the chain drive with gears. A last suggested improvement is that it is possible to design module G with a smaller outside diameter, in a stiffer material since it visibly deforms under the weight of the arm. In Chapter 2.3, the 3D model is used in dynamic simulations to establish the maximal torques that the servomotors will need to be able to provide. In order to do this, the arm is put in different poses for which the different joints are loaded maximally. The reason that these positions are used instead of the actual poses that the arm will perform for the gestures is that this way, the actuators are chosen with the possibility of adding new gestures in the future in mind. Due to the possibility of additional loading (due to the compliance or unknown external loading), the torque of the final servomotors is chosen with a certain safety factor.

In Chapter 2.4, the two methods of passive compliance are examined: in the elbow joint two springs are integrated in the chain drive, while in joint S3 a round wound spring that functions as a torsion spring is implemented. It was concluded that using a torsion spring is preferable to using the two springs in the chain transmission due to the absence of a preload on the joint and the ease of implementation. In Chapter 2.5, the passive gravity compensation mechanism is examined: a cable with a spring is wound around the shoulder axis and attached to the inside of the shoulder. Using this method, the arm is balanced for only the neutral position. It would be possible to statically balance the arm for all poses using one of the mechanisms given in Chapter 1.2.5, however the compliance of joint S3 prevented the implementation of such mechanisms in the design. Lastly, in Chapter 2.6, the method of collision detection is examined. An accelerometer is fitted to the lower arm and the measured values of the accelerations on three orthogonal axes are compared to predetermined values that have been recorded beforehand. A possible improvement is to measure the angles of the joints during the gestures to establish if a collision has taken place. With this method, there would be no need to determine any values beforehand, however due to the excessive flexibility of the compliance in the elbow joint, this was not implemented. Another method is to implement pressure sensors in the fur of Probo to establish if there is an external loading on the arm.

Part III: Testing the recognition rates

In Part 2, the complete design of the first prototype of an arm system for Probo is examined. Two physical prototypes have been built during the process: first a left arm, and then a right arm that implemented some improvement such as a lighter design, the compliance and the passive gravity compensation. In Part 3, the two arms are mounted on an upper body that can rotate to the front and to the back. Using this upper body, six gestures will be performed and videotaped. The footage of the gestures will be used for a survey to establish the recognition rates, in order to compare the rates to other studies and to check if additional degrees of freedom in the arms are desired.

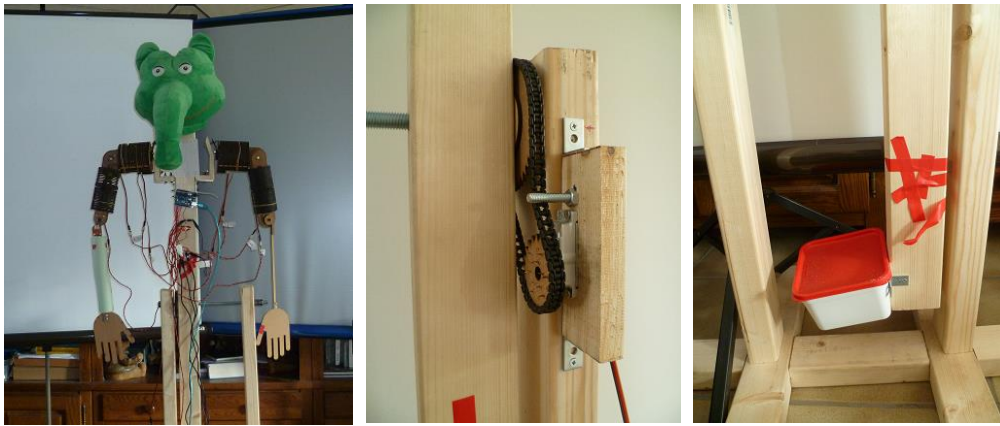## 3.1 Construction of the upper body and establishing the gestures

Fig. 62 (left) Complete upper body, (center) rotation of the hips and (right) counterweight for the upper body

The two arms are mounted on a structure that can rotate to the front and to the back, as the 1-degree of freedom hips also need to be actuated to perform the gestures (see Chapter 2.1.1). On top of the structure, a stuffed version of the head of Probo is mounted to give the impression of a complete upper body (pictured on the left of *fig. 62*). The rotation of the hips is done in a similar fashion to the joints in the arms: a chain drive transfers the torque from a Savöx SC-1283SG (see Chapter 2.3 for specifications) to a rotating wooden beam, using a 2:1 gear ratio (middle of *fig. 62*). On one end of this beam, the arms and the stuffed head are mounted. On the other end, a box filled with weights is attached, to provide the counterweight for the mass on the other end. The counterweight is chosen so that the torque from the weight of the arms and head is compensated; this way the servomotor only has to account for the inertia of the rotating beam and is not subjected to a static load torque (right side of *fig. 62*). This structure will only be used for testing the recognition rates through videos and is not meant to be used for any other purpose.
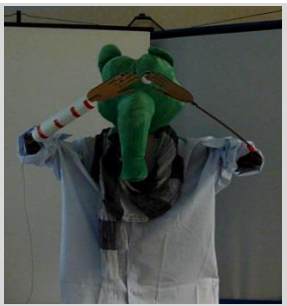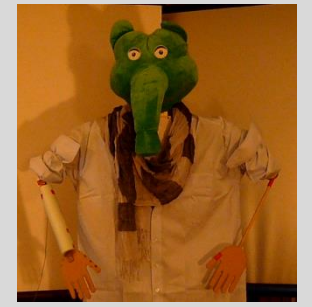
Videos of the gestures will be used, as they are claimed to yield much higher recognition rates compared to the use of static images [74] [75]. To record the videos of the gestures, a shirt and scarf are used to cover the wiring and the microcontroller (which is an Arduino Uno), to not distract the viewer. The six gestures that will be portrayed are discussed in Chapter 2.1.1. The upper body will start in the neutral position, then go to the expressive pose, hold this pose for 2.5 seconds, then go back to the neutral position. This whole progression is filmed with a camera that is put in front of the prototype, around 2.5m away. Sometimes, the camera is lowered or put to the side, since it can be difficult to see the position of the arms relative to the front of the body on the video. The transition

to and from the expressive pose is done by sending the trajectories in joint space, created with cubic splines with initial and final velocity zero, to the different servomotors. As alluded to at the end of Chapter 1.1.2, the generation of the motion trajectory plays an important role in recognition rates. However, the preliminary focus of the gestures in the first prototype is on creating a key expressive pose and then transitioning from the neutral pose to this expressive pose, rather than focusing on the motion itself. This has been claimed to produce a '*convincing and believable display*' [76].

In *Table 15*, the rotations of the joints and the durations, along with images of the gestures (screen captures from the videos that have been recorded) are given. The rotations for the hips are always done in 1.5 seconds, due to the high inertia of the construction. The rotations for joint S1 are displayed in the angles that are given to the servomotors; however, due to the gearing ratio, they needs to be multiplied with $\frac{22}{17}$ to obtain the real rotations. The same is valid for the rotation of the hips: these rotations needs to be multiplied with $\frac{22}{44}$.

Table 15 Expressive poses for the recognition rates tests

Neutral	Happiness	Surprise	Fear
Initial position: E_Left = 40° S3_Left = 180° S2_Left = 140° S1_Left = 25° E_Right = 160° S3_Right = 30° S2_Right = 30° S1_Right = 170° Hips = 90°	Rotation of joints in 1.5s: E = 30° S3 = 0° S2 = 0° S1 = 135° Hips = 30°	Rotation of joints in 1s: E = 140° S3 = 150° S2 = 85° S1 = 15° Hips = 30°	Rotation of joints in 1s: E = 135° S3 = 40° S2 = 20° S1 = 100° Hips = -30°

	Disgusted	Anger	Sadness
Note: The elements of compliance are removed for this test, so there is no need to account for the deflection in the joints (see Table 13)	Rotation of joints in 1s: E = 80° S3 = 10° S2 = 0° S1 = 80° Hips = 40°	Rotation of joints in 1.5s: E = 100° S3 = 20° S2 = 50° S1 = 15° Hips = -30°	Rotation of joints in 1.5s: E = 20° S3 = 0° S2 = 0° S1 = 25° Hips = -35°

3.2 Recognition rates survey and results

The videos of the different gestures are combined into one video (as the chosen survey software does not allow individual video embedding) and added to two surveys: one survey is in English, while the other is in Dutch. The reason for this is that the target is to get as many responses as possible from children, as Probo is being designed to specifically interact with children (see the Introduction). Translating the survey into Dutch makes it easier for Dutch-speaking children to fill in their responses. Regarding the two languages of the surveys, an attempt is made to translate the text and questions as literally as possible with no difference in content.

The surveys are performed with Limesurvey [77]. The participants are first asked to fill in their age and gender. Then, they can choose from a list of possible choices the emotion that they though best described the gesture seen in the video. At the end of the survey, the participants can indicate, on a scale from 1 to 5, how hard it was to label the gestures from the video.

An initial survey listed 10 possible choices: in addition to the six correct gestures *Happiness, Surprise, Fear, Disgusted, Anger* and *Sadness*, four other choices were added: *Confused, Excited, Interested* and *Neutral*. The four additional choices were chosen to test different values on the Valence-Arousal affect space plane [8]. This is illustrated on *fig. 63*.
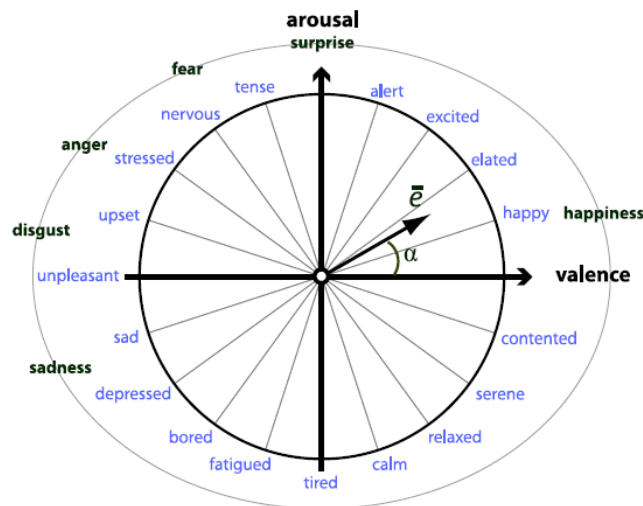

Fig. 63 Positions of the six basic emotions on the Valence-Arousal affect space plane [8]

The positions of the six basic emotions are indicated on the plot. The option *Confused* can be considered to be in the third quarter with negative valence and negative arousal while the option *Excited* is indicated in the first quarter of the plot. The option *Interested* is considered to be in the fourth quarter and *Neutral* is considered to be in the origin. These four options were considered to be distant enough from the other choices on the Arousal-Valence plot and were therefore added. This initial survey was distributed among 7 persons (mean age 29, median age 23). Of the seven respondents, 3 people identified the video for *Happiness* as *Excited* and 5 people identified the video for *Sadness* as *Interested*. The first difference may indicate that the gesture in the video for *Happiness* is positioned too high on the arousal axis. The second difference may indicated that the gesture in the video for *Sadness* is perceived with a correct negative value for arousal, but with a positive valence value. At this stage, it is unknown if this is due to the chosen expressive pose, motion trajectory or due to a lack of degrees of freedom (either in the arms or through the absence

of a working head and neck). It is assumed that increasing the number of possible choices that the respondents can choose from will negatively affect the recognition rates. Due to the small number of responses on this initial survey, no conclusions will be drawn.

An attempt will be made to compare the results from the survey to other recognition rates studies. In order to do this, the gestures and responses from a number of comparable studies (also given in Chapter 1.2.2 and Chapter 1.2.3) are examined. The first study that is analyzed, are the recognition rates of the actuated head of Probo [8]. In this study, the recognition rates of the same six emotions *Happiness, Surprise, Fear, Disgusted, Anger* and *Sadness* are compared for a virtual model of the head, an uncovered physical prototype and the physical prototype covered with a fur. In this research, the participants were shown pictures of the head in the expressive pose and could then indicate their preference from a list of the six correct emotions. The results of the tests with the physical prototype covered with the fur are given in *Table 16*.

Table 16 Recognition rates of the fur covered head of Probo [8]

Recognition rates of fur covered head of Probo using a multiple-choice questionnaire with 23 children [8]					
%Match	Happy	Sad	Disgust	Anger	Surprise	Fear
Happy	**100**	0	0	0	0	0
Sad	0	**87**	0	0	0	9
Disgust	0	0	87	4	4	4
Anger	0	9	**4**	**96**	0	0
Surprise	0	0	9	0	**70**	22
Fear	0	4	0	0	26	**65**

The study concludes that, in accordance with other studies of recognition rates of robotic heads, that the recognition of *Fear* tends to be the most difficult. However, since the objective of the research described in this document is to check the recognition rates of an upper body without actuated head, it would be beneficial to compared it to robots with similar configurations instead of to only an actuated head.

The study of the recognition rates of the robots WE-4 and WE-4R is examined [42]. In this research, the recognition rates of a photo of a human face, a photo of the head of WE-4 and a video of the whole upper body of WE-4R are compared for 6 gestures. It is not explicitly stated that only the six gestures were given as the possible choices that the observers could choose from. Looking at the results (see Chapter 1.2.2), there is a non-negligible but not significant difference in recognition rates between the actuated robotic face and a complete upper body. This means that in this study, the face has the largest share in determining the recognition of an emotion and since the upper body that will be used in this research has no actuated head or neck, comparison of the numerical results will be difficult. This conclusion can be drawn to other studies in which an actuated face is used: for example, the study of the recognition rates of KOBIAN [12] or the comparison of the recognition rates of WE-4R and WE-4RII [27].

In a study of the recognition rates using the robot NAO [43], the following six gestures are performed: *Anger, Sadness, Fear, Pride, Happiness* and *Excitement*. In the study it is explicitly stated that only these six emotions were given as the possible choices that the participants of the study could choose from. Making a comparison to the recognition rates of NAO would be interesting since it has 6 degrees of freedom in each arm (3 in the shoulder, 1 in the elbow, 1 in the wrist and a 1 degree of freedom gripper shaped as a hand), 1 degree of freedom in the hips with actuated legs (which can rotate the upper body to the sides) and 2 degrees of freedom in the neck without an actuated face. This means that the gestures, like in the prototype of the upper body of Probo, are performed mainly by the arms, instead of drawing the attention of the viewer to the face. However in the study, the participants were shown all gestures with 3 different orientations for the neck: looking straight ahead, tilted up and tilted down, while the rest of the portrayed by the body stayed the same. The results of the study indicate that the orientation of the head has a large impact on the recognition rates. Since the neck in the recognition rates test with the upper body of Probo is not actuated and the head is always looking straight ahead, the results will be compared to the recognition rates of NAO with the head straight.

Most of the participants in the test using NAO (with mean age 29.31) had the British nationality, which means that most of the participants of this research in Belgium will have a similar 'European' background. This is beneficial for a comparison of the recognition rates, as there are indications that the recognition and interpretation of emotions is dependent on cultural background [78]. In another study of the recognition rates using NAO, the gestures *Sadness*, *Anger*, *Fear* and *Joy* were performed each in different variations [79]. However, in this study the gestures were performed not only by assuming an expressive pose but also by movements during the gesture (such as shaking its head during *Sadness* and closing the hand to a fist during the expressive pose of *Anger*) [80]. These gestures are much more complex than those currently performed by the upper body of Probo and will not be used for comparison.

To summarize, in order to compare with the study of the recognition rates with NAO, the participants of this research will be able to choose only from the six correct emotions once (in the English version of the survey: *Happy, Surprised, Fear, Disgusted, Angry* and *Sad*; in the Dutch version: *Blij, Geschrokken, Bang, Gedegouteerd, Boos* and *Droevig*).

The results of the study will be examined. There were a total of 77 responses to the surveys, with the mean age of the participants 25.69 years old, the median age 23 years old and a standard deviation of 8.91. A histogram of the ages of the participants is plotted in *fig. 64*. An attempt was made to reach as much children as possible with the survey, however due to the very low number of responses from people in this range of ages, they will not be taken as a separate category. The recognition rates are given in *Table 17* (a comparison between female and male participants is given in *Appendix D*).
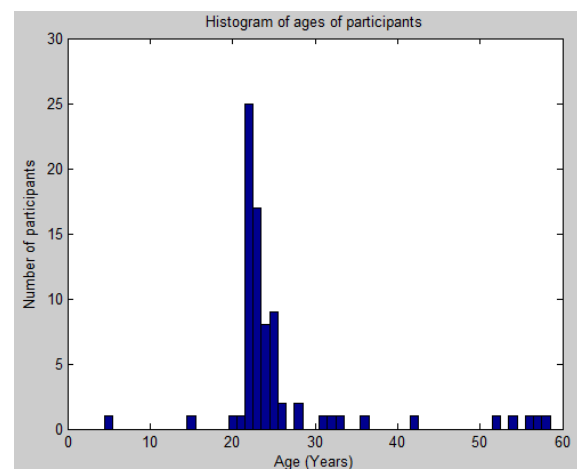

Fig. 64 Histogram of the ages of the participants

Table 17 Recognition rates of the prototype of the upper of Probo

Recognition rates of the upper body consisting of two actuated arms (4 degrees of freedom each) and one degree of freedom in the hips (Chance level would be 17%)						
% Match	Fear	Surprise	Anger	Happiness	Sadness	Disgust
GESTURE1 (Fear)	**55**	8	0	3	30	5
GESTURE2 (Surprise)	8	**60**	0	26	3	4
GESTURE3 (Anger)	0	6	**79**	0	4	10
GESTURE4 (Happiness)	5	22	1	**68**	1	3
GESTURE5 (Sadness)	9	6	14	6	**38**	26
GESTURE6 (Disgust)	34	19	1	4	3	**39**

The results of the study indicate that the recognition rates of the gestures are significantly above chance level. The Fleiss' Kappa value is calculated, which gives an indication on the mutual agreement of the participants of the study [81]. The value of the Fleiss' Kappa is calculated to be 0.30 in this study. A table with suggested interpretations of the value is added in *Table 18*. Take note that these interpretations are not universally accepted and are only indicative. Nevertheless, this rather low value is an indication that the participants have widely different opinions: this may be due to the fact that they are of different ages or backgrounds. This is assumed to be a logical consequence of doing an open and anonymous survey over the internet.

Table 18 Interpretation of Fleiss' Kappa value [81]

Fleiss' Kappa	Interpretation
<0	Poor agreement
0.0-0.20	Slight agreement
0.21-0.40	Fair agreement
0.41-0.60	Moderate agreement
0.61-0.80	Substantial agreement
0.81-1.00	Almost perfect agreement

A histogram on the results of the question '*Did you find that it was difficult to name the gestures? (1 is very easy, 5 is very difficult)*' is added in *fig. 65.* The mean value is equal to 3.59, the median 4 and the standard deviation 0.79. This may indicate that the gestures in the videos are hard to identify. After they had performed the survey, a number of participants were questioned on their reasoning for their answer on this question. They indicated that the non-actuated face was very distracting. This may indicate that a recognition rates study where the camera for the videos is placed further away from the upper body, so that the face is harder to see, may yield very different results.
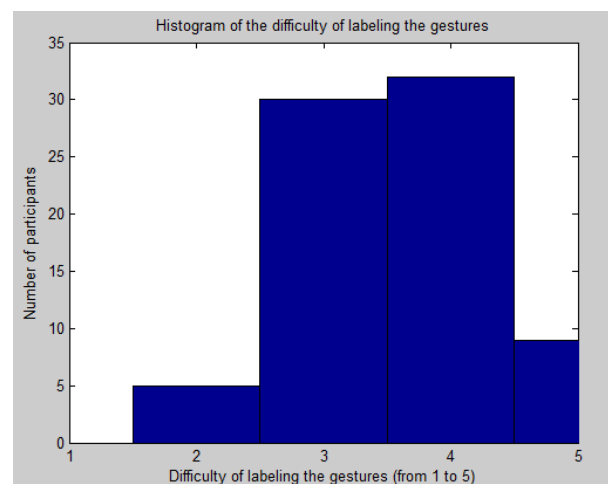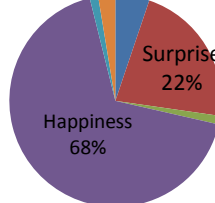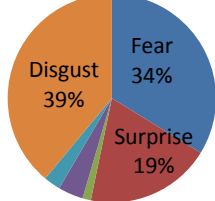
Fig. 65 Histogram of the difficulty of labeling the gestures

In conclusion, in Chapters 3.1 and 3.2, the construction of the upper body, generation of the motion trajectories and content of the recognition rates surveys are examined. The surveys are drafted in such a way so that they can be compared to the recognition rates in a study using the robot NAO, a social robot with similar functionalities. In Chapter 3.3, the results of the recognition rates test will be interpreted and compared to those of the study with NAO.

3.3 Interpretation and comparison of the recognition rates

The results of the recognition rates test described in Chapter 3.2 are plotted in *Table 19*, along with the relevant results of the recognition rates test of the robot NAO [43]. The pictures of the expressive poses of NAO are given in *fig. 16,* those of the upper body of Probo are given in *Table 15*.

Table 19 Comparison of the recognition rates

Gesture	Recognition rates of NAO with the neck straight [43]	Recognition rates of the prototype of the upper body of Probo
Anger		
Sadness		
Fear		
Happiness		
Surprise	This gesture was not performed, instead, *Pride* was portrayed.	
Disgust	This gesture was not performed, instead, *Excitement* was portrayed.	

The similarities or differences in recognitions rates between the two studies will be examined for each gesture individually. Regarding the gestures performed by NAO, as only static images of the expressive poses are available, no conclusions can be made on the difference in speed of gesturing between the two studies, only on the gesturing speed of the upper body of Probo individually.

Regarding the gesture *Anger*, the expressive pose is more or less the same (*fig. 66*): the elbows are bent outwards to make the upper body as large and imposing as possible. The recognition rates of the two studies are very similar: around 70 (NAO) to 79% (Probo) of the participants identified this gesture correctly. This may indicate that the pose of the arms plays a very large role in the correct recognition of this gesture. The added degrees of freedom that NAO possesses (1 degree of freedom in the wrist and actuated legs) do not seem to offer significant benefits over the prototype of the upper body of Probo. There are no indications that the speed of the gesturing influences the recognition rates.
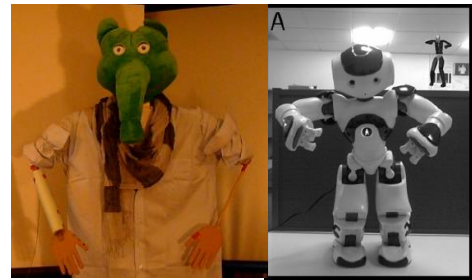

Fig. 66 Gestures for *Anger* **[43]**

For the gesture *Sadness*, the expressive poses seem to be similar (*fig. 67*): both the upper bodies lean forward with the arms hanging in front. A major difference is that the knees in the actuated legs of NAO are bent. Most of the participants in the study with NAO label this gesture either as *Sadness* or *Anger*, while in the study with the upper body of Probo, the participants label it mostly as either *Sadness* (38%) or *Disgust* (26%). It is remarkable that such a large part of the participants identify this gesture as *Disgust*, as they should be reasonably distant from each other on the Arousal axis (see *fig. 63*). The fact that the participants of the study incorrectly identified this gesture as *Disgust* can be possibly explained by the fact that *Sadness* was fifth out of the six gestures that the participants needed to label, with *Disgust* being the last. It is possible that some of the participants may not have recognized this gesture at all and saw that they had not yet chosen the option *Disgust* from the multiple choice question. The added degrees of freedom that NAO possesses in the arms do not seem to impact the recognition rates; rather, the orientation of the neck seems to be the most important factor (when the head of NAO is looking downwards, the recognition rates for this gesture increase from around 45% to 65%).
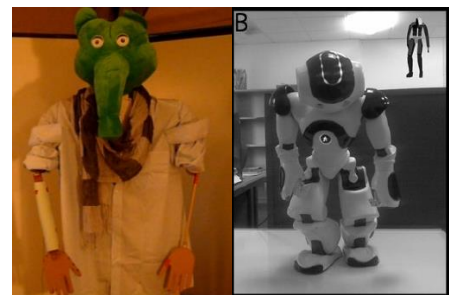
Fig. 67 Gestures for *Sadness* **[43]**

Looking at the gesture *Fear*, the arms of both the robots are lifted and held in front of the face (*fig. 68*). A major difference in the gesture is that the actuated knees of NAO are bent in order to make the body as small as possible and lean away, whereas the upper body of Probo can only rotate to the front to simulate this. This may be one reason that the number of participants that correctly identified this gesture in the study with NAO is higher (around 70%) than in the study with Probo (54%). For this gesture, the wrists of NAO are rotated so that the palms of the hands clearly face the camera, whereas in the study with the upper body of Probo, this is not so obvious (the fact that 30% of the participants of the study identify this gesture as *Sadness* may indicate that these participants interpret the gesture as using the hands to cover the eyes, as if Probo was crying). It is unknown if this directly adds to the increase in recognition rates or if the movement of the lower half of the body has a larger influence.

Fig. 68 Gestures for *Fear* **[43]**

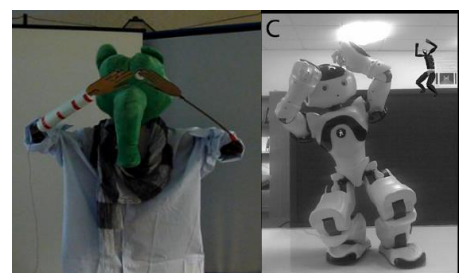Concerning the gesture *Happiness*, the expressive pose of the upper body of Probo is realized by lifting the arms high above the head, while the expressive pose of NAO seems to be more similar to Probo's gesture for *Surprise*: the upper body leans backwards and the lower arms are lifted in an angle of around 90° to the horizontal upper arms (*fig. 69*). However, since *Surprise* was not an option in the multiple choice question in this study with NAO, the participants could therefore not choose it. The recognition rate of this gesture in the study with the upper body of Probo is quite

Fig. 69 Gestures for *Happiness* **[43]**

similar (68%) to the results of the study with NAO when the options *Happiness* and *Excitement* are added together (around 65%). Since *Happiness* and *Excitement* are rather close to each other on the Arousal-Valence plane, the assumption is made that the rates can be combined. For this gesture, the wrist of the left arm of NAO is rotated, but as the recognition rates in both studies are very similar, this can be an indication that the added degree of freedom in the arms does not offer benefits.
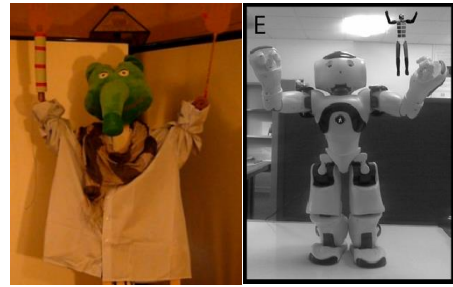
Regarding the gesture *Surprise* (*fig. 70*), as this was not performed in the study with NAO, no comparative conclusions can be drawn. The recognition rates of the study with the upper body of Probo of this gesture indicate a certain parallel to the results of the gesture *Happiness*: for this gesture, 68% of the people labeled this as *Happiness*, while 22% of the participants recognized it as *Surprise*. For *Surprise*, 60% of the participants labeled this as

Fig. 70 Gesture for *Surprise*

Surprise, with 26% of the participants calling it *Happiness*; which is very close to a complete reversal of the recognition rates. This indicates that there is a clear link between the two gestures and that they are too similar. It is unknown if this is due to the expressive poses being too similar or due to the fact that there is not enough difference in the speed of the gesturing. Nevertheless, there are no clear indications that added degrees of freedom in the arms would offer increased recognition rates.

Lastly, the gesture for *Disgust* (*fig. 71*) was recognized by 39% of the participants. The other two popular choices were *Fear* (34%) and *Surprise* (19%), meaning that the three most popular choices all lie rather close to each other (in the second quadrant of the Valence-Arousal plane), for a combined recognition rate of 92%. It is unknown if the individual recognition rates can be improved by either altering the expressive pose or by changing the speed of the gesturing, but as the vast majority of the participants could situate the gesture in the right quadrant, there are no indications that added degrees of freedom in the arms offer significantly increased recognition rates.

Fig. 71 Gesture for *Disgust*

In conclusion, in this Chapter 3.3 the recognition rates of the study using the prototype of the upper body of Probo, as described in Chapter 3.2, are compared to those of a study using the robot NAO since this is a similar study, both using social robots without an actuated face. Only for the gesture *Fear* are there are clear indications that the additional degrees of freedom in the arms of NAO increase the recognition rates. The gestures that were performed can however still be improved, either by modifying the expressive pose or by changing the speed of the gesturing. The fact that the participants indicate that the gestures are hard to recognize, may partly be explained by the lack of context regarding the gestures that the that the participants had during the survey.

Findings, conclusions and prospects for future work

In Part 1, the human arm and the state of the art of robotic arm systems for social robots are examined. It is established that the distinction can be made between arm systems developed for object manipulation and systems for gesturing, as they can implement other (or more) degrees of freedom, offer compliance or not, and need to cope with different amounts of external loading. A robotic arm that only needs to portray gestures does not always need the traditional 7 degrees of freedom. There are a number of social robots such as NAO [28], QRIO [37] and KASPAR II [40] that implement 3 degrees of freedom in the shoulder, one in the elbow and only 1 in the wrist (as an axial rotation of the forearm).

Based on this research and on the examination of the gestures that Probo [1] needs to be able to portray [13], the decision is made in Chapter 2.1 to implement 4 degrees of freedom in the arm: 3 degrees of freedom in the shoulder (XZX) and one in the elbow. Throughout Part 2, the mechanical properties that the arm needs to possess to accurately portray gestures are examined, starting from the method of transmitting the power from the actuators to the axis of the joints, then the entire 3D design and finally the choice of actuators based on simulations using the 3D model.

In Part 3, the prototype of the arm system is mounted to a temporary upper body, which can rotate to the front and to the back. This upper body is then used to portray six gestures: *Anger*, *Happiness*, *Surprise*, *Disgust*, *Sadness* and *Fear*, using motion trajectories generated by motion capturing [13]. The gestures are recorded and the videos are used in an electronic survey to test the recognition rates. The results of the survey are given in Chapter 3.3 and a comparison is made to a similar study using the robot NAO [43], which has one additional degree of freedom in the arm (apart from a 1 DOF hand-shaped gripper): an axial rotation of the forearm. This robot also has actuated legs, which may influence the recognition rates, in addition to an actuated neck (the recognition rates for the gestures with the head looking straight forward are used for the comparison).

It is concluded that for the gesture *Anger*, there are no indications that additional degrees of freedom in the arms offer increased recognition rates. Regarding the gesture *Sadness*, in both the studies that are compared, the recognition rates are rather low. This indicates that for this gesture, the largest influence on the rates may be an actuated face (the recognition rate of the isolated actuated head of Probo is much higher [8]) and neck (there is a large increase in recognition rates when the head of NAO is tilted downwards [43]), rather than the degrees of freedom in the arms. For the gesture *Fear*, the recognition rates of the study with NAO are higher than those of the upper body of Probo, however the actuation of the legs may have a significant influence. A large portion of the participants in the study with Probo identified this gesture as *Sadness*, which may indicate that an axial rotation of the forearms is needed to rotate the hands so that they are shielding the face, rather than covering the eyes, making it seem like Probo is crying. The speed of the gesturing may also have an influence. The recognition rates for the gesture *Happiness* are quite similar for both studies, while the gestures *Surprise* and *Disgust* were not performed by NAO, meaning that no comparison can be made. Regarding *Surprise*, the recognition rates indicate that this gesture and the gesture for *Happiness* are too similar, however it is assumed that this is caused by the motion trajectories and speed of gesturing. The gesture *Disgust* was identified by a large part of the participants as *Fear* or *Surprise*, but as those three emotions lie in the same quadrant of the Valence-Arousal plane, it can be assumed that a larger difference in arousal or speed of the gesturing is

needed, rather than an additional degree of freedom in the arms. In summary, for all of the performed gestures, there is no direct indication that adding degrees of freedom in the arms will have the single largest impact (from all other possible improvements such as an actuated neck or optimizing the speed of the gesturing) on the recognition rates.

Apart from the mechanisms that are needed purely for moving the arm, there are also a number of safety features implemented. In Part 1, the different methods of implementing compliance into a robotic arm in the state of the art are examined. Compliance can be done both active and passive, with different types of passive compliance being compared in Chapter 1.2.5. In Part 2, it is decided to use passive compliance in the form of non-variable stiffness SEA in the first prototype, which is a method in which an elastic element is used to transmit the power from the actuator to the joint [48]. The compliance will be implemented in the elbow joint and in the axial rotational of the upper arm, which causes compliant behavior in the arm for all directions of external forces except for those aligned with the axis of the lower arm. However, as there is no 'punching'-type gesture that Probo will perform, the external force should never be aligned with the axis. The compliance is implemented as two springs in the chain transmission for the elbow joint and using a servo saver (which simulates a torsion spring) for the joint S3. A comparison of the two methods is made in Chapter 2.4, where it is concluded that use of a torsion spring-type element is preferable. This element needs to be chosen with the optimal stiffness, so that it is flexible enough to deform at low external loads, but is still stiff enough to limit the deformation under the own weight and inertia.

Additionally, a method of collision detection is added under the form of an accelerometer that is 'calibrated' beforehand and measures the instantaneous accelerations of the last link during operation. This method gives adequate experimental results: the arm stops reasonably quick and blocking the arm never causes physical pain. However, the fact that the accelerations need to be established beforehand for every single movement of the arm makes it a rather unwieldy system.

For future work, the following improvements can be made regarding the recognition rates. The expressive poses and speed of gesturing (and motion trajectories) can be modified and optimized. Should there be the desire to implement additional degrees of freedom in the wrist or an actuated end effector, the design of the elbow joint and the lower arm needs to be fortified. The rest of the design can be optimized so that it is in correct proportion with the actual head and upper body of Probo. The arms can be attached to the real upper body of Probo and the gestures of the arms can be synchronized to the facial expressions in order to test the recognition rates and compare them to the rates of the isolated head or to the rates of the isolated arms and hips (described in this document). This comparison will give the best indication of the benefits of adding an actuated arm system to the body of Probo regarding the recognition rates.

Regarding the safety features implemented in the arm, the methods of compliance can be modified to use torsion springs. Additionally, this may be improved by expanding the systems to include variable stiffness. The method of collision detection can be improved by using a mechanism that uses the angles in the joints rather than the accelerations, to avoid having to calibrate for each new gesture or for every time that the design is modified. However, the accelerations may be used to obtain the position of the arm and this data can be used in the controller to identify a possible collision or malfunctioning once the kinematics and dynamics are implemented in the controller.

Bibliography

[1] Kristof Goris, "The Development of the Huggable Social Robot Probo: On the Hardware Design and Construction," Vrije Universiteit Brussel, Ph.D. dissertation 2009.

[2] C.L. Breazeal, *Designing Sociable Robots*.: MIT Press, 2004.

[3] MIT Media Lab. (2012) Personal robots group. [Online]. http://robotic.media.mit.edu

[4] Hasbro Inc. (2013) Furby, A Mind Of Its Own. [Online]. www.furby.com

[5] K. Goris, J. Saldien, I. Vanderniepen, and D. Lefeber, "The Huggable Robot Probo, a Multi-Disciplinary Research Platform," *Research and Education in Robotics*, vol. 33, pp. 29-41, 2009.

[6] B. Vanderborght, R. Simut, J. Saldien, C. Pop, A. S. Rusu, S. Pintea, D. Lefeber, and D. O. David, "Using the social robot probo as a social story telling agent for children with ASD," *Interaction Studies*, vol. 13, no. 3, pp. 348-372, 2012.

[7] Greet Van de Perre, Ramona Simut, Bram Vanderborght, Jelle Saldien, and Dirk Lefeber, "About the design of the social robot Probo, facilitator for ASD therapies," in *9th National Congress on Theoretical and Applied Mechanics*, 2012.

[8] J. Saldien, K. Goris, B. Vanderborght, J. Vanderfaeillie, and D. Lefeber, "Expressing Emotions with the Social Robot Probo," *International Journal of Social Robotics*, vol. 2, no. 4, pp. 377-389, 2010.

[9] J. Cassell, T. Bickmore, M. Billinghurst, L. Campbell, K. Chang, H. Vilhjálmsson, and H. Yan, "Embodiment in Conversational Interfaces: Rea," in *Proceedings of the SIGCHI conference on Human factors in computing systems: The CHI is the limit*, 1999, pp. 520-527.

[10] E.T. Hall, *The Dance of Life: The Other Dimension of Time*.: Anchor, 1984.

[11] Albert Mehrabian, *Silent Messages*.: Wadsworth Publishing Company, 1971.

[12] M. Zecca, Y. Mizoguchi, K. Endo, F. Iida, Y. Kawabata, N. Endo, K. Itoh, and A. Takanishi, "Whole Body Emotion Expressions for KOBIAN Humanoid Robot -Preliminary Experiments with Different Emotional Patterns-," in *Robot and Human Interactive Communication, 2009. RO-MAN 2009. The 18th IEEE International Symposium on*, 2009, pp. 381-386.

[13] Steven Depue, "Kinematics and Dynamics of the arm system of the social robot Probo," MA1 project dissertation, unpublished 2012.

[14] I.A. Kapandji, *Bewegingsleer*.: Bohn Stafleu van Loghum, 2009.

[15] N. Klopčar, M. Tomšič, and J. Lenarčič, "A Kinematic Model of the Shoulder Complex to Evaluate the Arm-reachable Workspace," *Journal of Biomechanics*, vol. 40, no. 1, pp. 86-91, 2007.

[16] C. Högfors, G. Sigholm, and P. Herberts, "Biomechanical Model of the Human Shoulder—I. Elements," *Journal of biomechanics*, vol. 20, no. 2, pp. 157-166, 1987.

[17] G. Rab, K. Petuskey, and A. Bagley, "A Method for Determination of Upper Extremity Kinematics," *Gait & posture*, vol. 15, no. 2, pp. 113-119, 2002.

[18] D. Matsui, T. Minato, K.F. MacDorman, and H. Ishiguro, "Generating Natural Motion in an Android by Mapping Human Motion," in *Intelligent Robots and Systems, 2005.(IROS 2005). 2005 IEEE/RSJ International Conference on*, 2005, pp. 3301-3308.

[19] G. ElKoura and K. Singh, "Handrix: Animating the Human Hand," in *Proceedings of the 2003 ACM SIGGRAPH/Eurographics symposium on Computer animation*, 2003, pp. 110-119.

[20] A. Albu-Schaffer, O. Eiberger, M. Grebenstein, S. Haddadin, C. Ott, T. Wimbock, S. Wolf, and G. Hirzinger, "Soft Robotics," *Robotics & Automation Magazine, IEEE*, vol. 15, no. 3, pp. 20-30, 2008.

[21] Honda Worldwide. (2012) Improved Task Performing Capabilities. [Online]. http://world.honda.com/ASIMO/technology/2011/performing/index.html

[22] B.R. Duffy, "Anthropomorphism and the Social Robot," *Robotics and Autonomous Systems*, vol. 42, no. 3, pp. 177-190, 2003.

[23] C. Ott, O. Eiberger, W. Friedl, B. Bauml, U. Hillenbrand, C. Borst, A. Albu-Schaffer, B. Brunner, H. Hirschmuller, and S. Kielhofer, "A Humanoid Two-arm System for Dexterous Manipulation," in *Humanoid Robots, 2006 6th IEEE-RAS International Conference on*, 2006, pp. 276-283.

[24] C. Breazeal, G. Hoffman, and A. Lockerd, "Teaching and Working with Robots as a Collaboration," in *Proceedings of the Third International Joint Conference on Autonomous Agents and Multiagent Systems*, vol. 3, 2004, pp. 1030-1037.

[25] C. Breazeal, M. Siegel, M. Berlin, J. Gray, R. Grupen, P. Deegan, J. Weber, K. Narendran, and J. McBean, *Mobile, dexterous, social robots for mobile manipulation and human-robot interaction*.: ACM, 2008.

[26] N. Tsagarakis, G. Metta, G. Sandini, D. Vernon, R. Beira, F. Becchi, L. Righetti, J. Santos-Victor, A. Ijspeert, and M. Carrozza, "iCub: The Design and Realization of an Open Humanoid Platform for Cognitive and Neuroscience Research," *Advanced Robotics*, vol. 21, no. 10, pp. 1151-1175, 2007.

[27] H. Miwa, K. Itoh, M. Matsumoto, M. Zecca, H. Takanobu, S. Rocella, M. Carrozza, P. Dario, and A. Takanishi, "Effective Emotional Expressions with Emotion Expression Humanoid Robot WE-4RII: Integration of Humanoid Robot Hand RCH-1," in *Intelligent Robots and Systems, 2004.(IROS 2004). Proceedings. 2004 IEEE/RSJ International Conference on*, vol. 3, 2004, pp. 2203-2208.

[28] D. Gouaillier, V. Hugel, P. Blazevic, C. Kilner, J. Monceaux, P. Lafourcade, B. Marnier, J. Serre, and B. Maisonnier, "Mechatronic design of NAO humanoid," in *Robotics and Automation, 2009.*

ICRA'09. IEEE International Conference on, 2009, pp. 769-774.

[29] H. Kozima, "Infanoid," *Socially Intelligent Agents*, vol. 3, pp. 157-164, 2002.

[30] T. Asfour, K. Regenstein, P. Azad, J. Schroder, A. Bierbaum, N. Vahrenkamp, and R. Dillmann, "ARMAR-III: An Integrated Humanoid Platform for Sensory-Motor Control," in *Humanoid Robots, 2006 6th IEEE-RAS International Conference on*, 2006, pp. 169-175.

[31] K.A. Wyrobek, E.H. Berger, H.F.M. Van der Loos, and J.K. Salisbury, "Towards a Personal Robotics Development Platform: Rationale and Design of An Intrinsically Safe Personal Robot," in *Robotics and Automation, 2008. ICRA 2008. IEEE International Conference on*, 2008, pp. 2165-2170.

[32] Willow Garage. (2012) PR2 Hardware Specs. [Online].
http://www.willowgarage.com/pages/pr2/specs

[33] E. Guizzo and E. Ackerman, "The Rise of the Robot Worker," *IEEE Spectrum*, vol. 49, no. 10, pp. 34-41, October 2012.

[34] R. Hirose and T. Takenaka, "Development of the Humanoid Robot ASIMO," *Honda R&D Technical Review*, vol. 13, no. 1, pp. 1-6, 2001.

[35] Honda Worldwide. (2012) ASIMO Key Specifications. [Online].
http://world.honda.com/ASIMO/technology/2011/specification/

[36] H. G. Marques, M. Jantsch, S. Wittmeier, O. Holland, C. Alessandro, A. Diamond, M. Lungarella, and R. Knight, "Ecce1: The first of a series of anthropomimetic musculoskeletal upper torsos," in *Humanoid Robots (Humanoids), 2010 10th IEEE-RAS International Conference on*, 2010, pp. 391-396.

[37] L. Geppert, "QRIO, the robot that could," *IEEE Spectrum*, vol. 41, no. 5, pp. 34-37, 2004.

[38] N. Mitsunaga, T. Miyashita, H. Ishiguro, K. Kogure, and N. Hagita, "Robovie-IV: A communication robot interacting with people daily in an office," in *Intelligent Robots and Systems, 2006 IEEE/RSJ International Conference on*, 2006, pp. 5066-5072.

[39] F. Guenter, L. Roos, A. Guignard, and A.G. Billard, "Design of A Biomimetic Upper Body for the Humanoid Robot Robota," in *Humanoid Robots, 2005 5th IEEE-RAS International Conference on*, 2005, pp. 56-61.

[40] K. Dautenhahn, C. Nehaniv, M. Walters, B. Robins, H. Kose-Bagci, N. Mirza, and M. Blow, "KASPAR: A Minimally Expressive Humanoid Robot for Human-Robot Interaction Research," *Applied Bionics and Biomechanics*, vol. 6, no. 3-4, pp. 369-397, 2009.

[41] Arjan Westerhuis, "Design and Evaluation of a 3-DOF Spherical Parallel Mechanism for Domestic Robot Arms," University of Twente, Master's thesis 2012.

[42] H. Miwa, K. Itoh, D. Ito, H. Takanobu, and A. Takanishi, "Design and Control of 9-DOFs Emotion Expression Humanoid Arm," in *Robotics and Automation, 2004. Proceedings. ICRA'04. 2004 IEEE International Conference on*, vol. 1, 2004, pp. 128-133.

[43] Aryel Beck, Lola Cañamero, and Kim A Bard, "Towards an affect space for robots to display emotional body language," in *RO-MAN, 2010 IEEE*, 2010, pp. 464-469.

[44] H. Ishiguro, T. Ono, M. Imai, T. Maeda, T. Kanda, and R. Nakatsu, "Robovie: An Interactive Humanoid Robot," *Industrial robot: An international journal*, vol. 28, no. 6, pp. 498-504, 2001.

[45] P. Kahn Jr, T. Kanda, H. Ishiguro, N. Freier, R. Severson, B. Gill, J. Ruckert, and S. Shen, ""Robovie, you'll have to go into the closet now": Children's social and moral relationships with a humanoid robot.," *Developmental psychology*, vol. 48, no. 2, pp. 303-314, 2012.

[46] S. Roccella, M. Carrozza, G. Cappiello, P. Dario, J. Cabibihan, M. Zecca, H. Miwa, K. Itoh, and M. Marsumoto, "Design, fabrication and preliminary results of a novel anthropomorphic hand for humanoid robotics: RCH-1," in *Intelligent Robots and Systems, 2004.(IROS 2004). Proceedings. 2004 IEEE/RSJ International Conference on*, vol. 1, 2004, pp. 266-271.

[47] M. Zinn, O. Khatib, B. Roth, and J.K. Salisbury, "Playing It Safe [Human-Friendly Robots]," *Robotics & Automation Magazine, IEEE*, vol. 11, no. 2, pp. 12-21, 2004.

[48] R. Ham, T. Sugar, B. Vanderborght, K. Hollander, and D. Lefeber, "Compliant Actuator Designs," *Robotics & Automation Magazine, IEEE*, vol. 16, no. 3, pp. 81-94, 2009.

[49] R. Alexander, "Three uses for springs in legged locomotion," *The International Journal of Robotics Research*, vol. 9, no. 2, pp. 53-61, 1990.

[50] A. Albu-Schaffer, C. Ott, U. Frese, and G. Hirzinger, "Cartesian impedance control of redundant robots: Recent results with the DLR-Light-Weight-Arms," in *Robotics and Automation, 2003. Proceedings. ICRA'03. IEEE International Conference on*, vol. 3, 2003, pp. 3704-3709.

[51] T. Wimbock, C. Ott, and G. Hirzinger, "Impedance behaviors for two-handed manipulation: Design and experiments," in *Robotics and Automation, 2007 IEEE International Conference on*, 2007, pp. 4182-4189.

[52] R. Wistort and C. Breazeal, "TOFU: A Socially Expressive Robot Character for Child Interaction," in *Proceedings of the 8th International Conference on Interaction Design and Children*, 2009, pp. 292-293.

[53] S. Nishio, H. Ishiguro, and N. Hagita, "Geminoid: Teleoperated android of an existing person," *Humanoid Robots: New Developments*, vol. 14, pp. 343-352, 2007.

[54] John McBean and Cynthia Breazeal, "Voice coil actuators for human-robot interaction," in *Intelligent Robots and Systems, 2004.(IROS 2004). Proceedings. 2004 IEEE/RSJ International Conference on*, vol. 1, 2004, pp. 852-858.

BIBLIOGRAPHY

[55] G.A. Pratt and M.M. Williamson, "Series Elastic Actuators," in *Intelligent Robots and Systems 95.'Human Robot Interaction and Cooperative Robots', Proceedings. 1995 IEEE/RSJ International Conference on*, vol. 1, 1995, pp. 399-406.

[56] M. Quigley, A. Asbeck, and A. Ng, "A Low-cost Compliant 7-DOF Robotic Manipulator," in *Robotics and Automation (ICRA), 2011 IEEE International Conference on*, 2011, pp. 6051-6058.

[57] ECCEROBOT (Embodied Cognition in a Compliantly Engineered Robot). (2013) Actuator Subsystem. [Online]. http://eccerobot.org/home/robot/actuatorsubsystem

[58] B. Verrelst, R. Ham, B. Vanderborght, F. Daerden, D. Lefeber, and J. Vermeulen, "The pneumatic biped "Lucy" actuated with pleated pneumatic artificial muscles," *Autonomous Robots*, vol. 18, no. 2, pp. 201-213, 2005.

[59] C. Ott, A. Albu-Schaffer, A. Kugi, S. Stamigioli, and G. Hirzinger, "A Passivity Based Cartesian Impedance Controller for Flexible Joint Robots - Part I: Torque Feedback and Gravity Compensation," in *Robotics and Automation, 2004. Proceedings. ICRA'04. 2004 IEEE International Conference on*, vol. 3, 2004, pp. 2659-2665.

[60] T. Rahman, R. Ramanathan, R. Seliktar, and W. Harwin, "A Simple Technique to Passively Gravity-Balance Articulated Mechanisms," *Journal of Mechanical Design*, vol. 117, pp. 655-657, 1995.

[61] Gabriëlle JM Tuijthof and Just L Herder, "Design, actuation and control of an anthropomorphic robot arm," *Mechanism and machine theory*, vol. 35, no. 7, pp. 945-962, 2000.

[62] Keenan A Wyrobek, Eric Berger, and J Kenneth JR Salisburger, "Electromechanically counterbalanced humanoid robotic system," US20100243344, 2010.

[63] A. De Luca, B. Siciliano, and L. Zollo, "PD control with on-line gravity compensation for robots with elastic joints: Theory and experiments," *Automatica*, vol. 41, no. 10, pp. 1809-1819, 2005.

[64] J. B. Spicer, C. J. Richardson, M. J. Ehrlich, J. R. Bernstein, M. Fukuda, and M. Terada, "Effects of frictional loss on bicycle chain drive efficiency," *Journal of Mechanical Design*, vol. 123, pp. 598-605, 2001.

[65] Irving Griffel, "Chain drive," US3495468, 1970.

[66] Hiroyuki Takeda and Tetsuji Kotera, "Low noise chain drive," US5419743, 1995.

[67] ServoCity. (2013) Plastic Chain. [Online]. http://www.servocity.com/html/plastic_chain.html

[68] Savöx. (2013) Coreless Motor. [Online]. http://www.savoxtech.com.tw/

[69] Preston Blair, *Cartooning: Animation 1 with Preston Blair*.: Walter Foster, 1947.

[70] AnimationArchive (Through WebArchive). (2013) Media: Preston Blair's Animation First Edition. [Online].

http://web.archive.org/web/20060508201758/http://www.animationarchive.org/2006/05/media-preston-blairs-animation-first.html

[71] RS Components. (2013) Electrical and Electronical Components. [Online]. http://be02.rs-online.com/web/

[72] Pirate4x4. (2013) The largest off roading website in the world. [Online]. www.pirate4x4.com

[73] JunFac. (2013) Online Store. [Online]. http://www.junfac.com/

[74] Kathy L Walters and Richard D Walk, "Perception of emotion from moving body cues in photographs," *Bulletin of the Psychonomic Society*, vol. 26, no. 2, pp. 112-114, 1988.

[75] Richard D Walk and Carolyn P Homan, "Emotion and dance in dynamic light displays," *Bulletin of the Psychonomic Society*, vol. 22, no. 5, pp. 437-440, 1984.

[76] Frank Thomas and Ollie Johnston, *The illusion of life: Disney animation*.: Hyperion New York, 1995.

[77] Limesurvey. (2013) The open source survey application. [Online]. http://www.limesurvey.org/

[78] Andrea Kleinsmith, P Ravindra De Silva, and Nadia Bianchi-Berthouze, "Cross-cultural differences in recognizing affect from body posture," *Interacting with Computers*, vol. 18, no. 6, pp. 1371-1389, 2006.

[79] M Haring, Nikolaus Bee, and Elisabeth Andre, "Creation and evaluation of emotion expression with body movement, sound and eye color for humanoid robots," in *RO-MAN, 2011 IEEE*, 2011, pp. 204-209.

[80] HCM Lab. (2013) Emotion Expression with NAO (RO-MAN 2011). [Online]. http://www.youtube.com/watch?v=IXoTM9apowE

[81] J Richard Landis and Gary G Koch, "The measurement of observer agreement for categorical data," *Biometrics*, vol. 33, no. 1, pp. 159-174, 1977.

[82] SKF. (2013) Deep groove ball bearings, single row 61802. [Online]. http://www.skf.com/group/products/bearings-units-housings/ball-bearings/deep-groove-ball-bearings/single-row/index.html?prodid=1010021802

[83] MakeItFrom.com. (2013) Compare Materials: MDF to PVDF. [Online]. http://www.makeitfrom.com/compare-materials/?A=Medium-Density-Fiberboard-MDF&B=Polyvinylidene-Fluoride-PVDF

[84 The Engineering Toolbox. (2013) Elastic Properties and Young Modulus for some Materials. [Online]. http://www.engineeringtoolbox.com/young-modulus-d_417.html
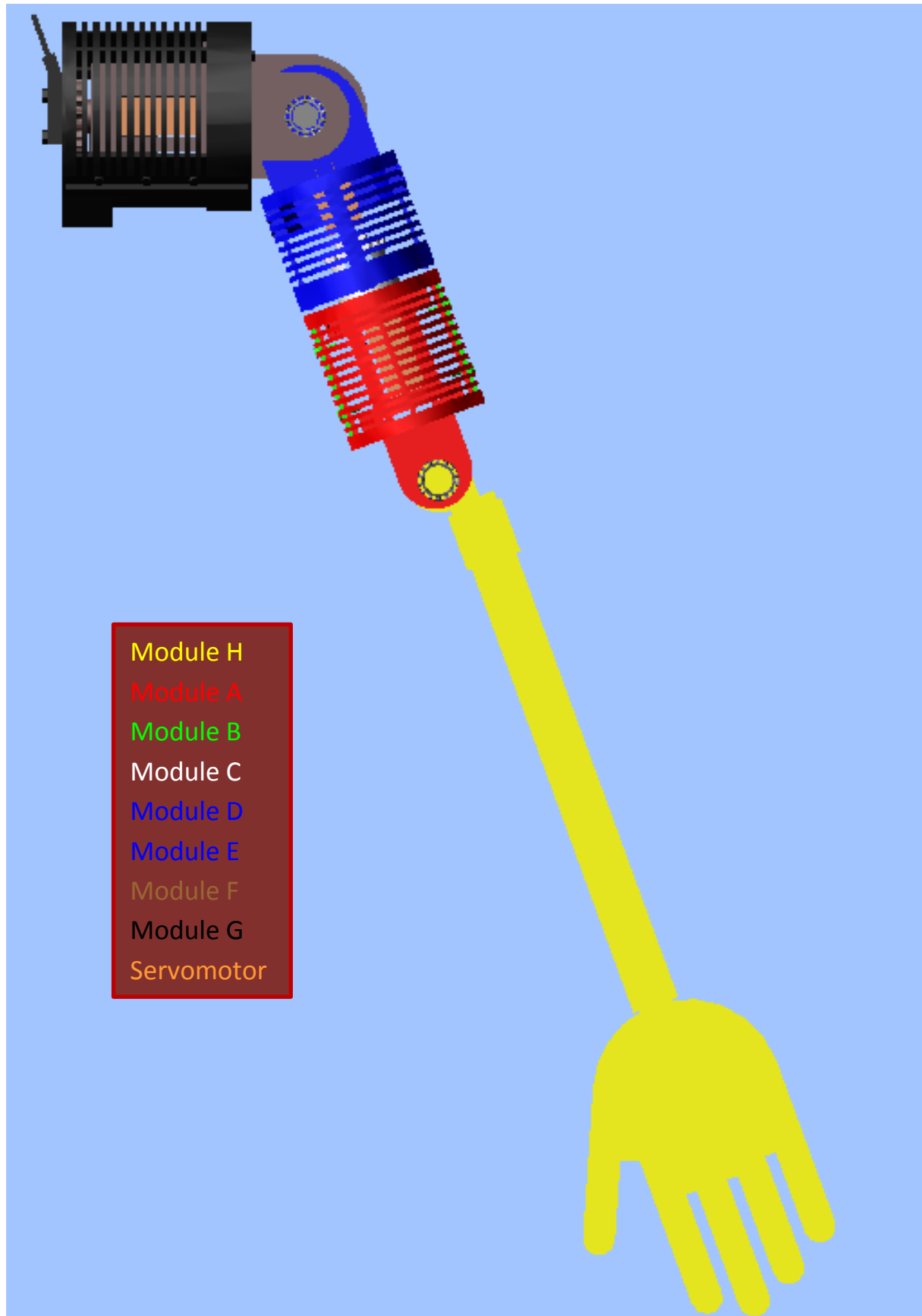
Appendix A: 3D model of the different modules

Module H
Module A
Module B
Module C
Module D
Module E
Module F
Module G
Servomotor

Fig. 72 Front view of the 3D model in MSC Adams 2012

Module H
Module A
Module B
Module C
Module D
Module E
Module F
Module G
Servomotor

Fig. 73 Rear view of the 3D model in MSC Adams 2012

Appendix B: Computation of the rotational stiffness of the elbow joint at no load

Arc length of a rotation of 1 rad on the driven sprocket of joint E:

$$Arc\ length\ (1rad) = r = \frac{26.54mm}{2} = 13.27mm$$

The spring is extended with this length. The force exerted by the spring by this extension is:

$$F = k * \Delta x = 0.9\frac{N}{mm} * 13.27mm = 11.94N$$

The moment on the joint caused by this force is equal to:

$$Moment = F * r = 0.158Nm$$

This means that the rotational stiffness of the elbow joint is equal to

$$k_{rot,spring} = 0.158\frac{Nm}{rad}$$
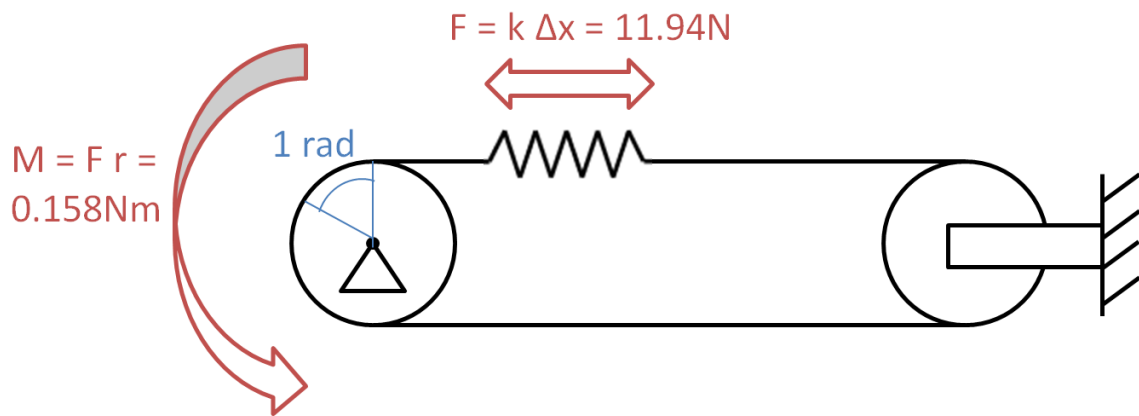
Fig. 74 Moment on the elbow joint at a rotation of 1 rad

Appendix C: Assessment of the stress in the structure due to the preload on the springs
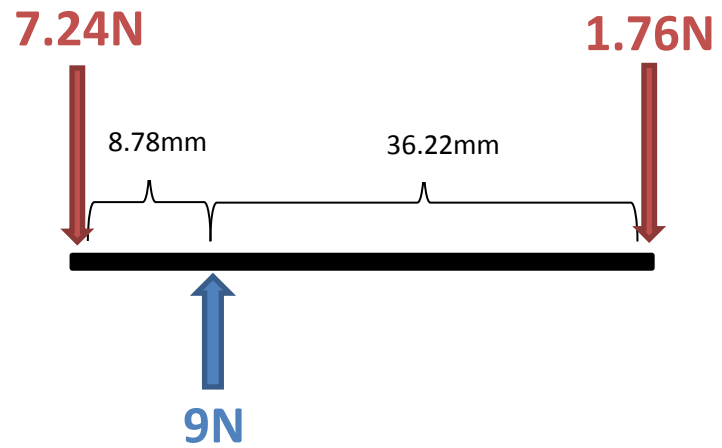
Fig. 75 (left) 3D model and (right) schematic overview of the preload forces working on the elbow axis

Load on the driven sprocket = 9N (2 identical springs with preload 4.5N in parallel)

Or if all dimensions stay the same, with only a change in spring stiffness k (in $\frac{N}{mm}$) :

Load on the driven sprocket = $2 * k * 5mm = k * 10mm$

Reaction force on left bearing: $F_L = \frac{36.22mm}{45mm} * 9N = 7.24N = k * 8.05mm$

Reaction force on right bearing: $F_R = \frac{8.78mm}{45mm} * 9N = 1.76N = k * 1.95mm$

Maximal allowable radial static load on bearings SKF 61802 = 800N (supplier given [82])

Maximal bending moment on elbow axis: $M_b = 7.24N * 8.78mm = 0.064Nm = k * 70.68mm$

In order to simulate the stresses resulting from the loading, a simplified model of the structure is used in a finite elements simulation in Altair Hyperworks 11.0. The MDF components that are in reality bolted together, are considered to be connected over the whole surface (the connections, which can be seen as the glue between the MDF slices, are considered to have the same properties as the MDF wood). Other simplifications of the structure are implemented, as finite elements stress analysis is a non-linear computation and the results are heavily dependent on the mesh quality.

The structure is meshed with a volume tetra-mesh with element size 3.6mm. Most of the structure is made out of MDF (Young's modulus = 4GPa, density = 0.75 g/cm³ [83]), while the M6 bolts that keep the servo holder into place, the servomotor itself and the bearings are elements with the properties of steel (Young's modulus = 210GPa, density = 7.9 g/cm³ [84]).

The forces coming from the preload on the springs are modeled as two point forces of 9N, one on the center of the elbow axis where the driven sprocket is and one on the actuated end of the servomotor, where the actuated sprocket is.
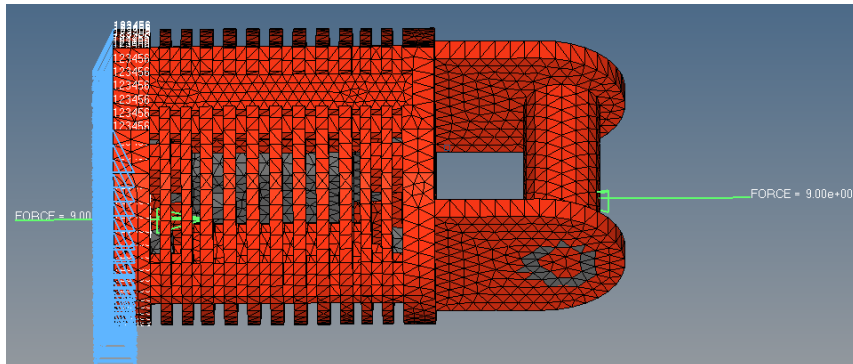
Fig. 76 Altair Hyperworks 11.0 simplified finite elements model of the elbow joint

The highest stresses (Von Mises) on the whole structure takes place on the end of the servomotor where the point force is located, and is equal to 1.06MPa (*fig. 77*). In reality, here the actuated sprocket is connected to the servomotor with a steel M3 bolt, therefore this should not pose a problem.
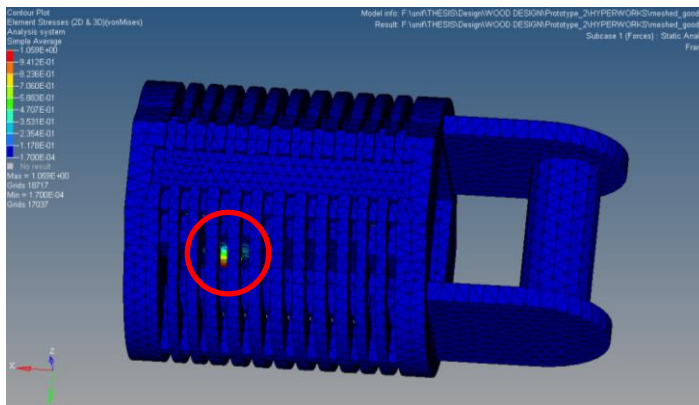
Fig. 77 Von Mises stresses on the structure

The highest stresses on the MDF are situated at the connections between the sides of the servomotor and the thin MDF plates in the servo holder (*fig. 78*). Here, the stress is approximately 0.47MPa. However, as this connection is done by steel M3 bolts in the real prototype; it is expected that there is no cause for failure anywhere in the structure due to the preload on the current springs.
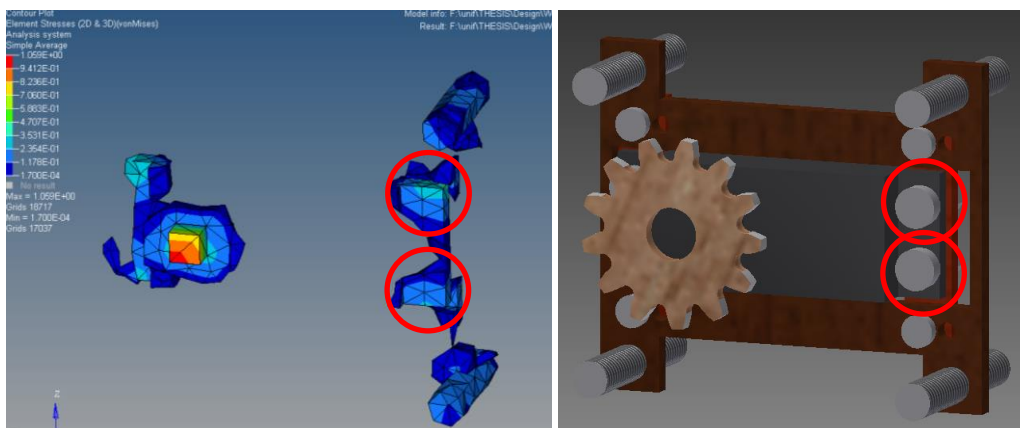
Fig. 78 Highest Von Mises stresses on the MDF

Appendix D: Comparison of recognition rates of female and male participants

Table 20 Comparison of the recognition rates of female and male participants

Recognition rates of the upper body of Probo: female/*male* participants (Chance level would be 17%)						
% Match	Fear	Surprise	Anger	Happiness	Sadness	Disgust
GESTURE1 (Fear)	59/*52*	4/*10*	0/*0*	0/*4*	30/*30*	7/*4*
GESTURE2 (Surprise)	11/*6*	48/*66*	0/*0*	30/*24*	7/*0*	4/*4*
GESTURE3 (Anger)	0/*0*	0/*10*	85/*76*	0/*0*	4/*4*	11/*10*
GESTURE4 (Happiness)	0/*8*	30/*18*	0/*2*	67/*68*	4/*0*	0/*4*
GESTURE5 (Sadness)	22/*2*	4/*8*	11/*16*	7/*6*	41/*36*	15/*32*
GESTURE6 (Disgust)	26/*38*	30/*14*	0/*2*	4/*4*	4/*2*	37/*40*

Table 21 Visual comparison of the recognition rates of female and male participants

Gesture	Recognition rates of 27 female participants	Recognition rates of 50 male participants
Anger		
Sadness		

Gesture	Recognition rates of 27 female participants	Recognition rates of 50 male participants
Fear	Disgust 7%, Sadness 30%, Fear 59%, Surprise 4%	Disgust 4%, Sadness 30%, Fear 52%, Happiness 4%, Surprise 10%
Happiness	Sadness 4%, Surprise 29%, Happiness 67%	Disgust 4%, Fear 8%, Surprise 18%, Anger 2%, Happiness 68%
Surprise	Sadness 7%, Disgust 4%, Fear 11%, Happiness 30%, Surprise 48%	Disgust 4%, Fear 6%, Happiness 24%, Surprise 66%
Disgust	Disgust 37%, Fear 26%, Surprise 29%, Sadness 4%	Disgust 40%, Fear 38%, Happiness 4%, Surprise 14%

Appendix E: Assembling the robotic arm for the social robot Probo in 23 steps

Part 1: Assembling modules H, A and B
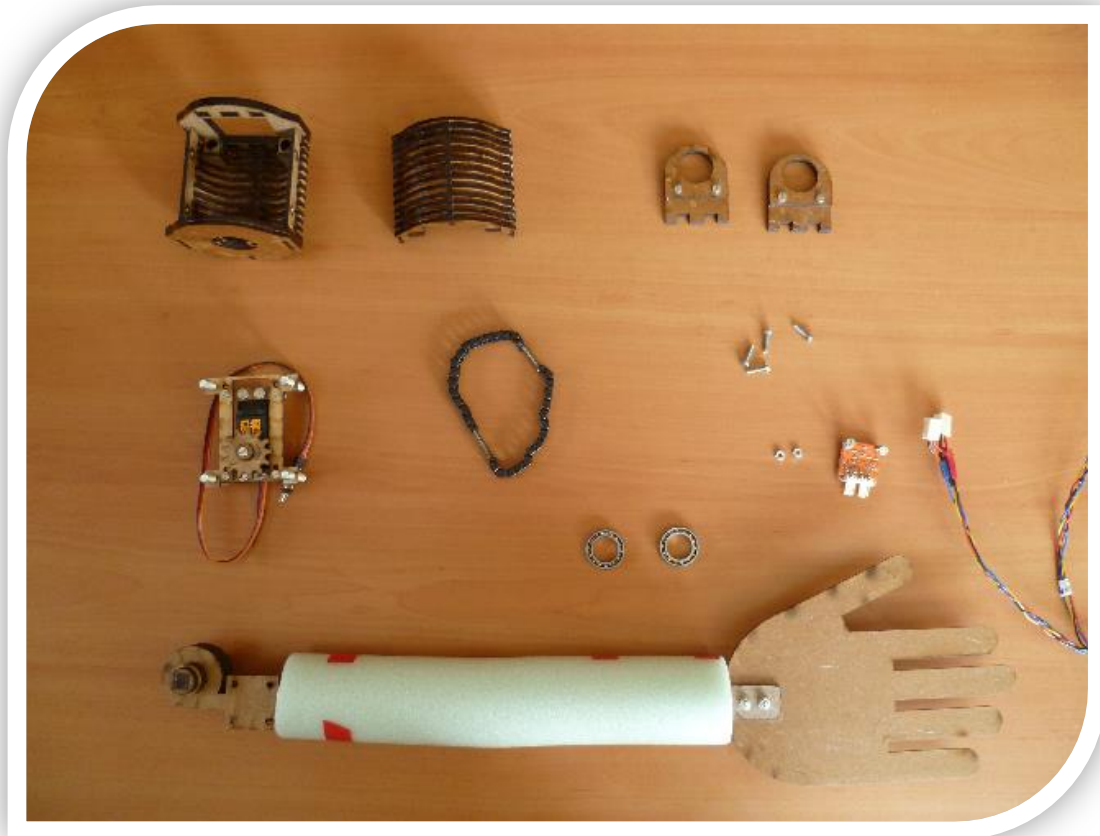
Fig. 79 Assembly: Step 1

1. Use a microcontroller to rotate servomotor *ServoE* to 180°.

2. Place the chain on the sprocket in such a way that the springs will not be pulled on the sprocket during rotation.
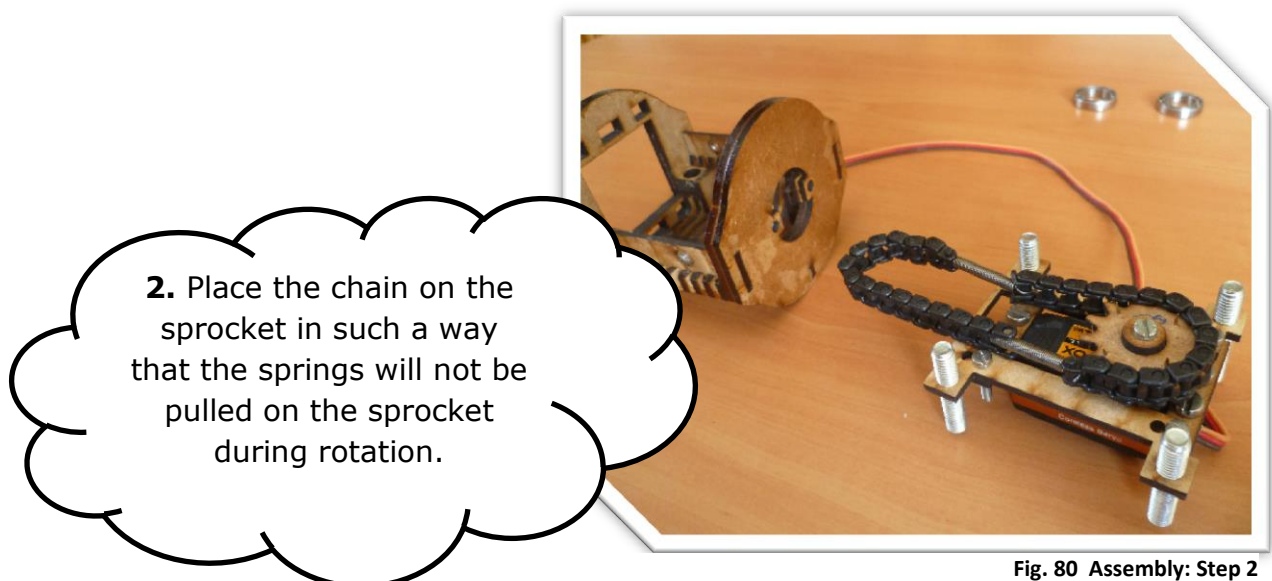
Fig. 80 Assembly: Step 2
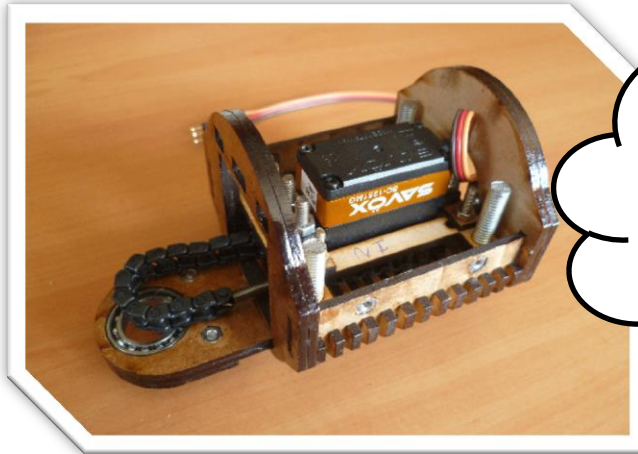
3. Place the holder for the servomotor in Module A. Place the first holder for the elbow axis, with its bearing, in Module A.

Fig. 81 Assembly: Step 3

4. Place the sprocket of the elbow axis in the chain and mount one side of the elbow axis in the bearing.
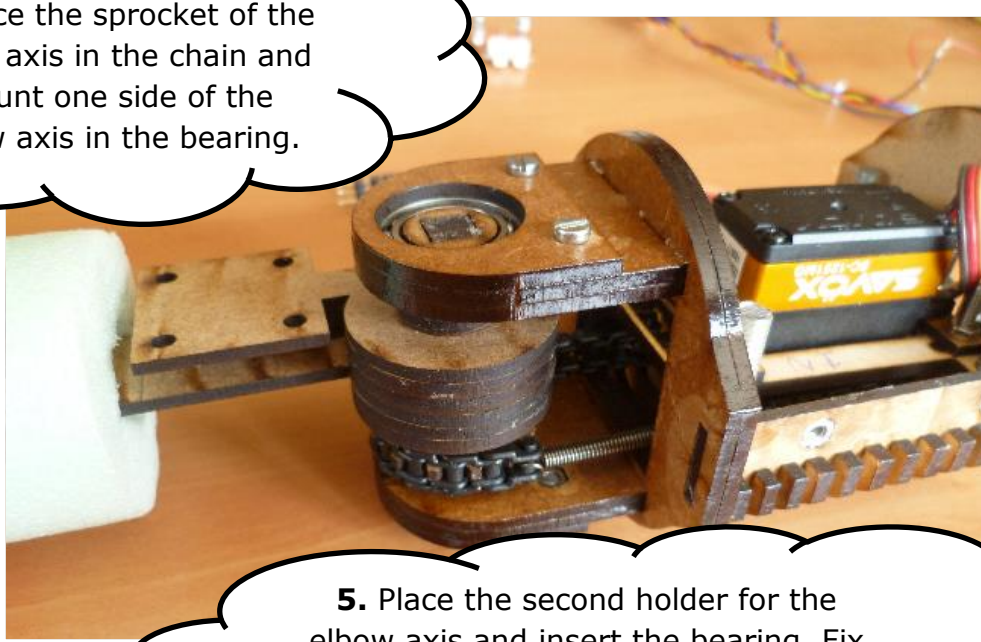
5. Place the second holder for the elbow axis and insert the bearing. Fix the bearing into place in the holder with the smaller piece and the two M3 bolts.

Fig. 82 Assembly: Step 4 and 5

6. Mount the accelerometer on Module H and attach the wires.
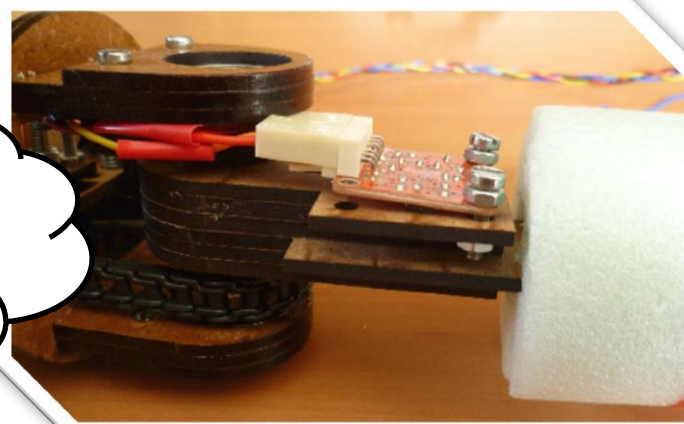
Fig. 83 Assembly: Step 6

Fig. 84 Assembly: Step 7

7. Guide the wires from the accelerometer and the servomotor through the end of Module A. Place Module B on Module A and close the modules up with four M3 bolts.

Fig. 85 Assembled modules H, A and B

Part 2: Assembling Modules C, D and E
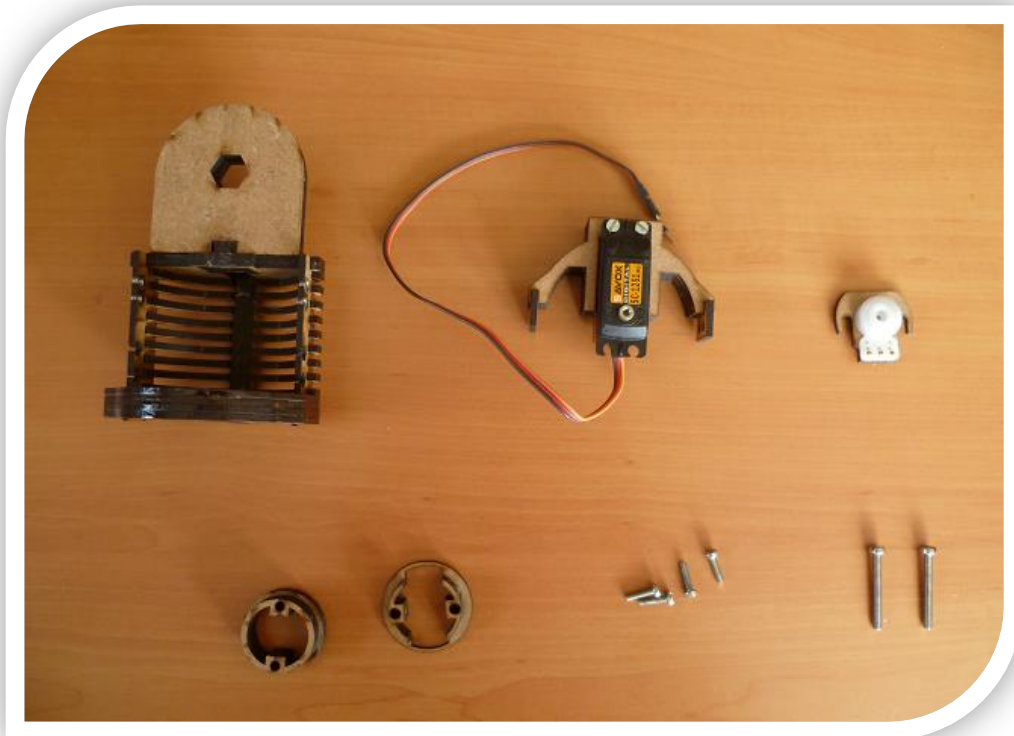
Fig. 86 Assembly: Step 8

8. Use a microcontroller to rotate servomotor *ServoS3* to 30°.
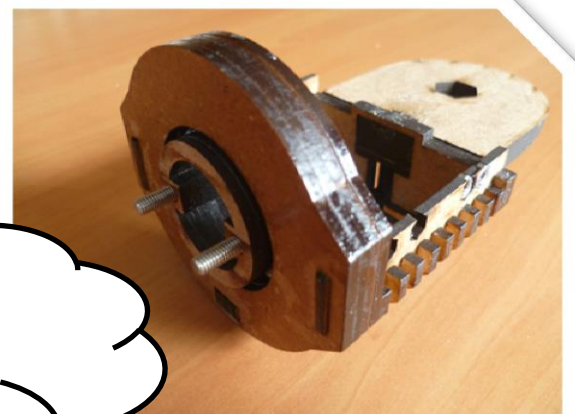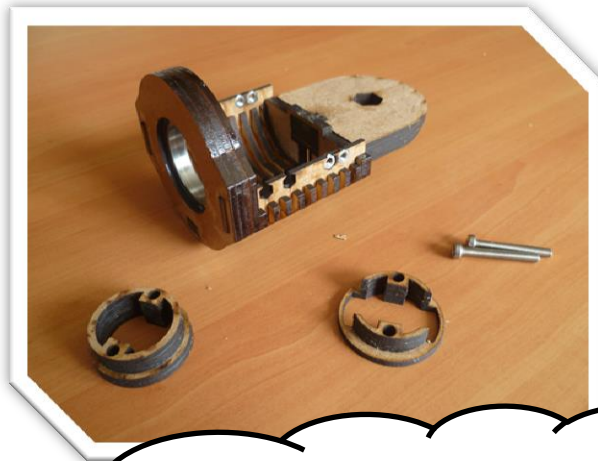
9. Place the two parts of Module C around the bearing and insert the two long M4 bolts.

Fig. 87 Assembly: Step 9
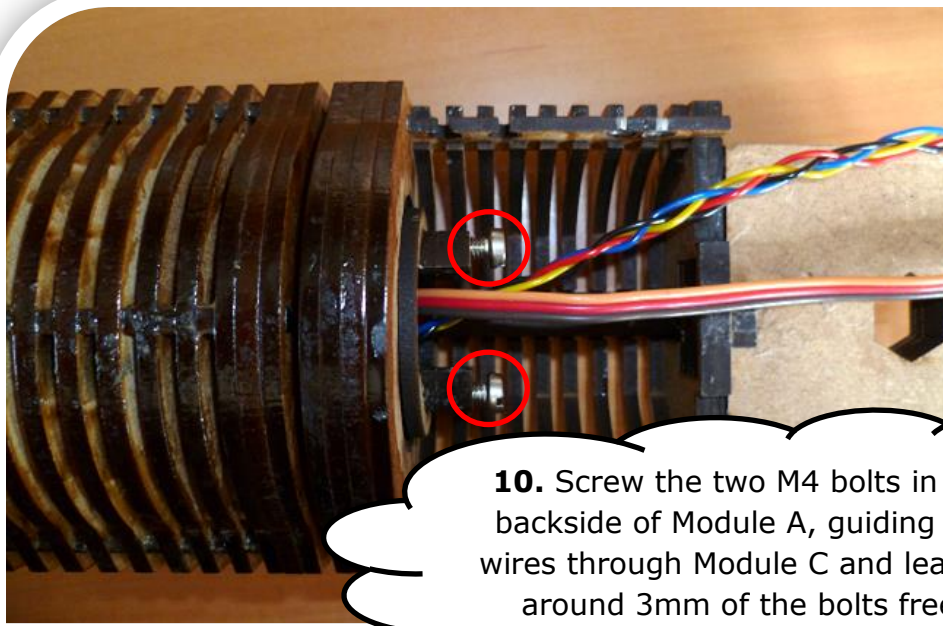
10. Screw the two M4 bolts in the backside of Module A, guiding the wires through Module C and leaving around 3mm of the bolts free.

Fig. 88 Assembly: Step 10

11. Place the servo saver with the attachment on the servomotor on Module E.
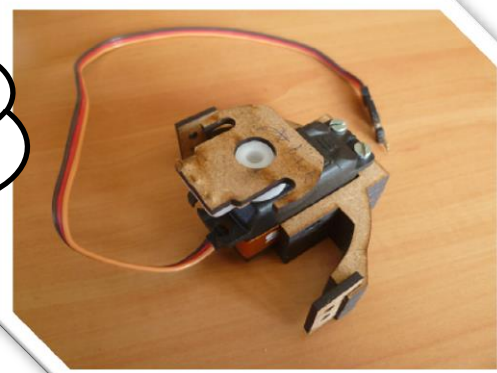
Fig. 89 Assembly: Step 11
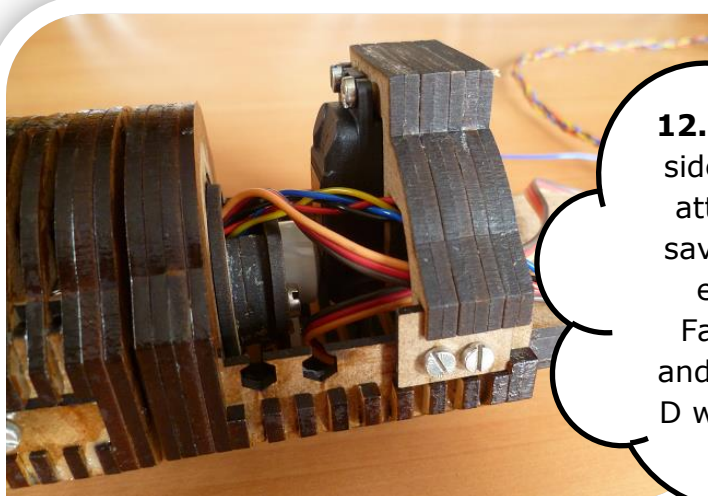
12. Slide Module E into the side of Module D, with the attachment on the servo saver sliding onto the free ends of the two bolts. Fasten the two M4 bolts and fix Module E to Module D with four short M3 bolts.

Fig. 90 Assembly: Step 12

Part 3: Assembling Module F
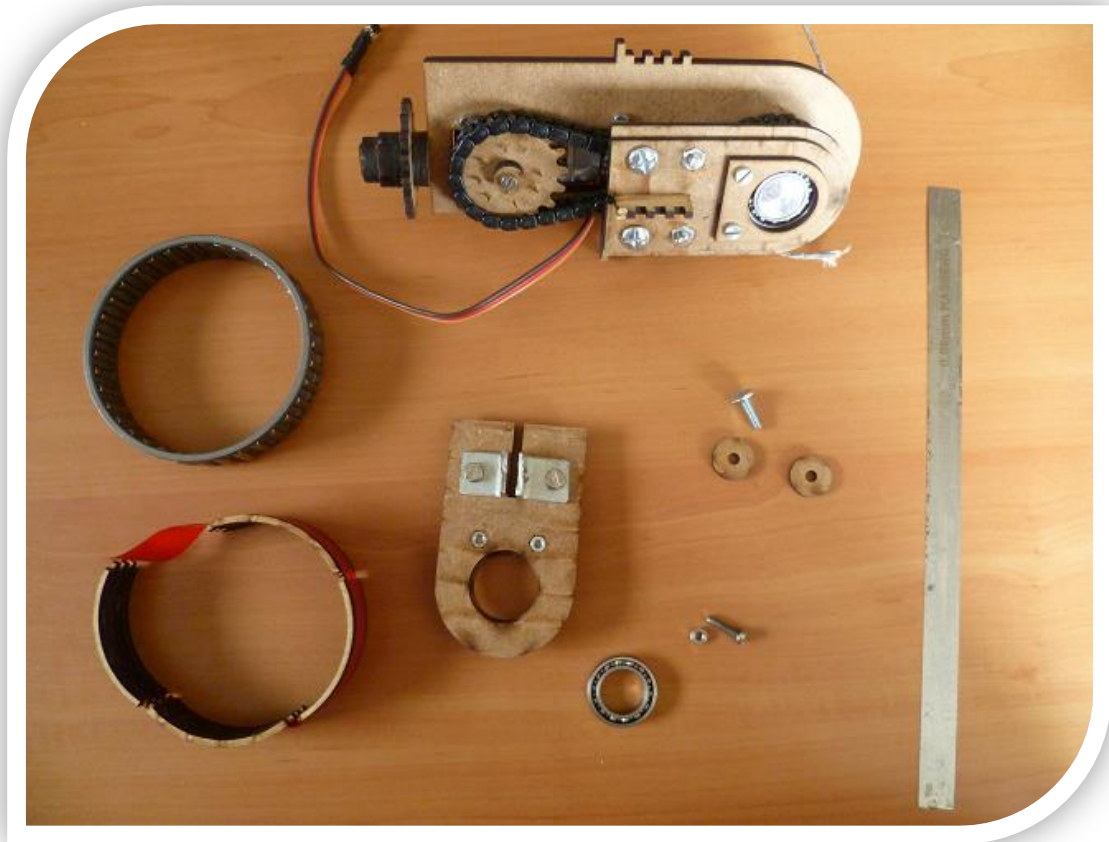
Fig. 91 Assembly: Step 13 (gravity compensation mechanism not pictured)

13. Use a microcontroller to rotate servomotor *ServoS2* to 43°.
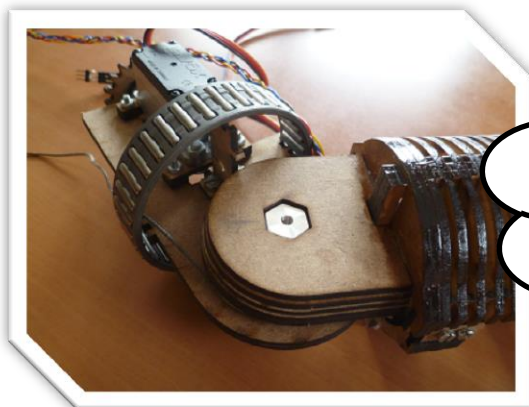
14. Place the needle bearing temporarily on Module F. Place Module D on the shoulder axis and bolt it onto the axis with the M4 bolt.
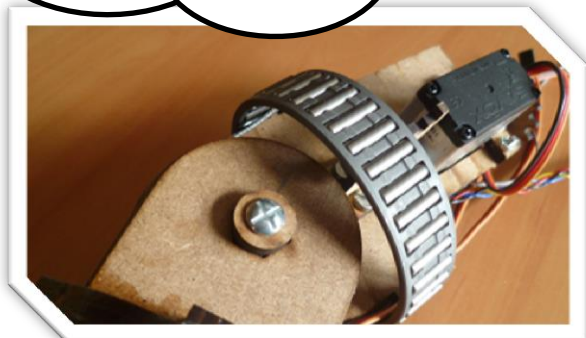
Fig. 92 Assembly: Step 14
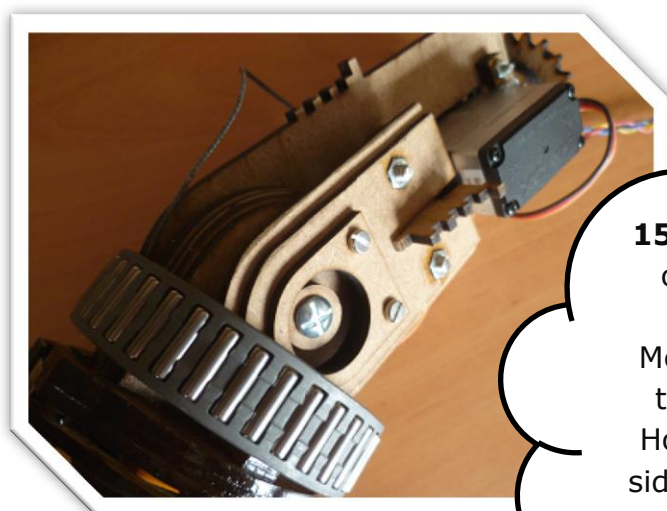
15. Move the needle bearing out of the way. Place the holder of the bearing on Module F. Place one M3 bolt through the corner joints. Hold an M3 nut at the other side and fasten the bolt to fix the holder into place.
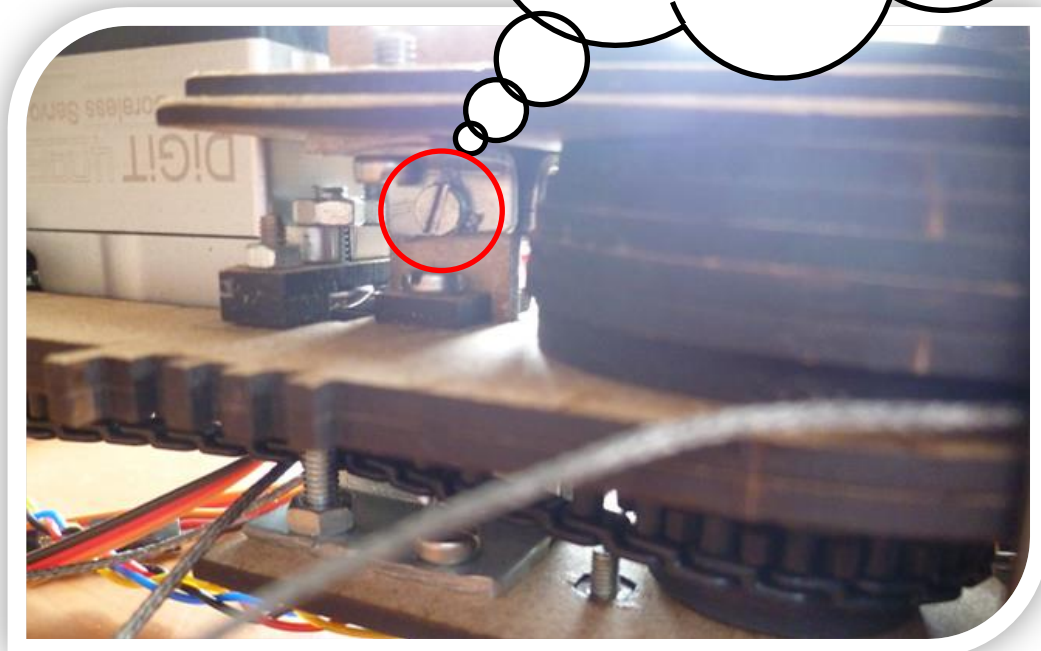
Fig. 93 Assembly: Step 15
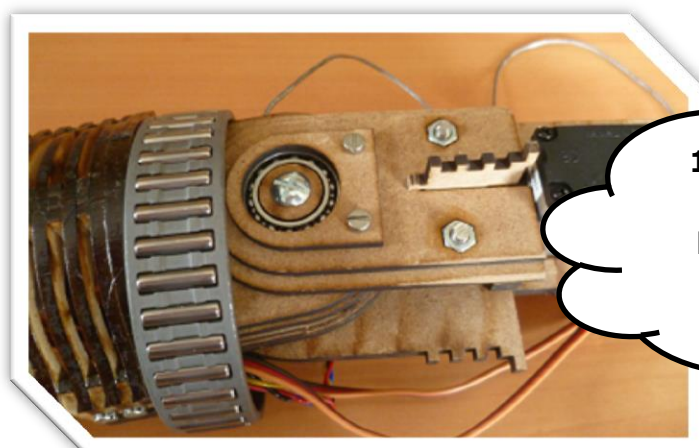
16. Remove the cover for the bearing, place the bearing and reattach the cover.

Fig. 94 Assembly: Step 16
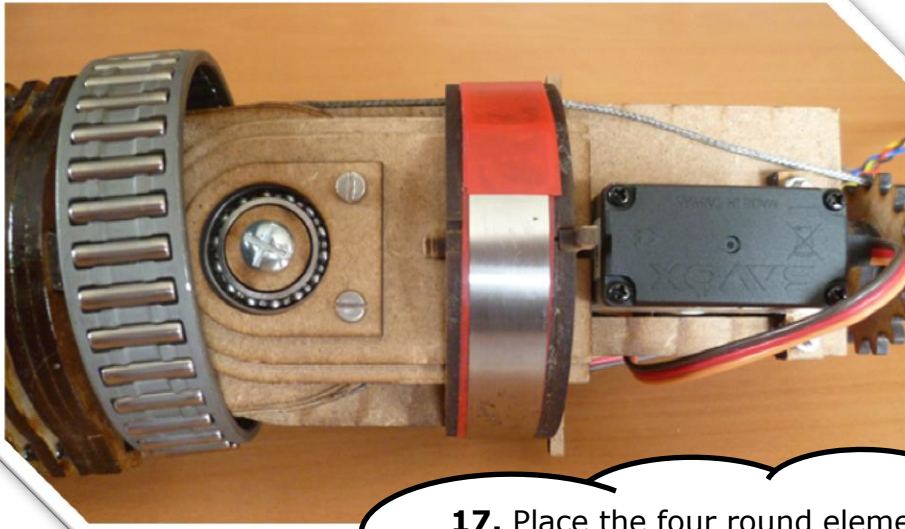
Fig. 95 Assembly: Step 17

17. Place the four round elements in the grooves of Module F. Place the metal strip around the round elements and fix it in place with tape.
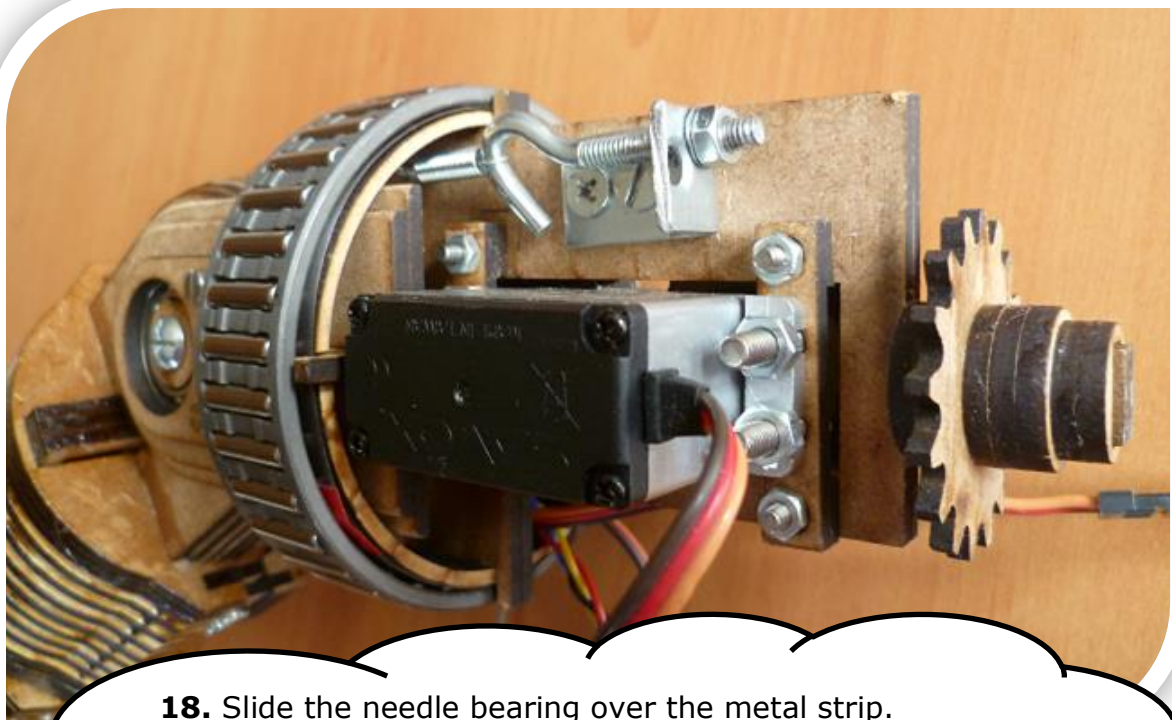
18. Slide the needle bearing over the metal strip. Attach the corner joint for the gravity compensation with two M4 bolts and nuts. Attach the spring on one end to the Kevlar cable and with the other end to the hook. Insert this hook in the hole in the corner joint and keep it in place with an M4 nut.

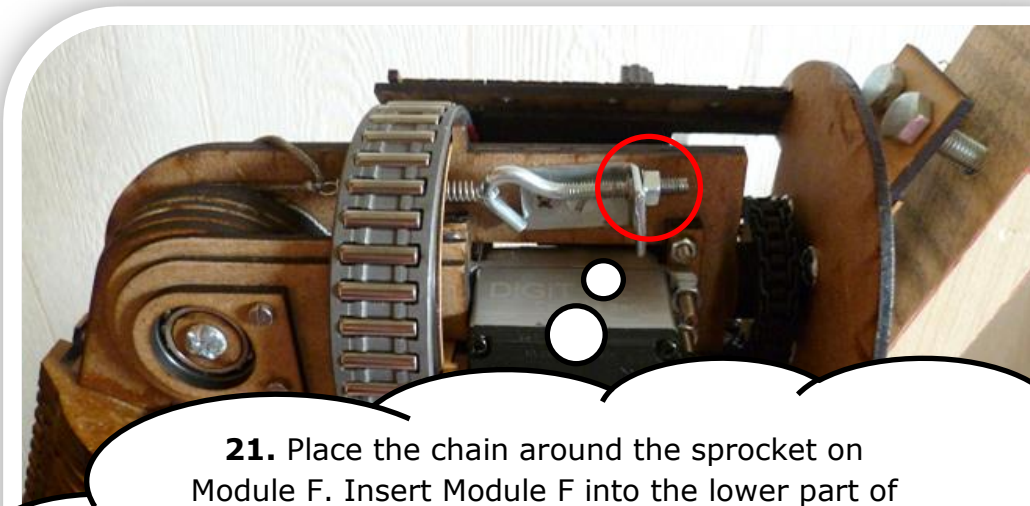**Fig. 96 Assembly: Step 18**

Part 4: Assembling Module G
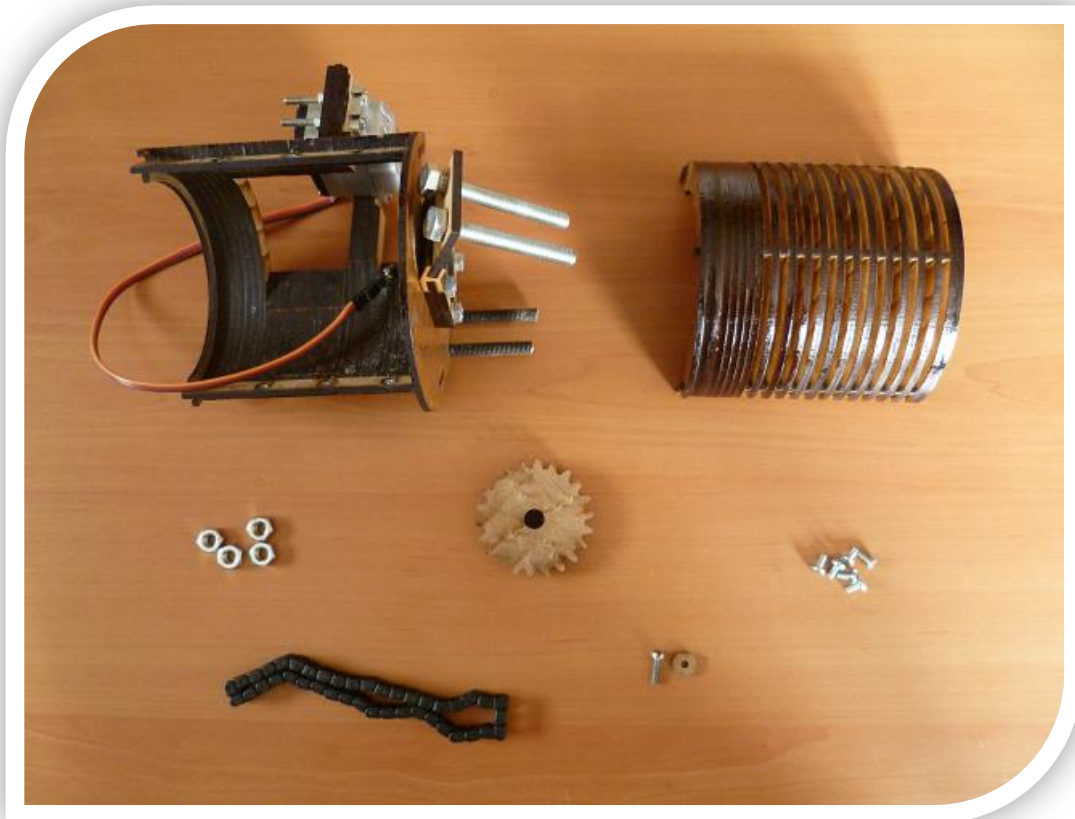
**19.** Use a microcontroller to rotate servomotor *ServoS1* to 170°.
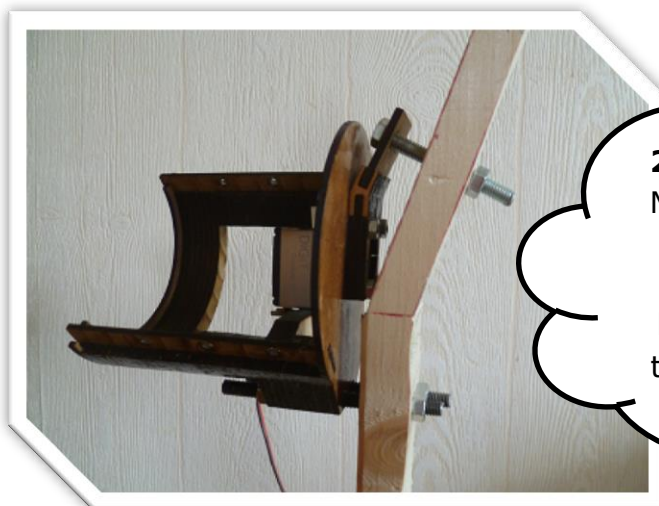
20. Mount the lower part of Module G to the frame, first inserting the top two M6 bolts, then inserting the lower two M6 bolts. Fasten the bolts with four M6 nuts.

Fig. 98 Assembly: Step 20

21. Place the chain around the sprocket on Module F. Insert Module F into the lower part of Module G. Fasten the M4 nut to increase the tension on the spring, until the upper arm is at an angle of 20° with the vertical. Guide all wires and the chain through the back of Module G.

Fig. 99 Assembly: Step 21
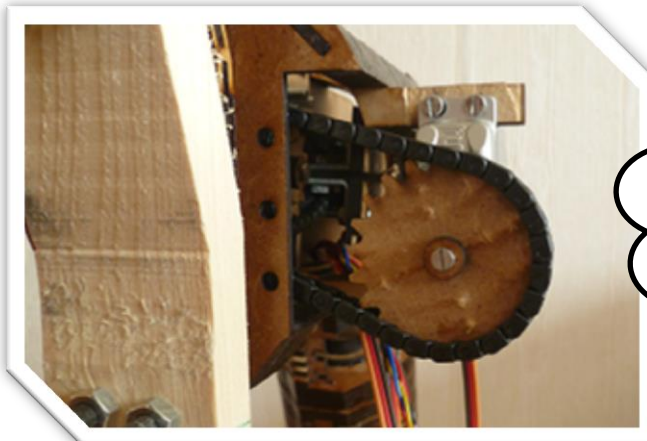
22. Place the sprocket in the chain and mount it on the servomotor on Module G. Fix it into place with an M3 bolt.

Fig. 100 Assembly: Step 22

23. Place the upper part of Module G on the lower part and connect them with six short M3 bolts.
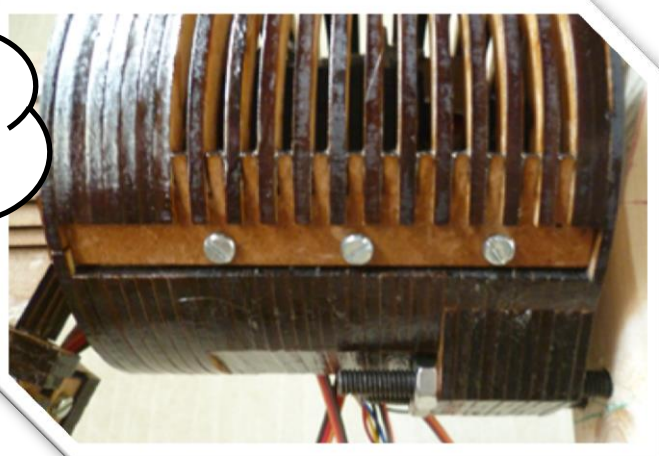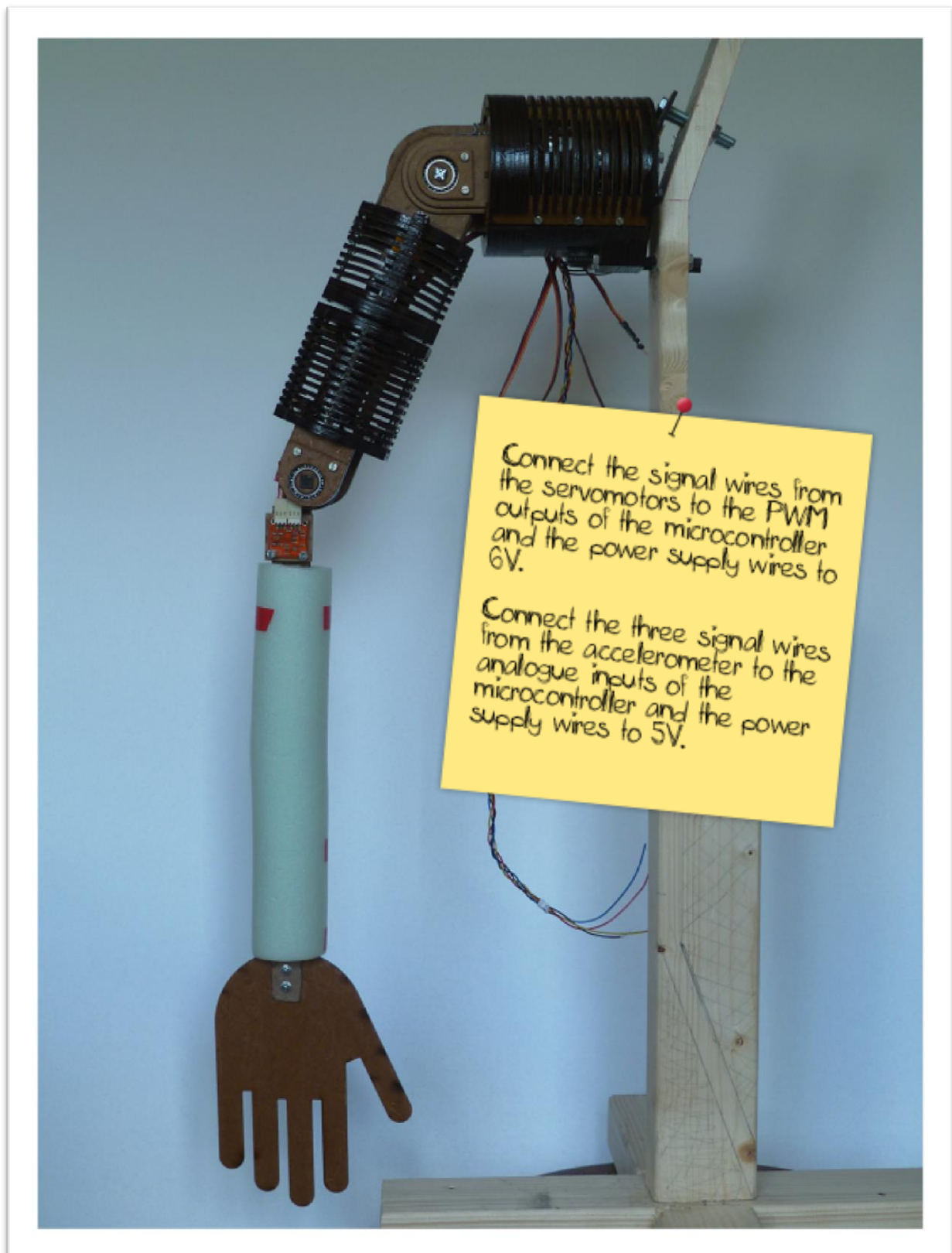
Fig. 101 Assembly: Step 23

Fig. 102 Final assembly and wires connections